ARAP REPORT NO. 96

A STUDY OF THE MEAN AND TURBULENT STRUCTURE OF A FREE JET AND JET IMPINGEMENT HEAT TRANSFER

A. R. A. P.

AERONAUTICAL RESEARCH ASSOCIATES of PRINCETON, INC.

HYPERVELOCITY KILL MECHANISMS PROGRAM
ARPA Order No. 149-60
Aerothermal Phase

ARAP REPORT NO. 96

A STUDY OF THE MEAN AND TURBULENT STRUCTURE OF A FREE JET AND JET IMPINGEMENT HEAT TRANSFER

by
Coleman duP. Donaldson
Richard S. Snedeker
and
David P. Margolis

This research was supported by the Advanced Research Projects Agency, Ballistic Missile Defense Systems Branch, and was monitored by the U.S. Naval Research Laboratory (Code 6240) under Contract No. Nonr-3903 (00)(X).

Aeronautical Research Associates of Princeton, Inc.
50 Washington Road, Princeton, New Jersey

December 1966

ABSTRACT

The results of an experimental study of the heat transfer below normally impinging jets are presented. These results are correlated on the basis of the local mean flow and turbulent characteristics of the free jet that would exist in the plane of impingement were this plane to be removed. In order to make these local correlations possible, a rather extensive survey of the turbulent characteristics of the free jet used in the experiments is made that can be used in connection with previous studies of the local mean character of the jet. On the basis of the method of local correlations which is developed, a rationale for computing heat transfer distributions below impinging jets is suggested.

TABLE OF CONTENTS

1. INTRODUCTION

The research that will be described in this report is part of a general study of the relationship between the local properties of axially symmetric free jets and the flows that result when such jets impinge upon a surface [1, 2]. One objective of this total program has been to gain an understanding of the heat transfer that results when the stagnation temperature of such a jet is different from that of the surface upon which it impinges.

If a laminar free jet impinges normally on a flat plate and if the flow is steady, the stagnation point heat transfer can be computed if one has a knowledge of the molecular transport properties of the gas in question, the centerline stagnation enthalpy of the jet, the temperature of the plate, and the pressure distribution in the region of impingement. The computation can be made since exact solutions of the Navier-Stokes equations can be obtained for laminar stagnation points. The key to obtaining such a solution is a knowledge of the stagnation point velocity gradient. For most Reynolds numbers of interest, this parameter may be determined from the measured pressure distribution in the region of impingement. Much attention has been given in the ARAP reports referenced above to relating this heat transfer parameter to the local mean properties that a free jet would have in the plane of impingement if the surface on which impingement takes place were removed.

Unfortunately, most free jets of practical importance are not laminar but are turbulent, and we are led to the problem of the effect of turbulence on stagnation point heat transfer. Over the past twenty years, a number of studies have been carried out on the effects of free stream turbulence on heat transfer [3 - 12]. The most recent of these studies have considered in detail the heat transfer in the vicinity of the stagnation line of cylinders placed normal to a turbulent air stream. In general, for relative turbulent intensities that are less than 10 percent

and for cylinders (two-dimensional flow), it has been found that stagnation heat transfer increases linearly with turbulence intensity, with the slope of this linear increase being larger with increase in Reynolds number. Unfortunately, there are large discrepancies among the slopes found by various investigators. The data are not sufficiently complete to enable the cause of these discrepancies to be determined at the present time, although it has been demonstrated [8] that the ratio of the integral scale of the turbulence to the diameter of the cylinder can be an important additional parameter.

In the case of heat transfer to spheres (axisymmetric flow), there is not so much information, but that which exists in the literature, as well as some unpublished results made available to the authors by Professor F. Costello,* indicates that the effect of turbulence on stagnation point heating in axisymmetric flow is less for small turbulence levels than for two-dimensional flow. In spite of all the quantitative uncertainty which is found in the data, it does appear that the best method of handling the computation of stagnation point heating in the presence of turbulence is to compute the normal laminar stagnation point heat transfer rate and then to apply a correction factor which is a function of the free stream turbulence level, an appropriate Reynolds number, and the ratio of the integral scale of the turbulence to the length used in defining Reynolds number. Correction factors as high as 1.8 for turbulence levels as low as 2.7 percent have been reported in the literature [11].

In considering the heat transfer to a surface due to the impingement of a turbulent jet, it was decided, in the present study, that the correction factor method outlined above should be used in trying to correlate the stagnation point heat transfer rates which were to be measured. To adopt this approach requires that detailed measurements of the turbulent character of the jet

---

*Department of Mechanical and Aerospace Engineering, University of Delaware

studied in [1] be made. Thus a considerable portion of this report will be devoted to the determination of the jet microstructure.

In addition to the usual measurements of turbulent velocity correlations and their spectra, measurements were also made of the fluctuation of total pressure on the centerline of the free jet and at the stagnation point for the case of jet impingement.

Since we are primarily interested in the distribution of heat transfer under an impinging free jet, the remainder of the results presented in what follows are concerned with measurements of the heat transfer from a heated flat plate to a cooler jet which impinges normally. In particular, we will, following the procedure of [1,2], attempt to correlate the resulting local heat transfer rates with the properties of the free jet in the plane of impingement, an appropriate local temperature difference, and the distance from the point of impingement made nondimensional with respect to the half-breadth r_5 of the free jet in the plane of impingement.

Before going on to present these results, a review of some previous work on impingement heat transfer is in order. Until quite recently, very little information on the details of jet impingement heat transfer existed. However, within the past five or six years several most useful studies have been made. Vickers [13] studied the local heat transfer coefficients due to a laminar axisymmetric fluid jet impinging normally on a flat surface. Results are presented for Reynolds numbers based on the jet exit velocity and diameter from 250 to 950 and for impingement distances $8 < z/d_N < 20$.* Gardon and Cobonpue [14] measured local heat transfer coefficients for both single and multiple circular turbulent jets. Reynolds numbers varied from 7×10^3 to 1.12×10^5 and the range of z/d_N studied was $1.5 < z/d_N < 50$. It is interesting to note the variation of stagnation

*The notation used in this report for the jet axis system and velocity components differs from that used in [1, 2]. The present system, which is convenient for expressing turbulence parameters in an axisymmetric flow, is shown in the Appendix.

point heat transfer with z/d_N reported in this work for single jets. In Fig. 1.1 we have reproduced the pertinent figure from Gardon and Cobonpue's paper. Note the large variation in heat transfer between $z/d_N = 1.5$ and $z/d_N = 15$. This is primarily due to the variation in the stagnation point velocity gradient $(\partial u_e/\partial r)_{r=0}$ as a result of the elimination of the potential core and formation of a developed jet. This may be seen by comparing the results shown in Fig. 1.1 with the results shown in Fig. 1.2 which is taken from [1].

Huang [15] also studied the heat transfer below an impinging axially symmetric jet. Measurements were made for impingement distances from $z/d_N = 1$ to $z/d_N = 12$ and for the region $0 < r/d_N < 20$. Jet Reynolds numbers were varied from 10^3 to 10^4. Huang does not indicate a variation of stagnation point heat transfer coefficient with z/d_N for the range $1 < z/d_N < 12$ where significant variations were observed by Gardon and Cobonpue. This result is probably due to the lower Reynolds numbers at which these data were taken, as might be expected from an inspection of Fig. 1.1.

Gardon and Akfirat [16, 17] report measurements of local heat transfer below two-dimensional slot jets impinging on a flat plate. The range of Reynolds numbers (based on slot velocity and slot breadth b_N) was from 450 to 50,000. These data show the rapid variation of heat transfer with z/b_N in the range $1 < z/b_N < 15$ due to the elimination of the potential core and formation of a developed jet, as has been discussed above. The effect, however, appears to be somewhat more pronounced in two-dimensional jets than it is in axisymmetric jets. Of considerable importance is the observation by Gardon and Akfirat that increasing the initial turbulence level of the jet increased the stagnation point heat transfer in the core region ($z/b_N \cong 2$). In particular, by increasing the turbulence intensity from 2.5 percent to 6 and 18 percent through the use of turbulence promoters, the heat transfer was increased over its value for 2.5 percent intensity by 1.2 and 1.7 times, respectively.

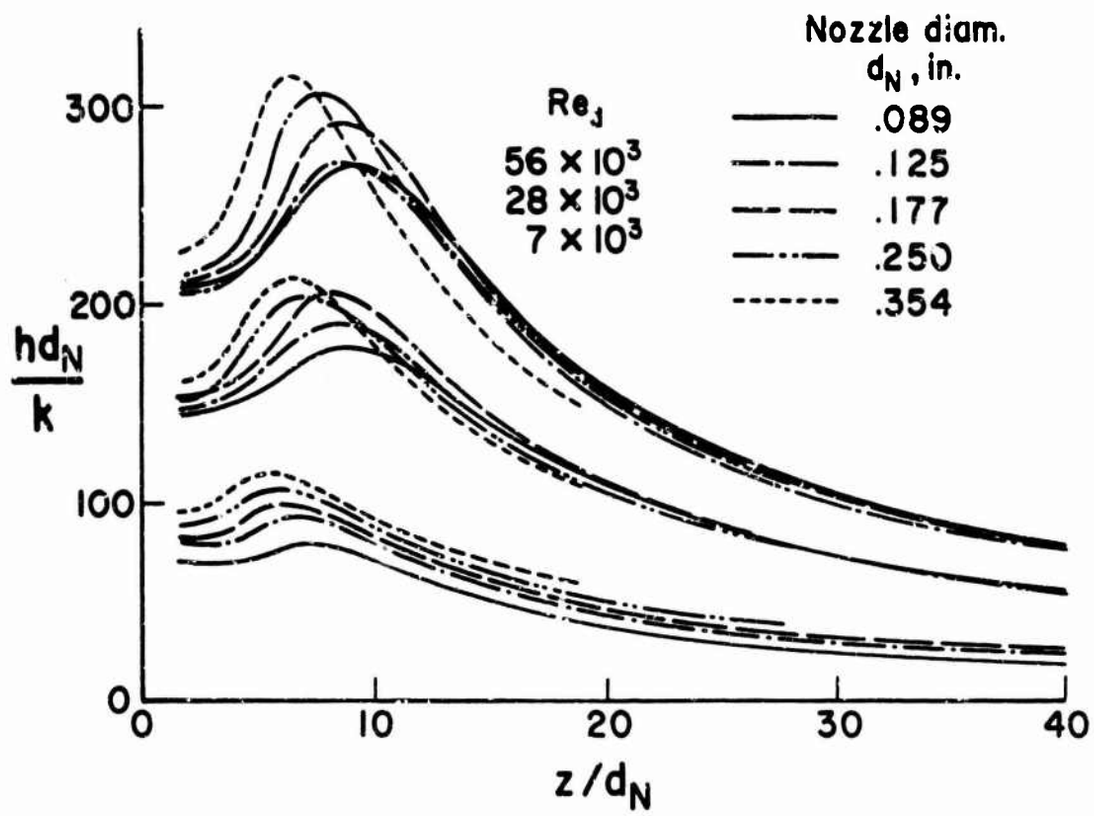

Figure 1.1. Stagnation point heat transfer measured by Garlon and Cobonpue [14].

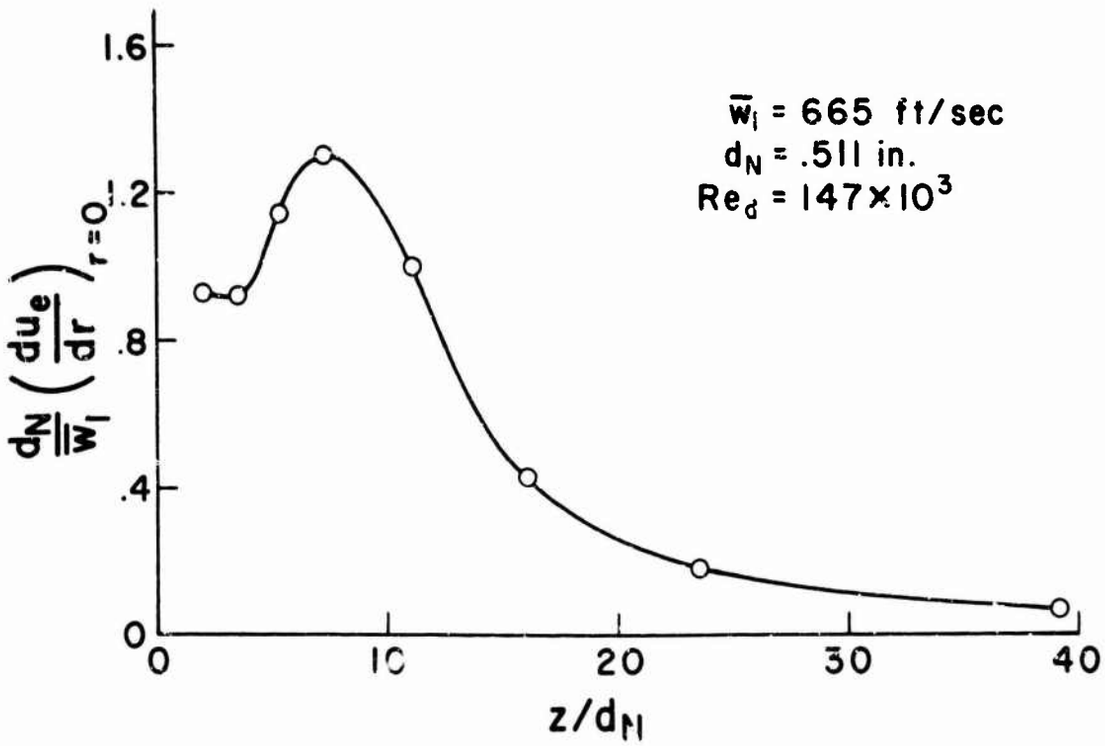

Figure 1.2. Measured stagnation point velocity gradients from [1].

O'Connor, Comfort, and Cass [18] have measured the heat transfer below an impinging arc jet at distances such that $6 < z/d_N < 20$ and at Reynolds numbers from 8×10^3 to 1.8×10^4. In this work a detailed study of the mean structure of the free jet was carried out so that the stagnation point heat transfers might be compared with appropriate computations made for a laminar stagnation point having the same velocity gradient $(\partial u_e/\partial r)_{r=0}$. The result when such a comparison was made was that the theoretical prediction was low by a factor of the order of 2.

The factor of 2 found by O'Connor, et al is, as will be seen in what follows, roughly equal to the factor found in the measurements reported here for fully developed jets. According to the philosophy that has been adopted, this factor must be ascribed to the existence of turbulence in the fully developed impinging jet.

As found in the studies referred to above, the general character of the heat transfer that results from impinging jets is quite dependent on the jet Reynolds number as well as the position of impingement relative to the core. For fully developed jets, the stagnation point heat transfer is found to be proportional to the square root of the local free jet Reynolds number $Re_5 = \rho_c w_c r_5/\mu_c$ times a factor of the order of unity which accounts for the effect of jet turbulence. Away from the stagnation point, under the wall jet which develops on the impingement surface, the heat transfer is found to be proportional to the eight-tenths power of the local free jet Reynolds number. The different dependence of these two heat transfers on Reynolds number causes the relative magnitudes of stagnation point heat transfers and wall jet heat transfers to vary over wide ranges with Reynolds number. A plot of the Nusselt number $\dot{q}r_5/k\Delta T$ divided by the eight-tenths power of the Reynolds number Re_5 versus r/r_5 for several values of Re_5 has, in general, the character shown in Fig. 1.3. Note that for small Reynolds number the stagnation point heat transfer is large compared to the wall

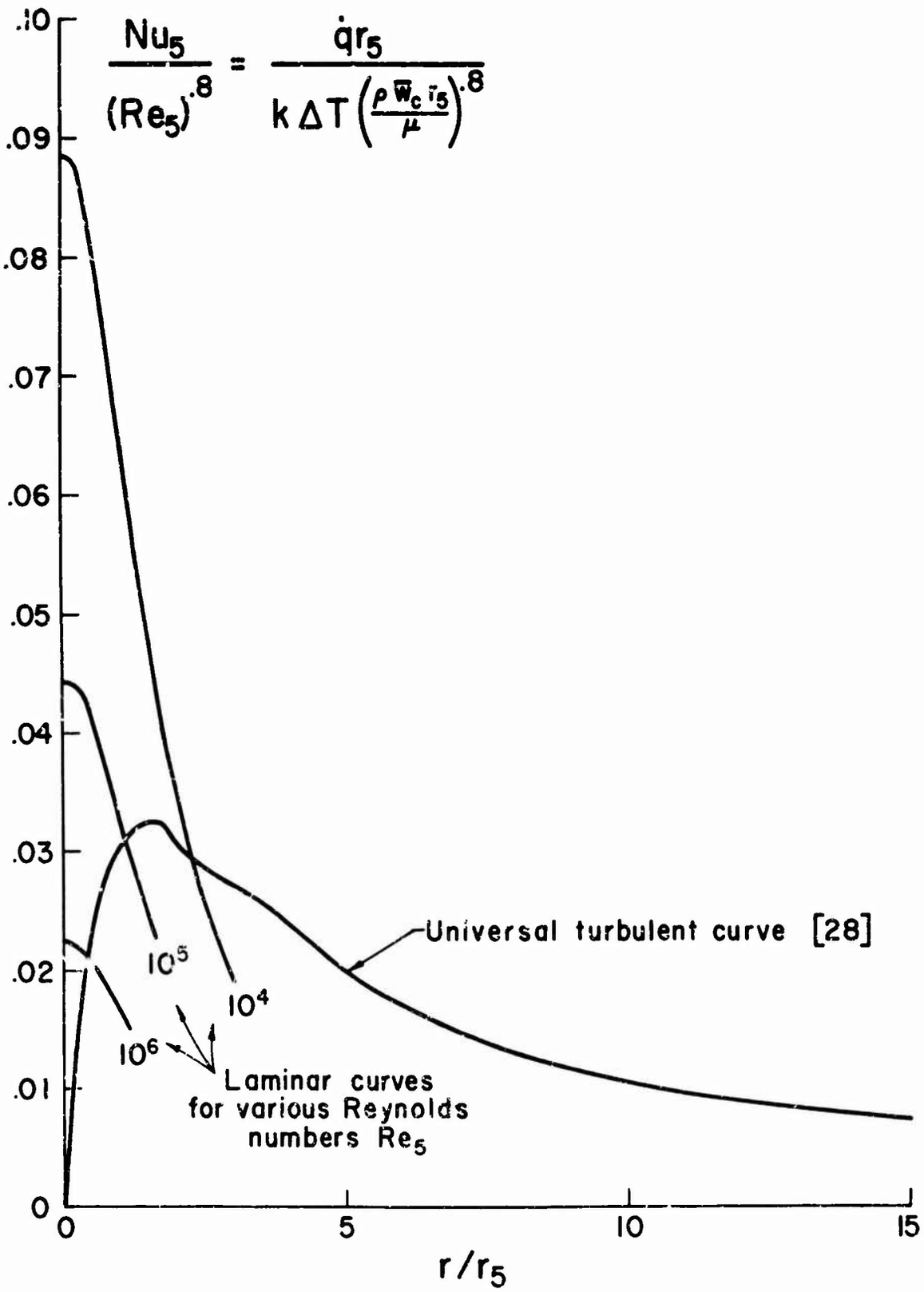

Figure 1.3. General character of jet impinge[illegible] heat transfer as a function of distance from the stagnation point.

jet heat transfer and one observes a monotonic drop-off of heat transfer with radius.* When the Reynolds number is large, on the other hand, the stagnation point heat transfer is small compared to the wall jet heat transfer and one observes an initial rise in heat trarsfer as r/r_5 increases before observing the usual fall-off at large r/r_5. In the experiments that will be discussed in this report, the Reynolds number was such that the break in the curve that occurs on transition from laminar to turbulent flow is so small as to be obscured by the scatter of the experimental data.

*This behavior is found provided the impingement takes place sufficiently far from the nozzle so that nozzle interference effects are not present.

2. EXPERIMENTAL APPARATUS AND TECHNIQUE

General Description.

The jet apparatus used in these experiments was the same as that used in the earlier studies performed at ARAP on free and impinging jets [1, 2]. The jet was produced by a convergent nozzle with an exit diameter of .511 in. (see Fig. 2.1) using air supplied from a blow-down system which was capable of running indefinitely at jet exit velocities of up to 300 ft/sec. The automatic pressure regulator maintained the desired exit velocity, in general, within ±1 percent. Supporting hardware for the probes and impingement surfaces was designed to produce a minimum of interference with the jet flow field.

Details of the apparatus, instrumentation, and techniques used in measuring the turbulence, fluctuating pressure, and heat transfer characteristics of the jet are given in the following sections.

Free Jet Turbulence Measurements.

Apparatus and instrumentation. Measurements of the turbulence intensities and shear stress in the free jet were made using a Thermo-Systems linearized, constant temperature, hot film anemometer. A block diagram of this instrumentation is shown in Fig. 2.2. The basic elements in this system are two Model 1010 Thermo-Systems anemometers with two Model 1035 linearizers. An x-probe was used with 0.001-in. diameter platinum film sensors. In Fig. 2.1, this probe is shown mounted in the jet on a traversing mechanism. Signals from the sensor were fed through the anemometer and linearizer which produced an output voltage proportional to the instantaneous velocity at the sensor. Mean velocity values were determined by feeding the linearizer output directly to an electronic integrator. Root-mean-square values of the fluctuating quantities were determined by feeding the linearizer output through a sum-difference network and a Ballantine Model 320A true rms voltmeter. Such a meter, of

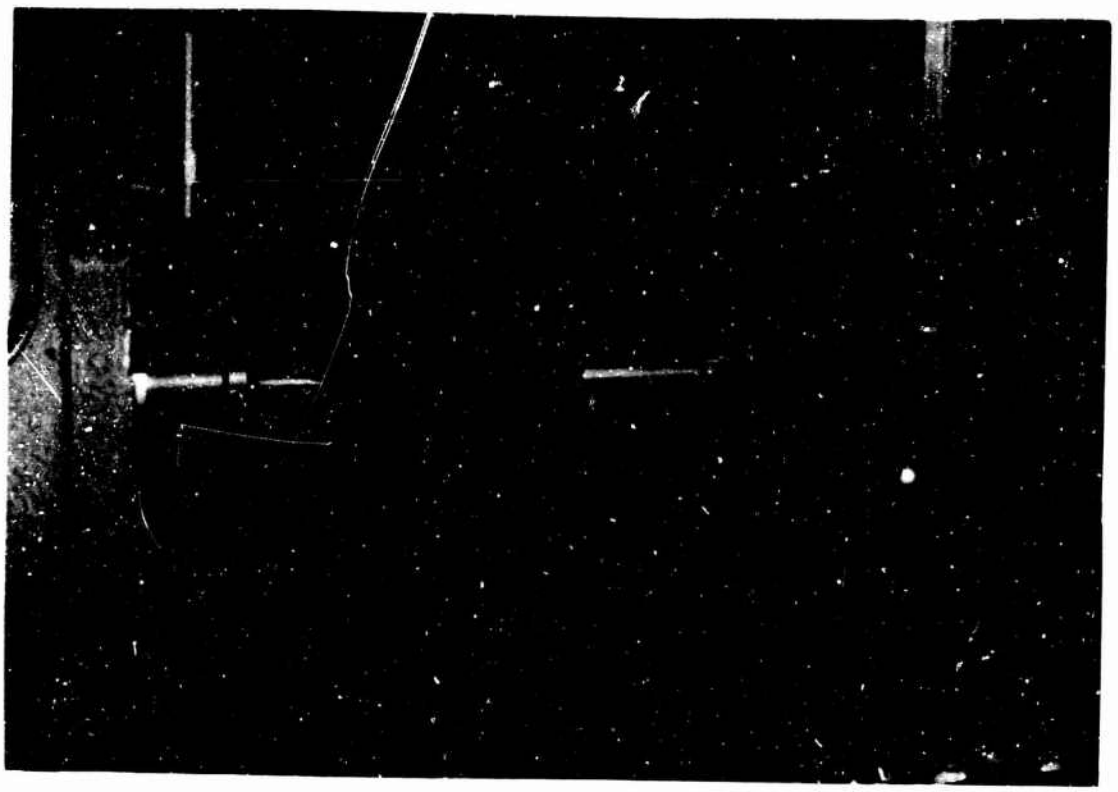

Figure 2.1. Photograph of nozzle and hot film x-probe.

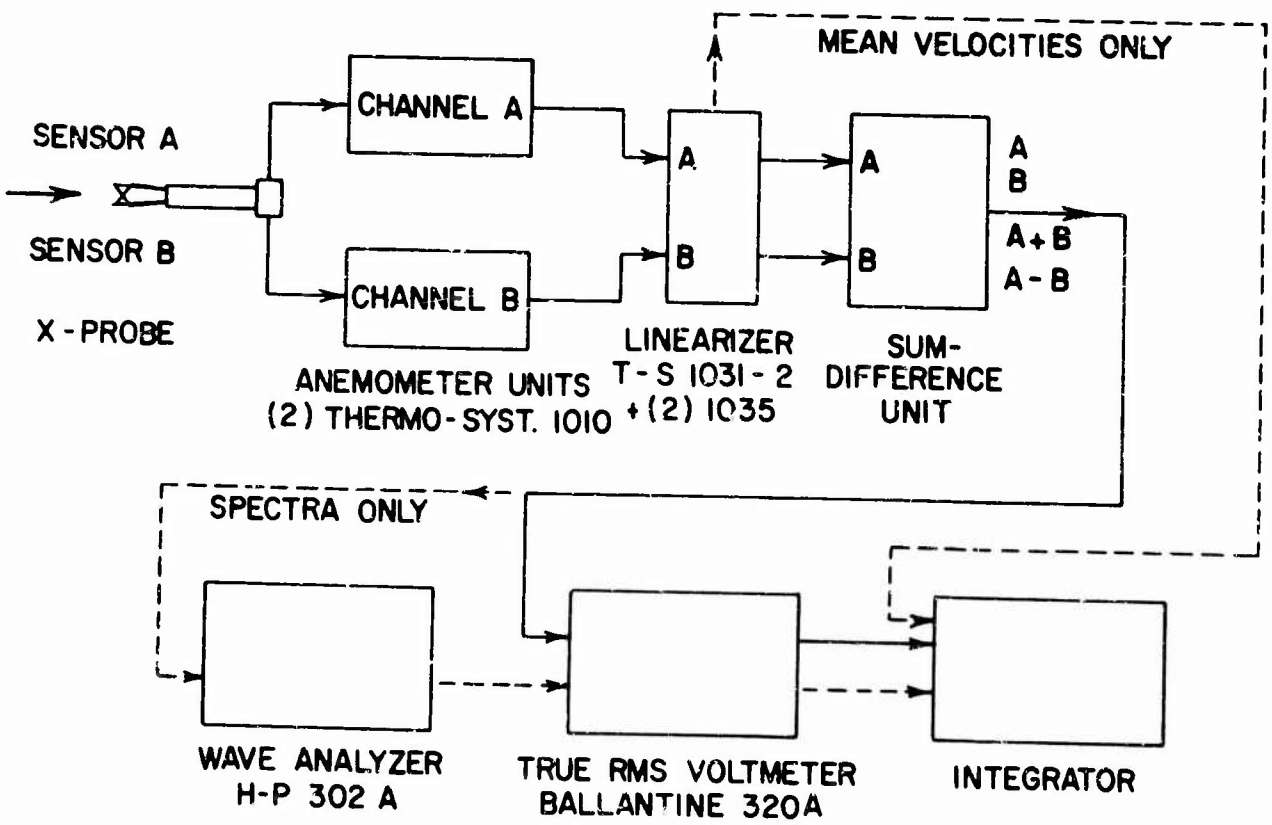

Figure 2.2. Block diagram of turbulence measuring equipment.

course, responds only to the fluctuating portion of the signal. A dc output signal proportional to the mean square from the rms voltmeter was then integrated electronically. The sum-difference network and the electronic integrator were designed and built at ARAP.

One-dimensional energy spectra of $\overline{w'^2}$ and $\overline{u'^2}$ were measured on the jet centerline using a Hewlett-Packard Model 302A wave analyzer The analyzer has a fixed bandwidth of 8 Hz and a range of 20-50,000 Hz.

Technique. Radial surveys were made by traversing the probe across the jet from edge-to-edge in a vertical plane through the jet centerline. Proper alignment with the centerline was achieved with the aid of a four-tube Pitot array which could be mounted on the shaft of the x-probe. The x-probe was aligned at the exact center of the Pitot array and the position of the probe was adjusted until all four Pitot tubes gave the same response on a multiple manometer. The x-probe was then assumed to be on the jet mean centerline and the Pitot array was removed.

The measurements of turbulent shear stress were made by traversing the jet twice, once with the probe in its "normal" position and once with the probe "inverted" or rotated about its axis 180° . The average of the two profiles produced was taken to represent the actual measured shear stress distribution. This technique, of course, serves, in an axisymmetric flow, to eliminate the error caused when x-probe sensors have different angles relative to the mean flow as long as the axis about which the probe is rotated is parallel to the mean flow. An alignment check showed that the probe shaft was parallel with the jet centerline within 0.2° . The equal opposing symmetries of the measured profiles confirmed that this was a negligible alignment error. The degree to which the resulting measurement actually represents the true shear stress distribution is limited by further considerations, namely, effects of intermittency in the flow and

nonlinear response of the sensor (see Rose [19]). In the present case, no corrections for these effects were applied.

Measurements of Fluctuating Stagnation Pressure.

Apparatus and instrumentation. The measurement of fluctuating stagnation pressures levels in the free and impinging jet was accomplished using a Brüel and Kjaer condensor microphone Model 4136 with matching cathode follower and microphone amplifier Model 2603. Signals from the microphone amplifier were fed to the wave analyzer and integrating circuitry used in the turbulence measurements. A block diagram of this system is shown in Fig.2.3.

Pressure level measurements were made on the centerline of the free and impinging jets by exposing the microphone diaphragm to the oncoming flow through a small probe tube. Since a primary consideration in the design of the probe was minimum flow interference, the smallest available microphone of the desired performance characteristics was used. The B&K 4136 has a diaphragm 0.234 in. in diameter, a sensitivity of 89.0 μvolts/μbar, and a flat frequency response from 25 to 80,000 Hz. A special enclosure was designed for the microphone cartridge and cathode follower assembly. Detailed drawings of the assembly and mounting are shown in Fig. 2.4. The design of the microphone enclosure and the probe tube involved a compromise among several factors in addition to minimum flow interference. The tube leading to the diaphragm had to be large enough in diameter and short enough in length not to cause excessive attenuation of the pressure signals and, at the same time, had to be stiff enough so that its natural frequency was not in the frequency range of interest. Because of the exposure of the microphone diaphragm to the full dynamic pressure of the flow, it was also necessary to provide an additional path to allow for the equalization of the mean pressure on the front and rear surfaces of the diaphragm. If the pressure equalization hole in the B&K 4136, located on the side behind the threads of the microphone grid cap, had merely been exposed to the

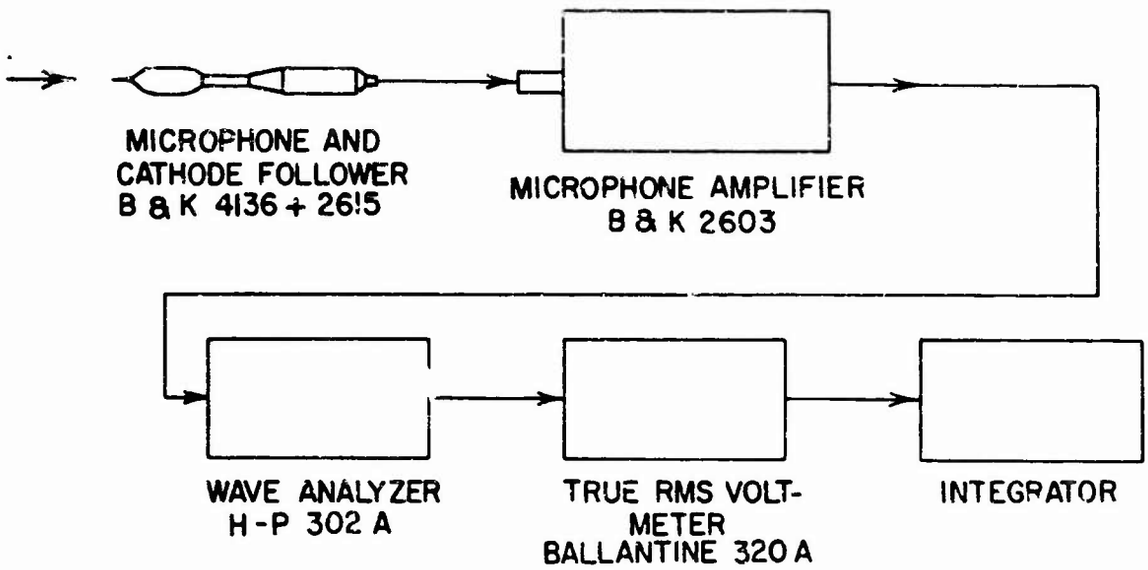

Figure 2.3. Block diagram of fluctuating pressure measuring equipment.

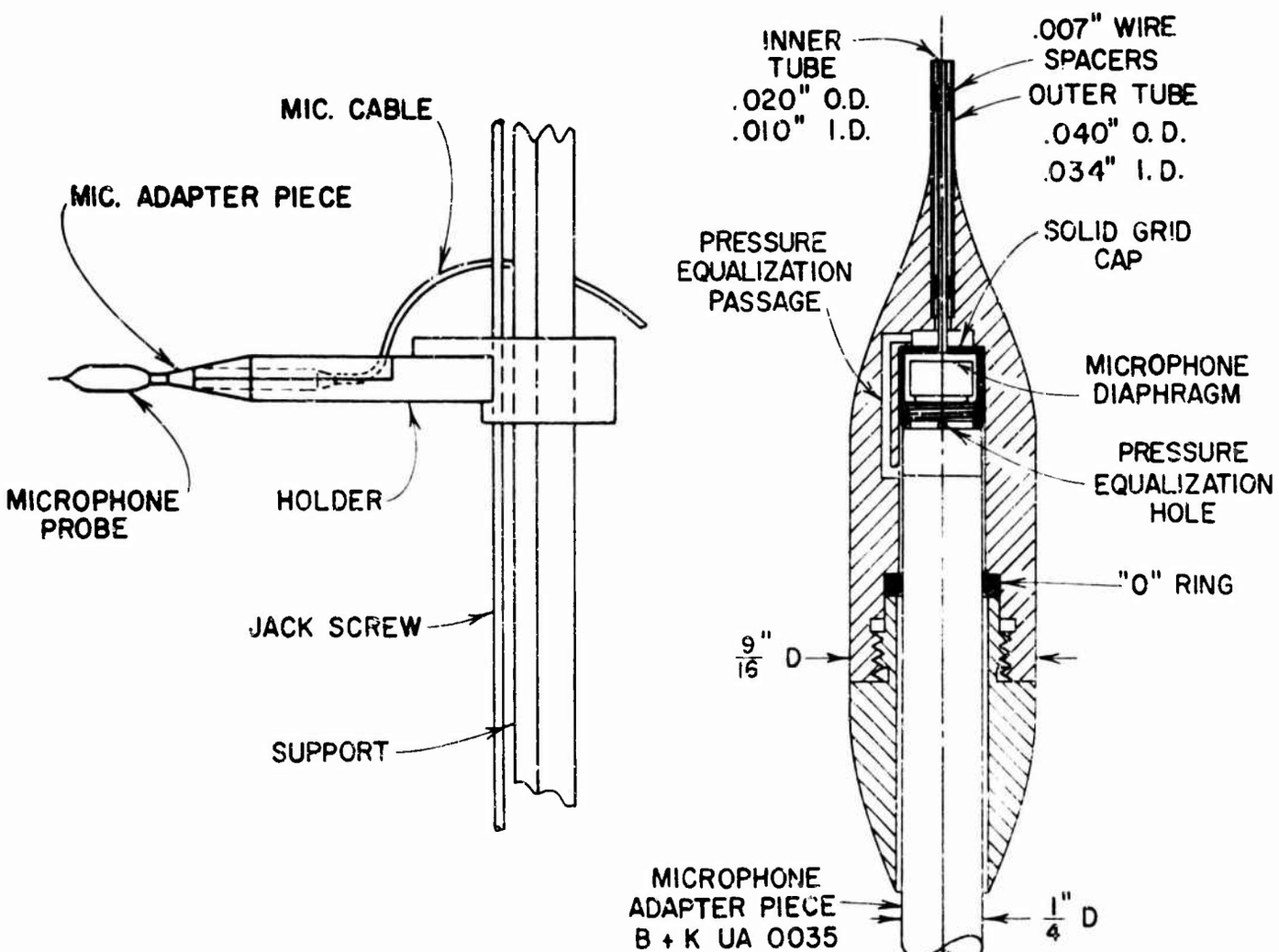

Figure 2.4. Microphone mounting assembly and probe detail.

static pressure, the resulting mean pressure imbalance across the diaphragm would have seriously altered the microphone's frequency response. Therefore, an outer concentric tube was mounted around the inner microphone tube and connected to a chamber within the microphone enclosure which led to the equalization hole at the rear of the cartridge. The chamber itself was sealed from the static pressure outside the enclosure with an "O" ring. The inner tube was mounted in a solid B&K 4136 grid cap (i.e., one without slots) which facilitated attachment to the cartridge. The natural frequency of the outer tube, considered as a cantilever and without the stiffening effect of the inner tube, was calculated to be about 24,000 Hz, well above the range of interest. The theoretical fundamental "organ pipe" resonant frequency of the inner tube was about 3400 Hz. Although this falls within the range of interest, its presence could not be detected during either the probe calibrations or the spectral measurements.

Because of the nonuniform frequency response of the probe tube, it was necessary to determine the over-all fluctuating pressure levels by making spectral measurements and integrating them over the range of interest after applying a probe tube correction at each frequency.

The frequency response characteristics of the microphone probe assembly were determined by mounting the probe with its tube through the wall of a 2-cubic centimeter coupling chamber in which a calibrated sound source was produced.* The actual response curve for this assembly is shown in Fig. 2.5 as the ratio of the output voltage of the microphone cartridge to the voltage equivalent of the sound applied at the end of the tube.

For the measurements in the free jet, the microphone was clamped rigidly in position on the traversing mechanism shown in Fig. 2.1. The impinging jet measurements were performed using

---

*The authors wish to thank Professor E. G. Wever and members of the staff of the Auditory Research Laboratory at Princeton University for their help in performing this calibration.

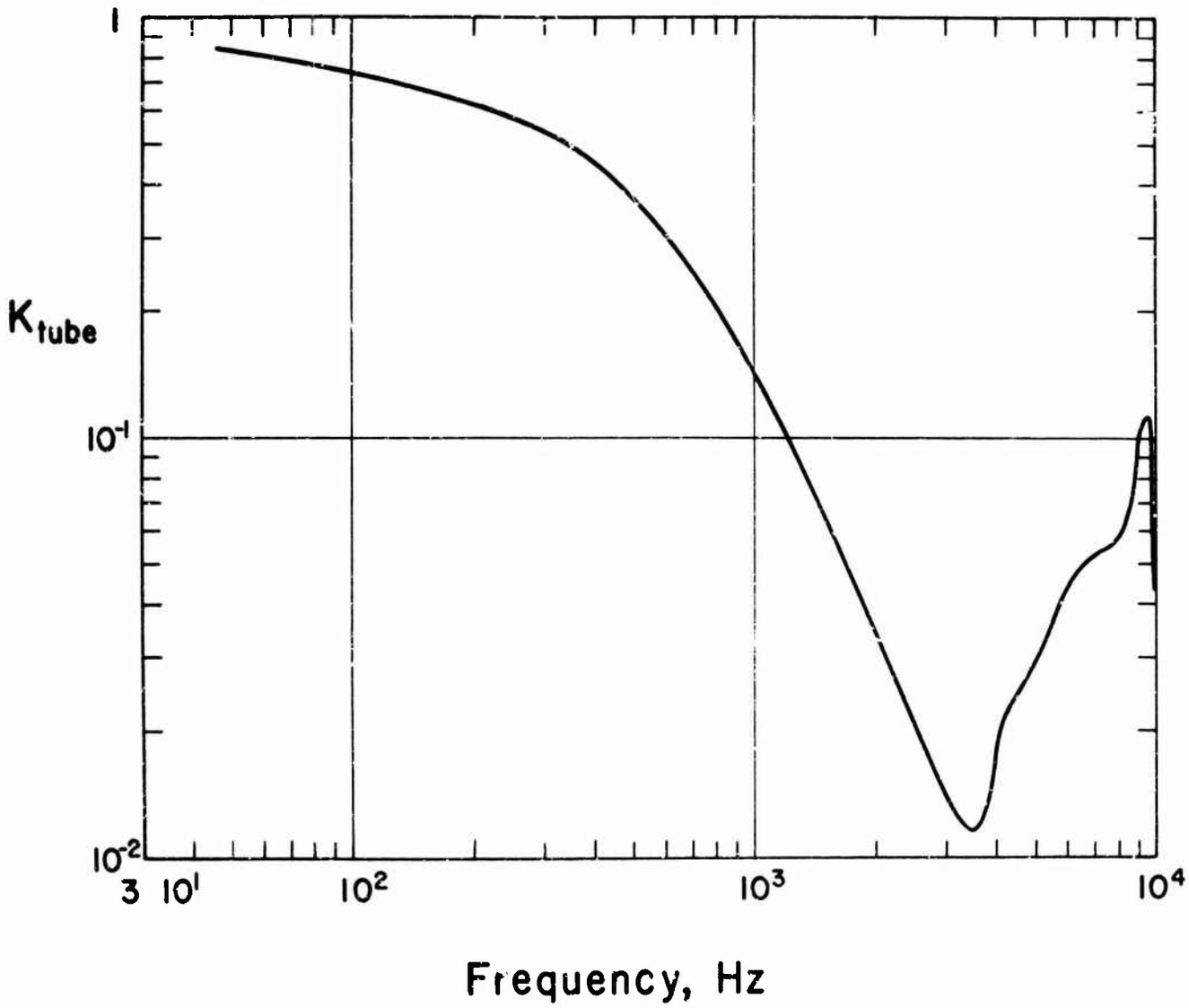

igure 2.5. Calibration of frequency response of ARAP probe tube using B&K 4136 microphone.

the same microphone probe assembly. In this case, however, the probe tube was fitted snugly into a hole at the center of a 1/2-in. thick aluminum plate and positioned flush with the surface. The adapter piece and cathode follower were supported rigidly at the rear of the plate. The plate itself was held in the adjustable mounting jig shown in Fig. 2.8.

Technique. The measurements of spectra at each location were made with the jet stabilized at the desired velocity and running continuously during the scan of the frequency range. In general, the range in which data were taken was from 100 Hz to 10,000 Hz. At each frequency, the signal was integrated for an appropriate time and the range settings of each element in the system were recorded. Calibrations were made of the effective gain constants of the microphone amplifier, wave analyzer, and rms meter-integrator system for the various combinations of range settings. These constants were applied to the integrated output along with the microphone and probe calibration constants in order to arrive at the actual spectral sound pressure level in the flow. A separate set of measurements was made with the microphone tube blocked in order to determine the level of noise due to mechanical vibration and other sources. Since the highest value of such noise was less than one percent of the sound level measured with the tube open, the spectral levels were not corrected. The measured spectra were then integrated graphically to give the over-all sound pressure levels.

Heat Transfer Measurements.

Introduction. The measurements of convective heat transfer coefficients were made with the cold jet impinging on a flat, circular heated plate containing 14 flush-mounted calorimeter disks with thermocouples attached. The initial portion of the recorded temperature-time response of each thermocouple was used to determine the heat transfer at that point by matching the response with a suitable analytical expression.

In the design of the plate, the usual considerations for establishing the most valid behavior of the calorimeters were taken into account (see, e.g., [20-22]). The plate itself and the calorimeters were of the same material, so that conductive heat fluxes due to temperature gradients or differing thermal properties along the plate surface could be minimized. At the same time, the plate and the calorimeters were thin enough to assure negligible internal thermal resistance to heat flux normal to the surface. In order to minimize conductive heat loss from the back, the plate was mounted on a rigid piece of insulating material of low density, thermal conductivity, and heat capacity. Finally, the calorimeter gages were thermally insulated from the surrounding surface by a ring of low conductivity material. The diameter of this ring was kept as small as possible compared to the diameter of the gage in order to minimize any effects due to lack of thermal continuity of the surface. At the same time, of course, the insulation had to be sufficiently thick to minimize conductive heat transfer along the surface between the gage and the surrounding surface.

Apparatus and instrumentation. The heat transfer plate consisted of a copper sheet .015 in. thick and 12 in. in diameter bonded to an insulating back-up plate of rigid polyurethane foam 1 in. thick (see Fig. 2.6). The foam used was Emerson and Cuming "Eccofoam SH", a material designed for use at temperatures up to 400°F. Its density was 8 lb/ft^3 and its thermal conductivity was .020 $Btu/hr\text{-}ft^2\text{-}^\circ F/ft$. The copper was bonded to the foam using a high temperature epoxy adhesive, Emerson and Cuming "Eccobond 106". This material was used because of its flexibility at high temperatures which permits the bonding of materials having dissimilar coefficients of expansion. In making the bond, a minimum of adhesive was used to minimize changes in the insulating performance of the foam.

The calorimeter gages were small copper disks, .015 in.thick

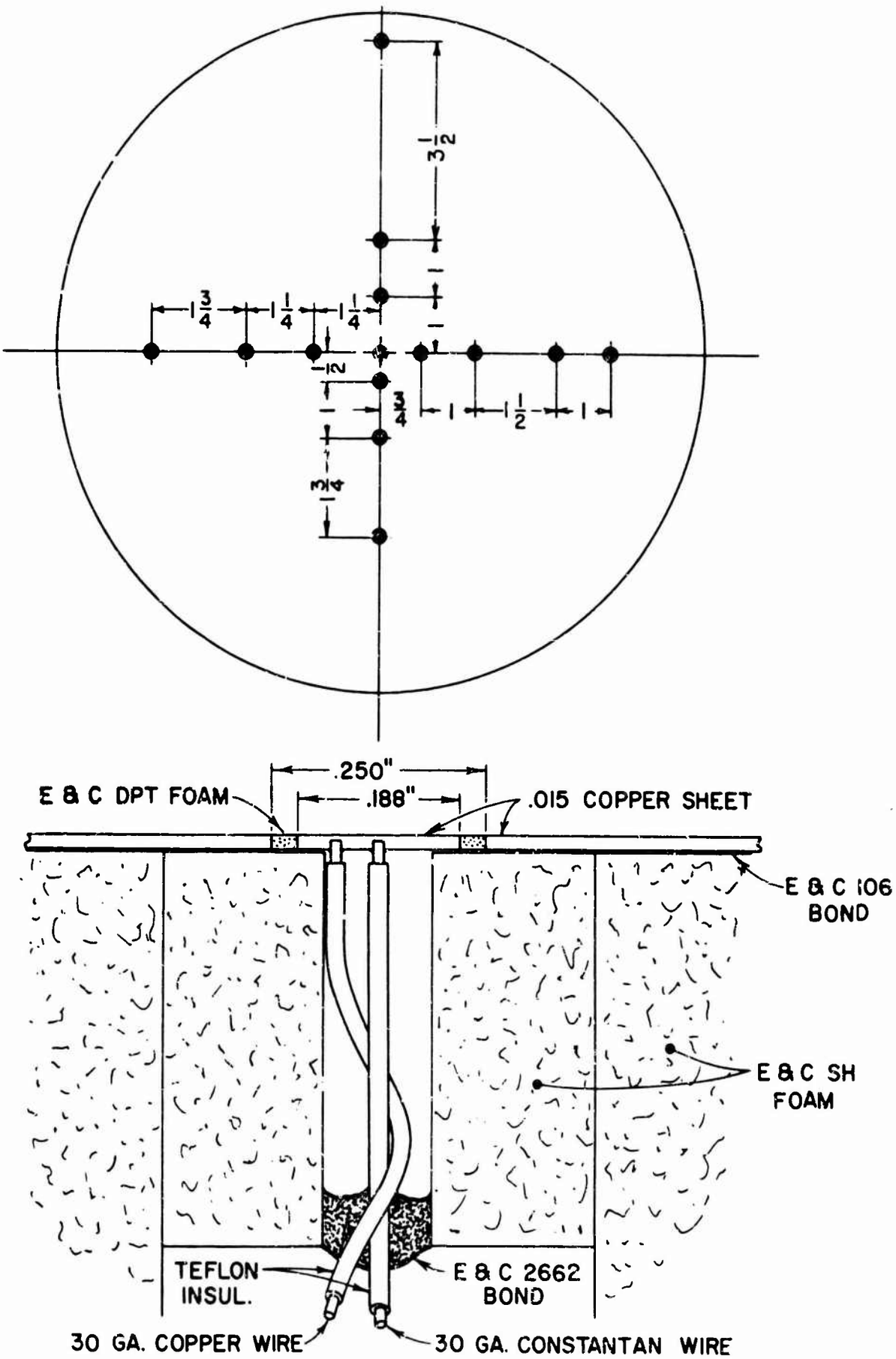

Figure 2.6. Layout of gages on heat transfer plate and detail of gage construction.

and 3/16 in. in diameter. Each disk contained a copper-constantan thermocouple junction at the center. The .010-in. diameter thermocouple wires were fastened by inserting them into holes drilled in the back of each disk and then soldering them to the disk with a minimum quantity of solder. Each calorimeter was mounted in a hole 1/4 in. in diameter in the copper plate, thus leaving a circular gap 1/32 in. wide around each gage. This gap was filled with a high temperature pack-in-place epoxy foam, Emerson and Cuming "Eccofoam DPT". This material has a density of about 18 lbs/ft^3 and a thermal conductivity of .025 Btu/hr-ft^2-F^o/ft. The surface texture of this fine-grain material was smooth enough not to produce boundary layer effects due to changes in surface roughness near the gages.

Because it was necessary to know the exact mass of each calorimeter gage, it was decided to weigh each disk prior to assembly. This dictated that the gages be mounted flush with the plate surface initially rather than making them flush after assembly by machining the entire surface. The latter procedure would have required that the gages be weighed after disassembly. The method devised for flush-mounting each gage and for the final assembly is described below.

The 1/4-in. holes in the copper sheet were drilled undersize and then finished with an end mill tool while the sheet was held clamped between two aluminum plates. This method produced holes without burrs or dents which required no further finishing. The drilled copper sheet was then clamped face down on a rigid jig plate and the gages with wires attached were positioned at the center of each hole. A special spring-loaded jig assembly (see Fig. 2.7) was used to hold each gage firmly against the jig plate. An outer clamping ring held the copper sheet against the jig plate around each gage. The pack-in-place epoxy material was then tamped into each ring-shaped gap from above and cured in an oven. The clamping jigs were then removed and a cylindrical piece of SH foam (see Fig. 2.6) was bonded in place at the back

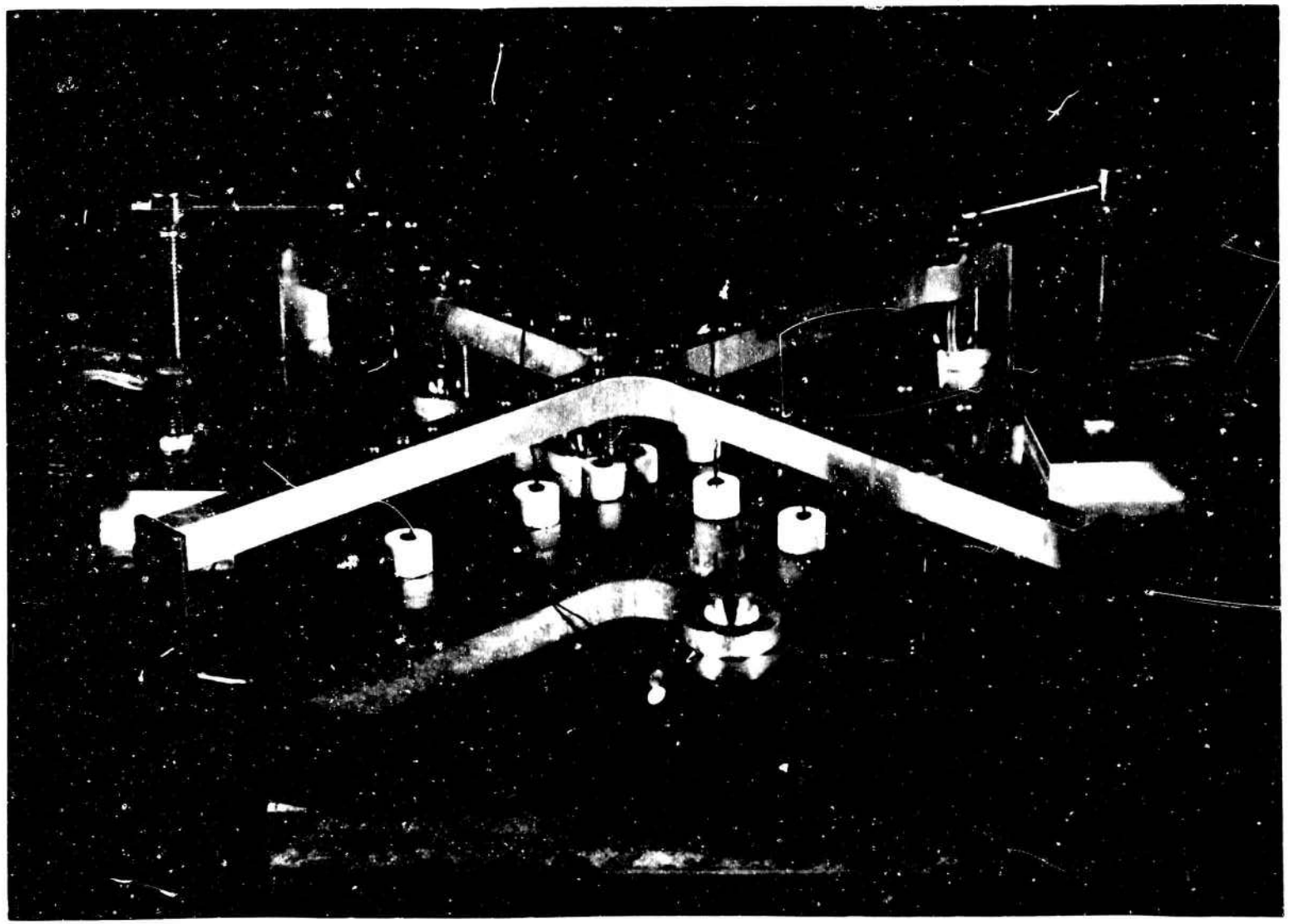

Figure 2.7. Mounting jig for heat transfer gages showing various stages of assembly.

of each gage using "Eccobond 106". These pieces served to reinforce the gages during the final assembly while maintaining the continuity of the back-up insulation layer. The final step was the bonding of the plate to the 1-in. SH foam sheet with the required holes cut to accomodate the gage reinforcing pieces. A slight bowing due to excessive shrinkage of the foam during curing of the bond material was corrected by bonding the rear surface of the foam to a 1/4-in. thick aluminum plate.

Before final assembly, eight pressure taps were drilled in a symmetrical pattern around the center of the copper plate to provide a check on the alignment of the plate in the flow.

A heater was designed which could be held against the surface of the test plate and then removed suddenly when the surface reached the desired temperature. This heater consisted of a circular, buried-element, electric heating pad, 12 in. in diameter and 1/16 in. thick, bonded to a backing sheet of flexible silicone rubber foam "Eccofoam SR", 1/4 in. thick, and an insulating layer of "Eccofoam SH", 1/2 in. thick. The heating pad, manufactured by Watlow Electric Company of California, was made of glass-cloth reinforced silicone rubber. The heater assembly was mounted on the end of a pivoted arm so that it could be removed quickly from the vicinity of the plate. Another pivoted arm was used to deflect the jet stream until after the heater was removed.

The output of each thermocouple was recorded directly on a Model 906C Honeywell "Visicorder" oscillograph. The thermocouple cold reference junction was maintained at 32°F in an ice bath, and the response of the oscillograph galvanometers was calibrated using a separate thermocouple junction at the same point in the circuit at which the gages were finally attached. Calibration was made at 212°F and room temperature (70°F) by comparison with the response of a Thermo Electric "Mini Mite" portable pyrometer.

Two views of the complete heat transfer apparatus are shown in Fig. 2.8.

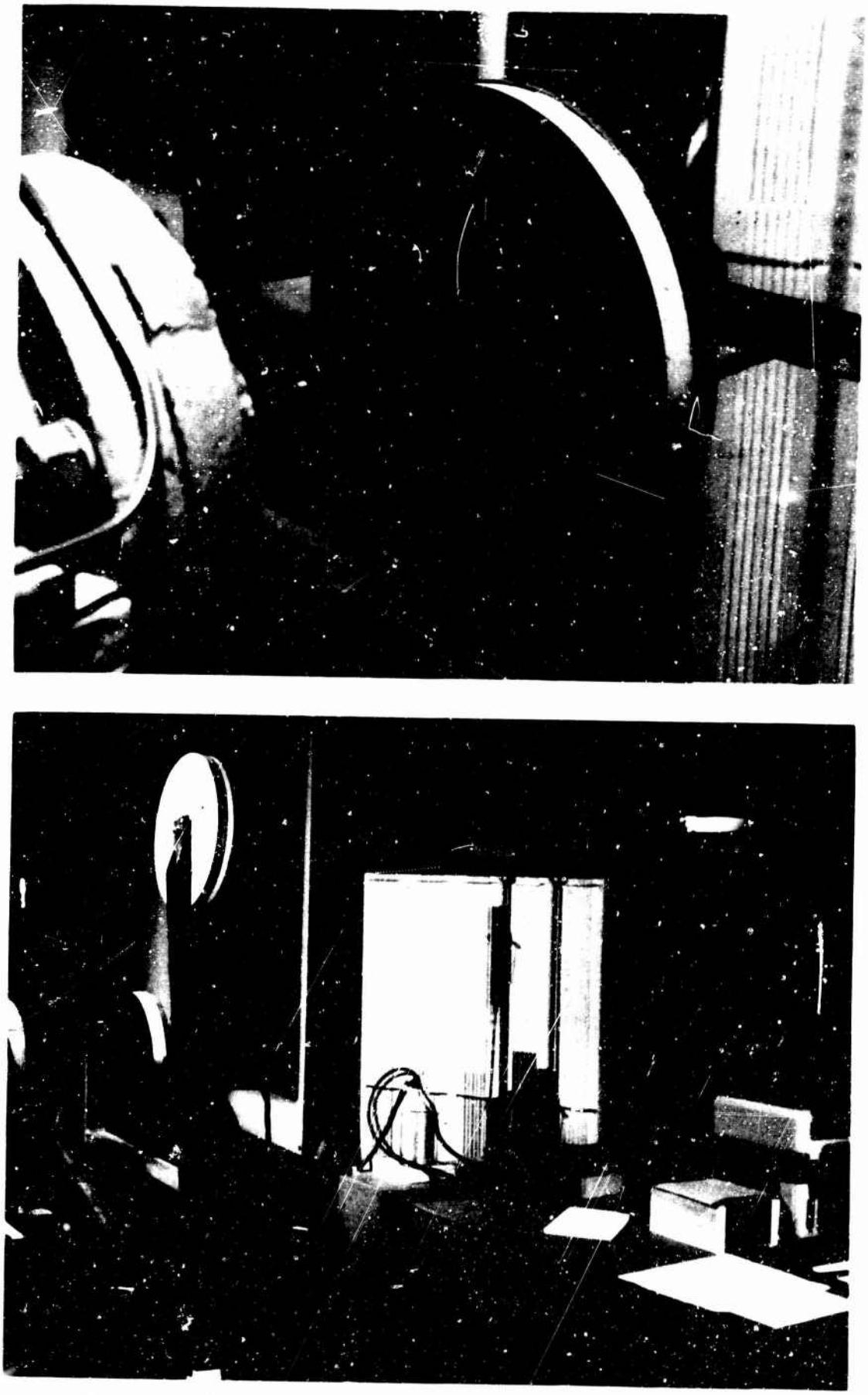

Figure 2.8. Views of the heat transfer apparatus.

Calibration of heat transfer gages. Prior to assembly of the heat transfer plate, the desired response of the gages was verified by tests using a radiant heat input to produce a predictable gage response. For this purpose, a single gage assembly was made and mounted exactly as were the 14 gages in the plate. The copper sheet surrounding the gage was 2 in.square. Another gage,identical but unmounted, was also prepared in order to measure the heat input. This gage was blackened with lamp-black to insure an emissivity of unity. It was held only by its thermocouple leads and exposed to the beam of three infrared heat lamps.

It was assumed that the response of the calibration gage was governed by the following differential equation:

$$mc_p \frac{dT_w}{dt} = \dot{q}_{in} - hA_c(T_w - T_0) - \sigma\epsilon A_r(T_w^4 - T_0^4) \qquad (2.1)$$

where

m = mass of the gage disk = .060 gm
c_p = specific heat of copper
T_w = gage temperature
T_0 = ambient temperature
$\dot{q}_{in}$ = unknown heat flux input
h = convective heat transfer coefficient
A_c = area of gage subjected to convective cooling
A_r = area of gage subjected to radiative cooling
σ = Boltzmann constant
ϵ = emissivity of gage (= 1 for lampblack coating)

Using Eq. (2.1) and the measured response dT/dt, the values of $\dot{q}_{in}$ and h were determined. It was found that the reradiation heat transfer was negligible.

Having obtained the values of $\dot{q}_{in}$ and h in the radiant test environment, the mounted gage was also blackened and mounted at the same point in this environment. The measured response of

the mounted gage (temperature change as a function of time) was found to agree with that computed using Eq. (2.1) within 5 percent after 2 seconds.

In order to estimate the magnitude of differences among the 14 gages in the plate without having to calibrate each one separately, three additional gages were made in the same way and tested in the heat lamp beam. Each gage was heated by the lamps repeatedly and the response curves were recorded. It was found that the initial slopes of these response curves for each gage were repeatable within 6, 8, and 12 percent. After 10 seconds, the magnitudes of the responses were repeatable within 6, 4, and 3 percent. A comparison of the average initial slope of all three gages showed a spread of 11 percent. It was assumed that a similar degree of accuracy would be expected for other gages constructed in this manner.

Procedure for making heat transfer measurements. The impingement heat transfer measurements were made using the following procedure. The heating pad was first brought to a temperature slightly below its maximum operating temperature (450°F) and then applied to the surface of the test plate. The air jet was started and stabilized at the desired exit velocity. When the plate temperature approached the desired value, usually about 225°F, the recorder paper was started and the jet deflector was put in place. The heating pad was lifted away from the plate and the jet deflector removed about one or two seconds later. The temperature-time response was then recorded. Since only three galvonometer channels were available on the recorder, seven runs were required to cover all 14 gages for a given impingement flow condition with the center gage repeated for reference on each run.

3. EXPERIMENTAL RESULTS - VELOCITY MEASUREMENTS

Free Jet Measurements.

The results of surveys of the free jet used in this study are presented below. Most of the detailed hot film surveys of turbulent phenomena were carried out at jet velocities of 200 ft/sec. This resulted in an initial jet Reynolds number Re_d of 5.2×10^4. Although, as will be seen, certain spot checks at other velocities showed slight variations of pertinent parameters from the values measured at 200 ft/sec, the Reynolds number was sufficiently high for the surveys made so that the general character of the turbulence did not change with further increase in velocity. Complete jet surveys were made at axial stations z/d_N of 10, 20, 30, 40, and 50. Certain other local measurements were made so as to have complete data on certain variables although no detailed surveys were made at these stations. Only certain typical portions of the total amount of data obtained will be presented below.

Mean quantities. In the process of surveying with hot film anemometers the free jet reported in [1], certain mean flow quantities were measured. It is instructive to compare these mean flow measurements with those reported in [1] which were obtained with a Pitot tube.

Figure 3.1 is a plot of the decay of the mean axial velocity on the centerline of the free jet as a function of distance from the nozzle exit. It may be seen that the agreement between hot film and Pitot tube measurements of jet centerline velocity is excellent. Figure 3.2 shows the results of a typical radial survey of axial velocity. Over the central portion of the jet the agreement between hot film and Pitot tube techniques is excellent. There is, however, a tendency for the Pitot tube to underestimate the velocities at the outer edges of the jet.

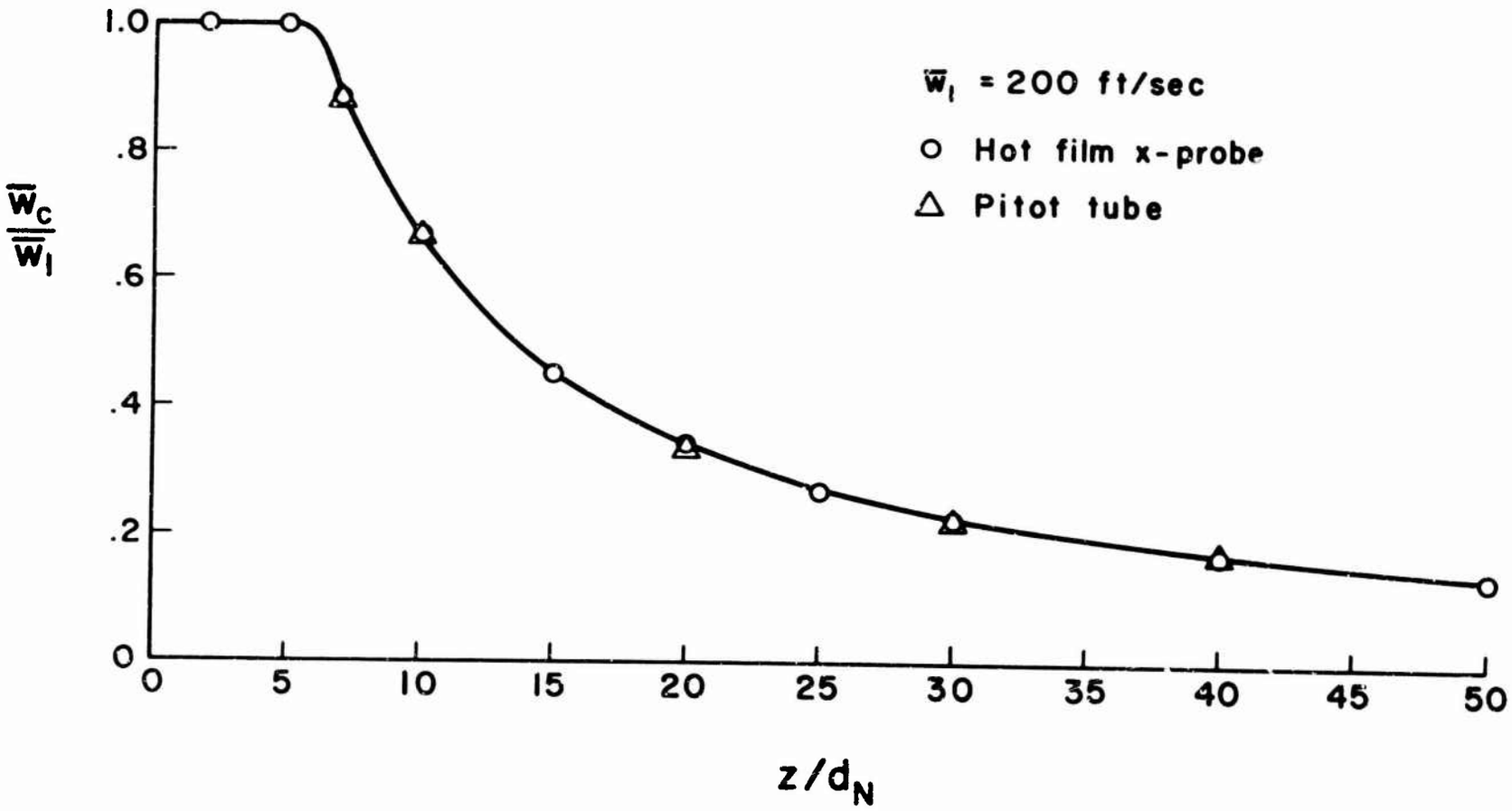

Figure 3.1. Axial decay of jet centerline velocity measured with a Pitot tube and a hot film x-probe.

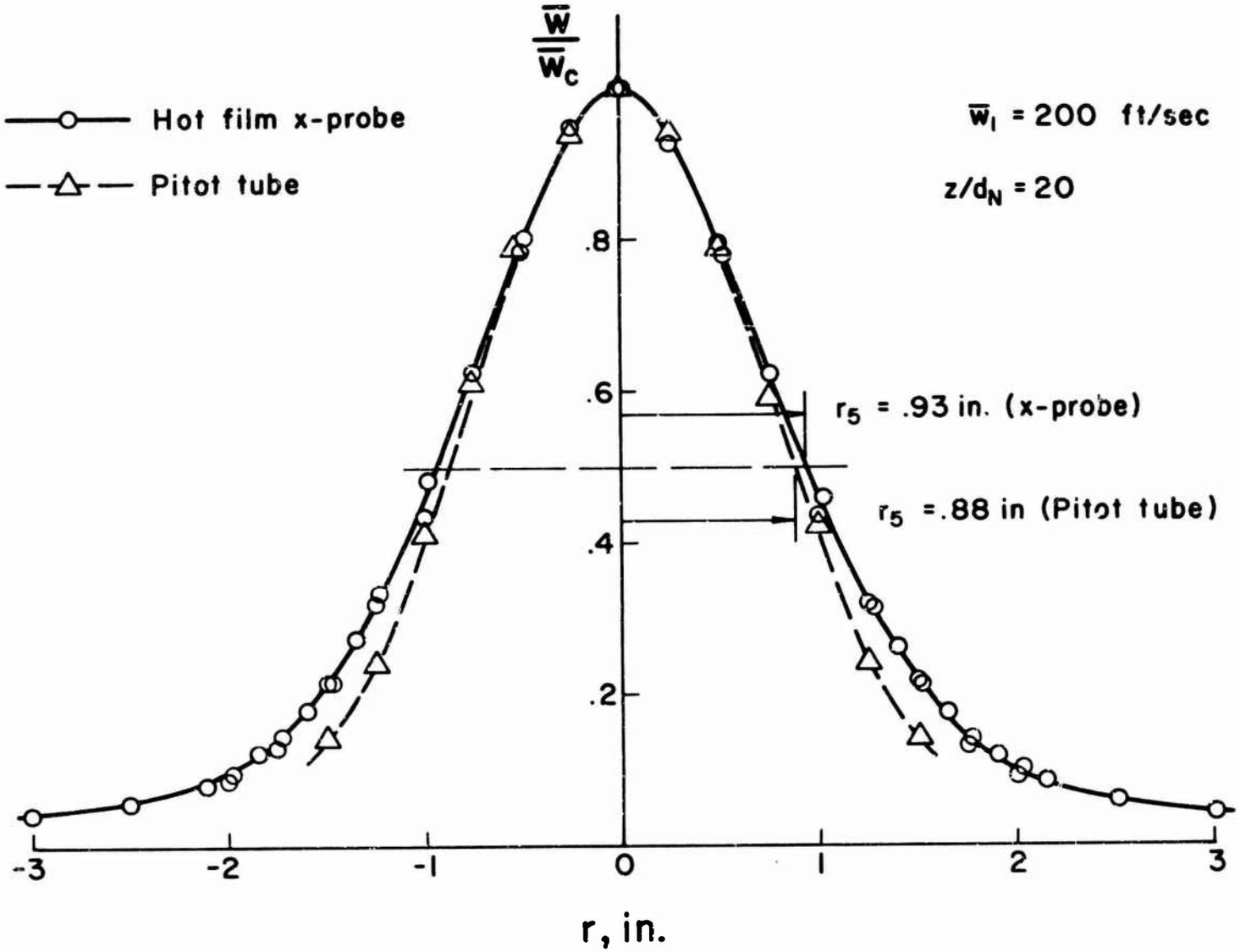

Figure 3.2. Typical free jet velocity profile.

This results, as may be seen, in there being two measured half-breadths at a point in a given jet. The difference is not large (only some 5 percent). As may be seen from Fig. 3.3, which is a plot of jet half-breadth as a function of distance from the nozzle, while, typically, a Pitot tube defines a narrower half-breadth than does a hot film probe, the half-breadths measured in the present studies sometimes fell outside the breadth previously defined by Pitot measurement. Such behavior is, in all probability, indicative of the lack of repeatability of free jet measurements in the same laboratory from one year to the next as a result of subtle changes in the position and shape of nearby laboratory equipment related to the measurements. Finally, and for comparative purposes, the two profiles shown in Fig. 3.2 are replotted in Fig. 3.4 in the nondimensional form that has been used throughout our studies of jet impingement. For comparison, the commonly used Gaussian velocity profile has been included in this figure.

In the remainder of this report, the basic reference length r_5 that is used is that obtained from the hot film measurements.

Turbulent correlations. Figure 3.5 is a plot of the behavior of the root-mean-square turbulent velocity fluctuations in the radial and axial directions on the centerline of the free jet. As mentioned previously, most of the data shown were taken at 200 ft/sec, but some data taken at 300 and 500 ft/sec are also included. This figure also shows the results of similar measurements obtained by Corrsin [23], Corrsin and Uberoi [24], Lawrence and Stickney [25], and Gibson [26]. It is seen that the data are, on the whole, in excellent agreement with the results of previous investigations except for the original low Reynolds number data obtained by Corrsin. An interesting point may be made in connection with the data presented in Fig. 3.5. It was observed during these studies that the region just downstream of the core, i.e., the region $10 < z/d_N < 25$, was particularly sensitive, in regard to turbulence levels, to changes in nozzle velocity. Indeed, the

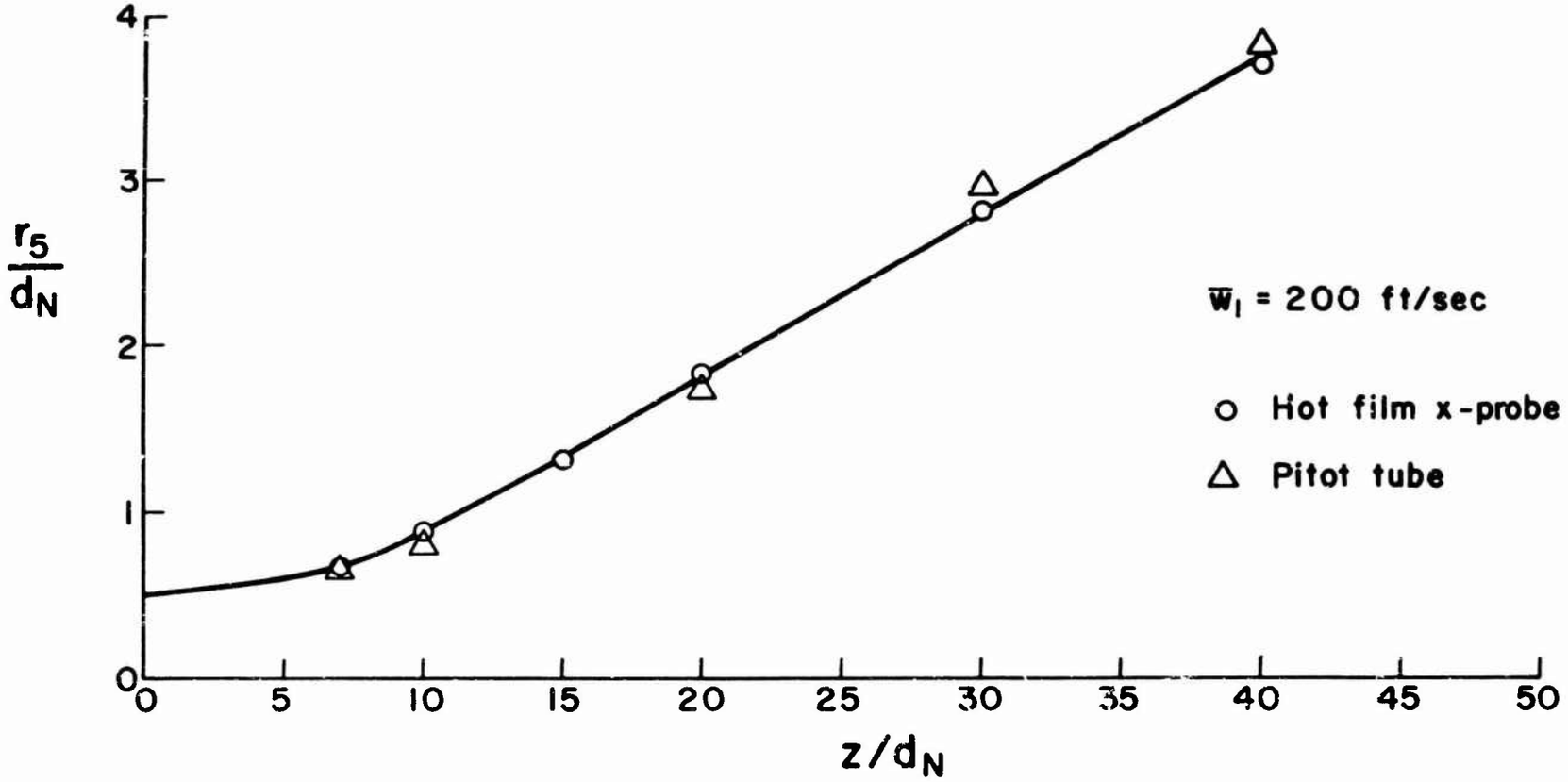

Figure 3.3. Free jet spread as a function of axial distance.

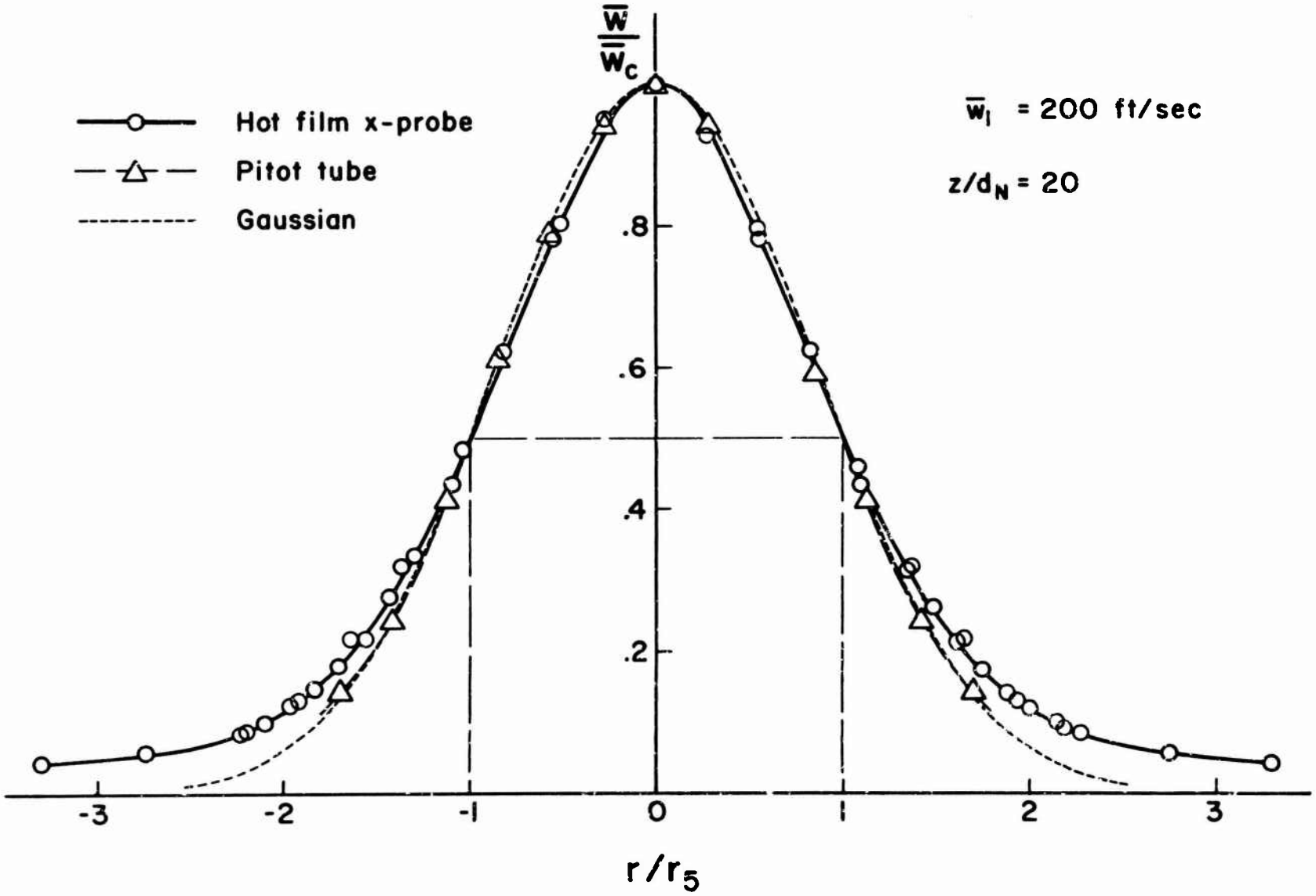

Figure 3.4. Normalized free jet velocity profile.

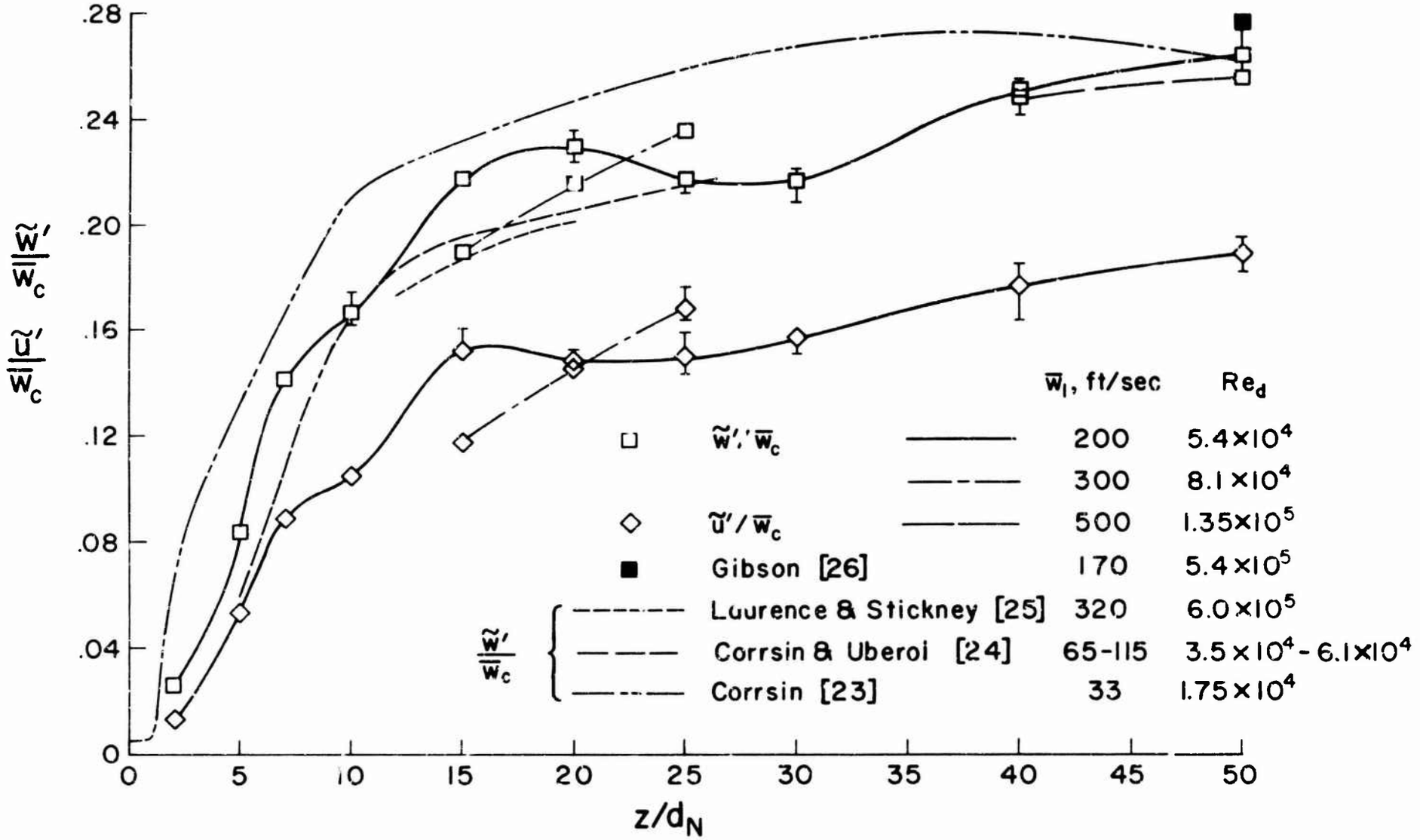

Figure 3.5. Free jet turbulence measured on the centerline.

small humps observed in the turbulent intensity curves in this region at 200 ft/sec (which have not been observed by other investigators) may have been due to a very slight flapping of the jet being studied.

The one-dimensional spectra of the centerline $\overline{w'^2}$ and $\overline{u'^2}$ just presented were obtained at the five reference stations z/d_N = 10, 20, 30, 40, and 50.* The $\overline{w'^2}$ spectra for z/d_N = 20, 30, 40, and 50 are plotted in Fig. 3.6, while the spectrum for z/d_N = 10 is shown in Fig. 3.7. Careful comparison of these two figures indicates that turbulent similarity has been achieved at approximately z/d_N = 20. At z/d_N = 10, although from previous measurements [1] it was established that similarity of the mean velocity profiles had been achieved, it is obvious from a comparison of the data in Figs. 3.6 and 3.7 that turbulent similarity is not yet achieved. The $\overline{w'^2}$ spectra obtained in the developed free jet agree well at the lower wave numbers with a similar spectrum obtained by Gibson [26]. As might be expected, Gibson's data, having been obtained at an order-of-magnitude higher Reynolds number, do not indicate as rapid a fall-off with increasing wave number as do the present data. Also as expected, Gibson's spectrum exhibits a larger region in which the $-5/3$ power fall-off typical of high Reynolds number turbulent spectra is adhered to.

Radial velocity spectra are shown in Fig 3.8. Again it appears that the spectrum for z/d_N = 10 has not yet achieved similarity. Indeed, the general similarity of spectra for $z/d_N > 10$ is not so pronounced as in the case of the $\overline{w'^2}$ spectra.

---

* The spectra are presented in the form of normalized power spectra based on the nondimensional frequency $r_5 k$. Thus

$$F_{\overline{w'^2}}(r_5 k) = \frac{1}{\overline{w'^2}} \frac{d\overline{w'^2}}{d(r_5 k)} \qquad \text{and} \qquad \int_0^\infty F_{\overline{w'^2}}\, d(r_5 k) = 1$$

where $k = 2\pi f / w_c$

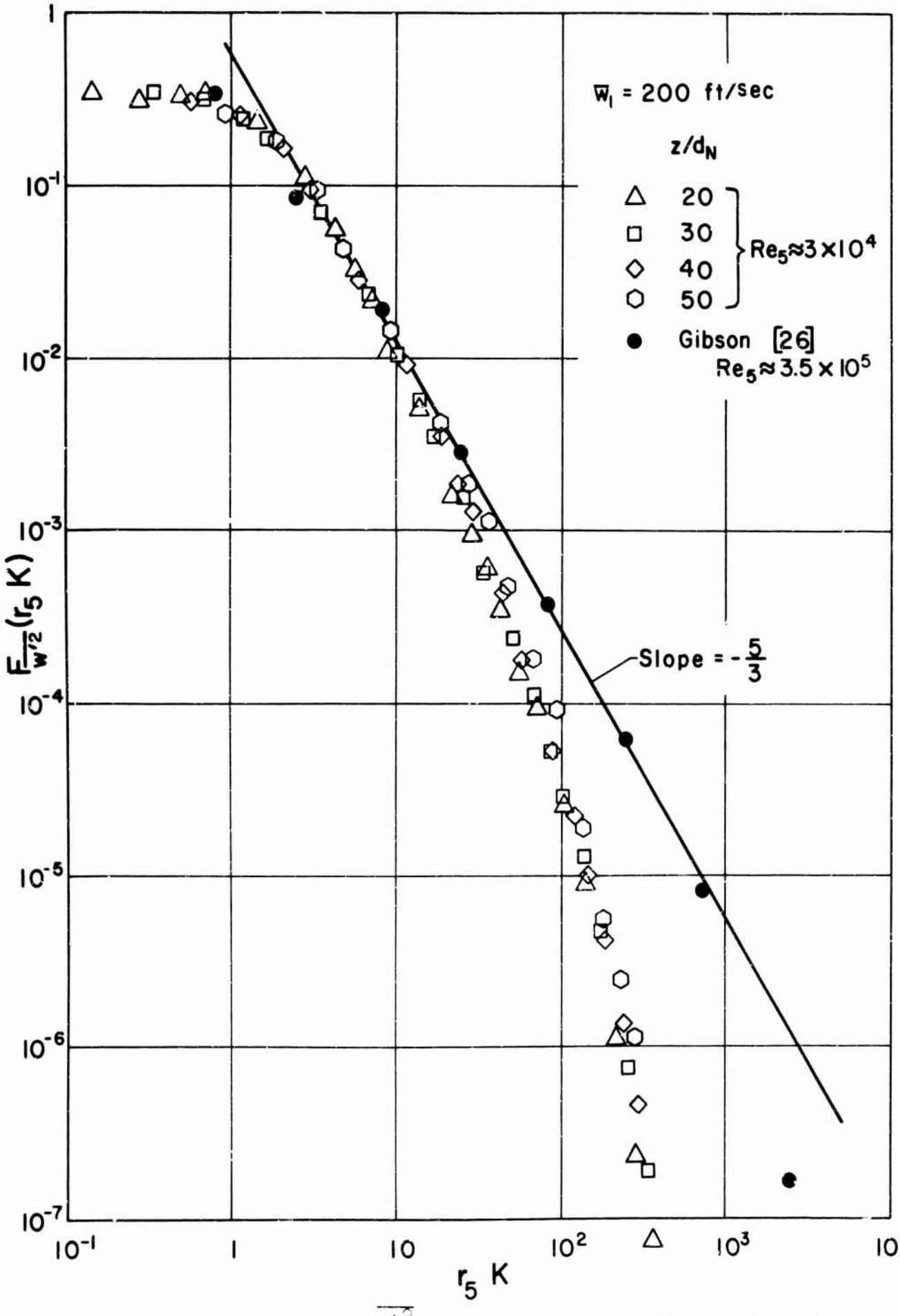

Figure 3.6. Spectra of $\overline{w'^2}$ measured on centerline of free jet.

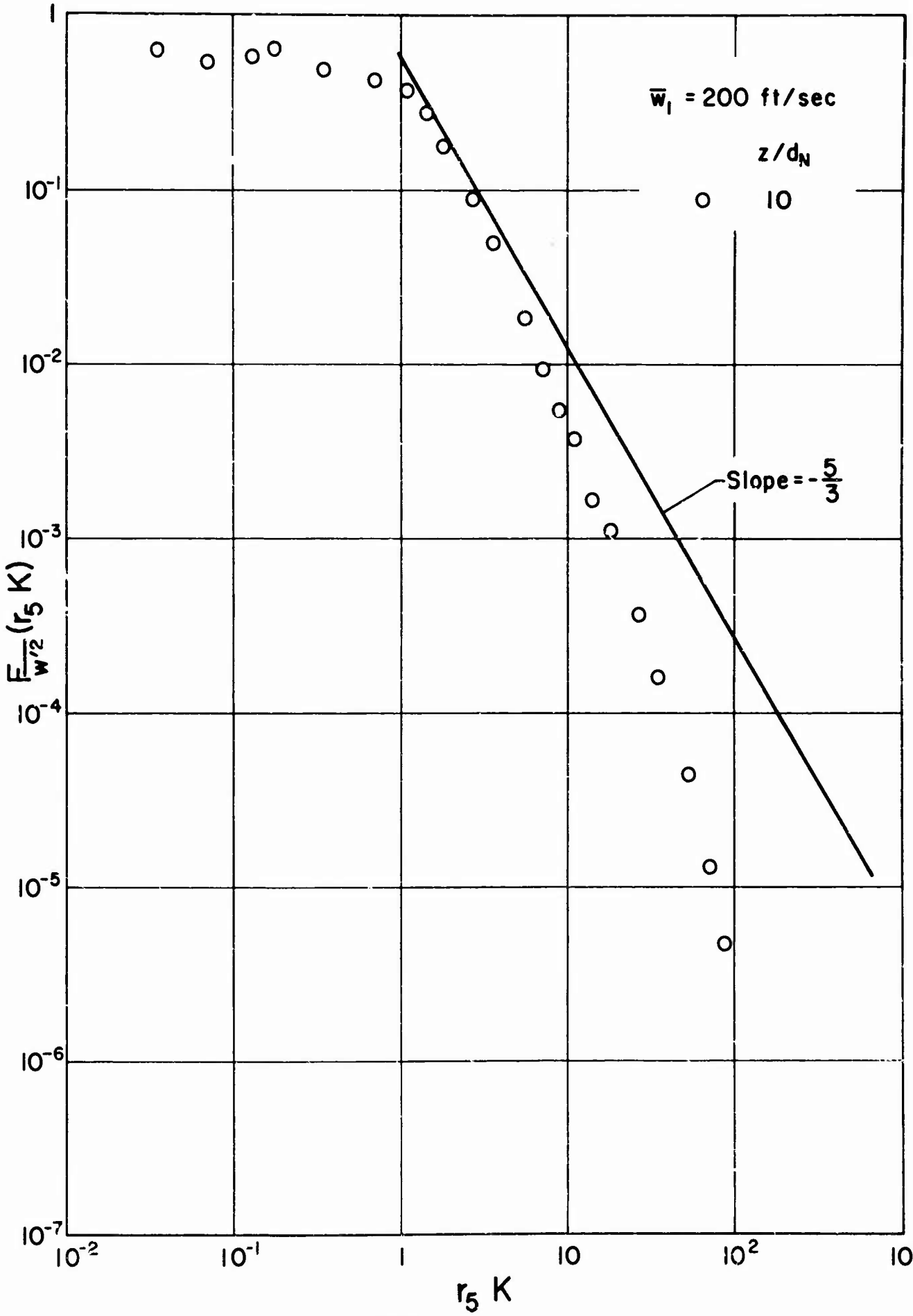

Figure 3.7. Spectra of $\overline{w'^2}$ measured on centerline of free jet.

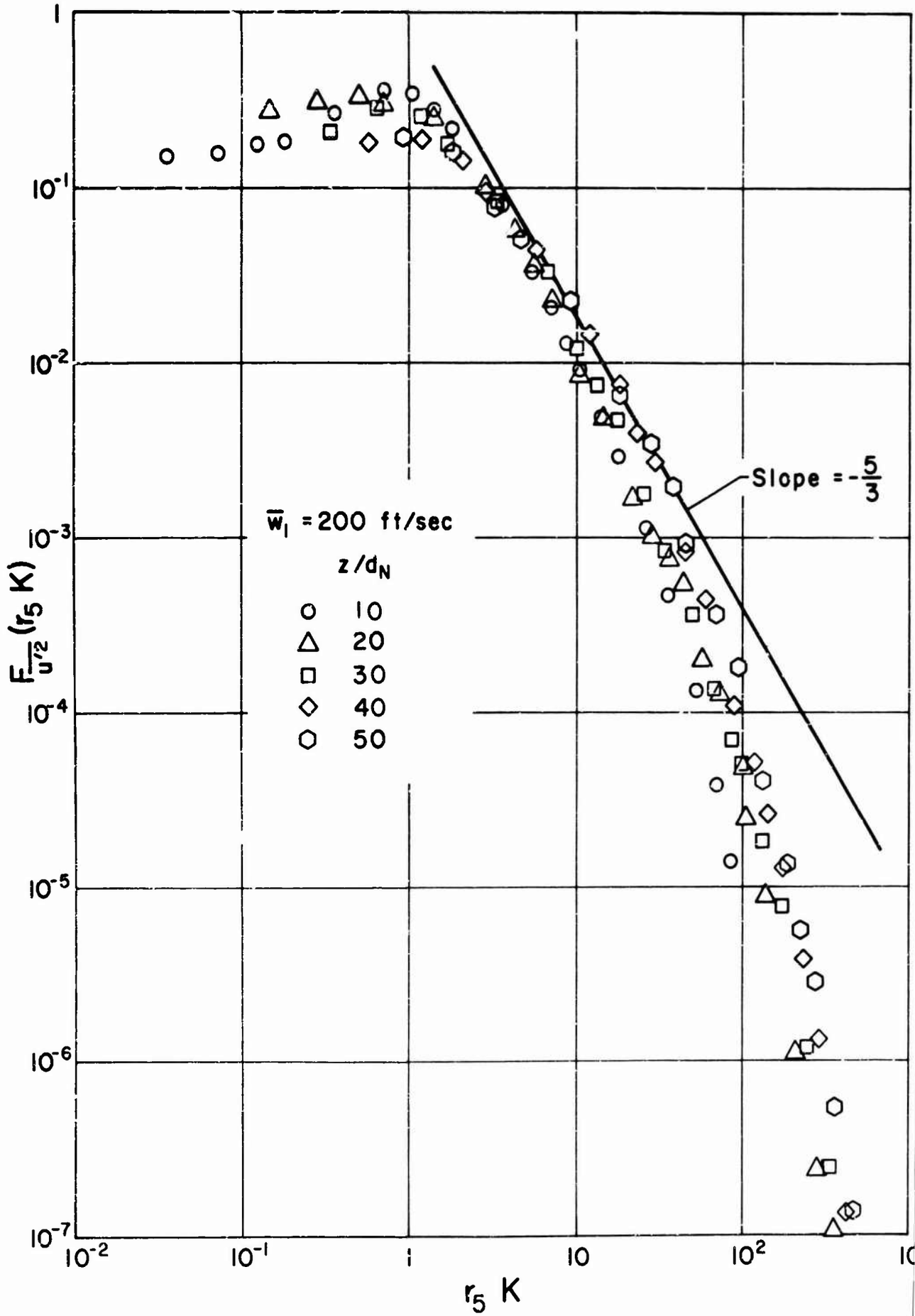

Figure 3.8. Spectra of $\overline{u'^2}$ measured on centerline of free jet.

Some of this lag is due to experimental error, but a portion of the lag is probably due to the longer time taken for the $\overline{u'^2}$ spectra to achieve complete similarity - a result that is expected from theoretical considerations.

From the $\overline{w'^2}$ spectra just presented, the integral scale L_z of the turbulence on the centerline of a developed free jet may be evaluated from the relation

$$L_z = \frac{\pi}{2} F_{\overline{w'^2}}(0) \cdot r_5 \qquad (3.1)$$

where $F_{\overline{w'^2}}(0)$ is the zero intercept of the nondimensional spectrum function $F_{\overline{w'^2}}(r_5 k)$. Estimating the zero intercepts of the power spectra shown in Fig. 3.6 to be approximately 0.4 results in an integral scale in the developed region of the free jet that is roughly 63 percent of the local half-breadth of the jet.

In Figs. 3.9 and 3.10, distributions of the root-mean-square values of $\overline{u'^2}$ and $\overline{w'^2}$ that are typical of a developed jet are plotted. In Fig. 3.9 $\tilde{u}'$ and $\tilde{w}'$ are made dimensionless using the local mean velocity $\bar{w}$, while in Fig. 3.10 the centerline velocity $\bar{w}_c$ is used. It will be noted in Fig. 3.10 that a small dip appears in the magnitude of $\tilde{u}'$ and $\tilde{w}'$ on the axis of the jet. This dip represents the last vestige of the effect of the core region of the jet, since, in the core, the maximum turbulent velocities are found away from the axis. The disappearance of the dip in the $\tilde{u}'$ and $\tilde{w}'$ distributions may be taken as another indication of the jet having become fully developed at $z/d_N \approx 20$ as has previously been noted by Corrsin [23].

In Figs. 3.11 and 3.12 a distribution of the turbulent shear correlation $\overline{u'w'}$ across the jet that is typical of the developed region is shown. As before, two methods of making this stress correlation nondimensional are depicted. In Fig. 3.12, our measurements are compared with those of Corrsin [23] and the agreement is seen to be excellent.

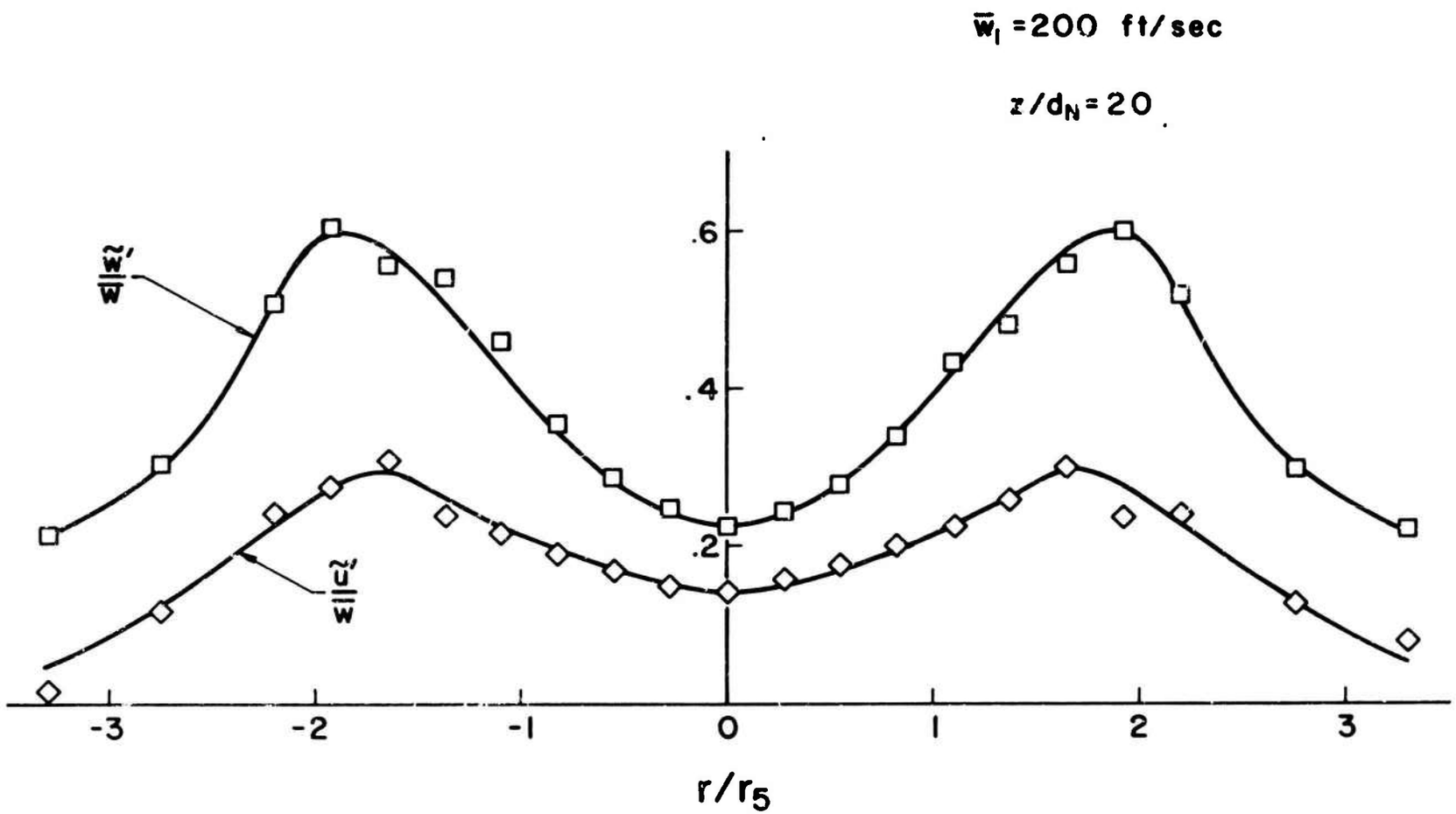

Figure 3.9. Radial distribution of rms turbulent velocity components in the free jet.

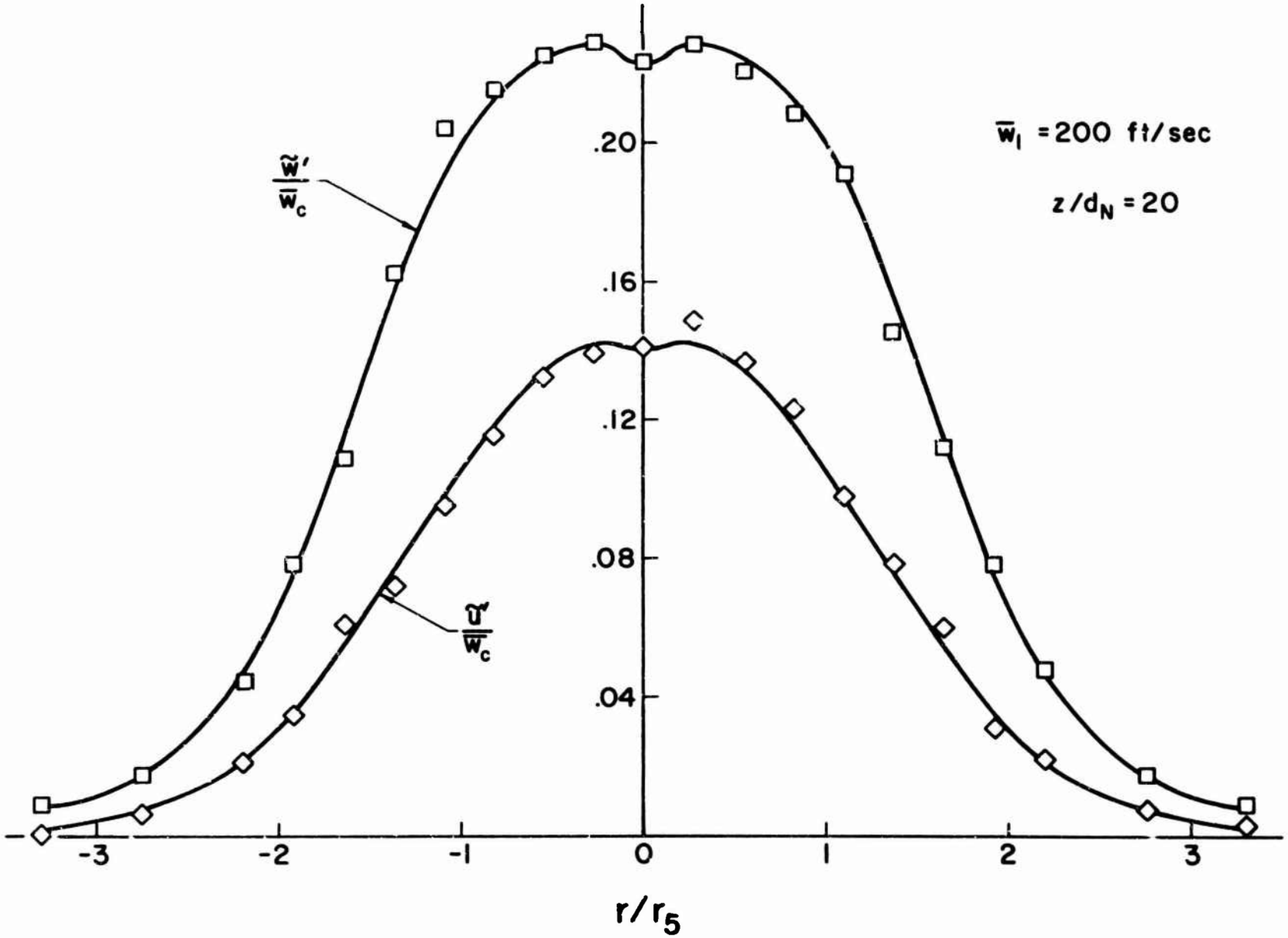

Figure 3.10. Radial distribution of rms turbulent velocity components in the free jet.

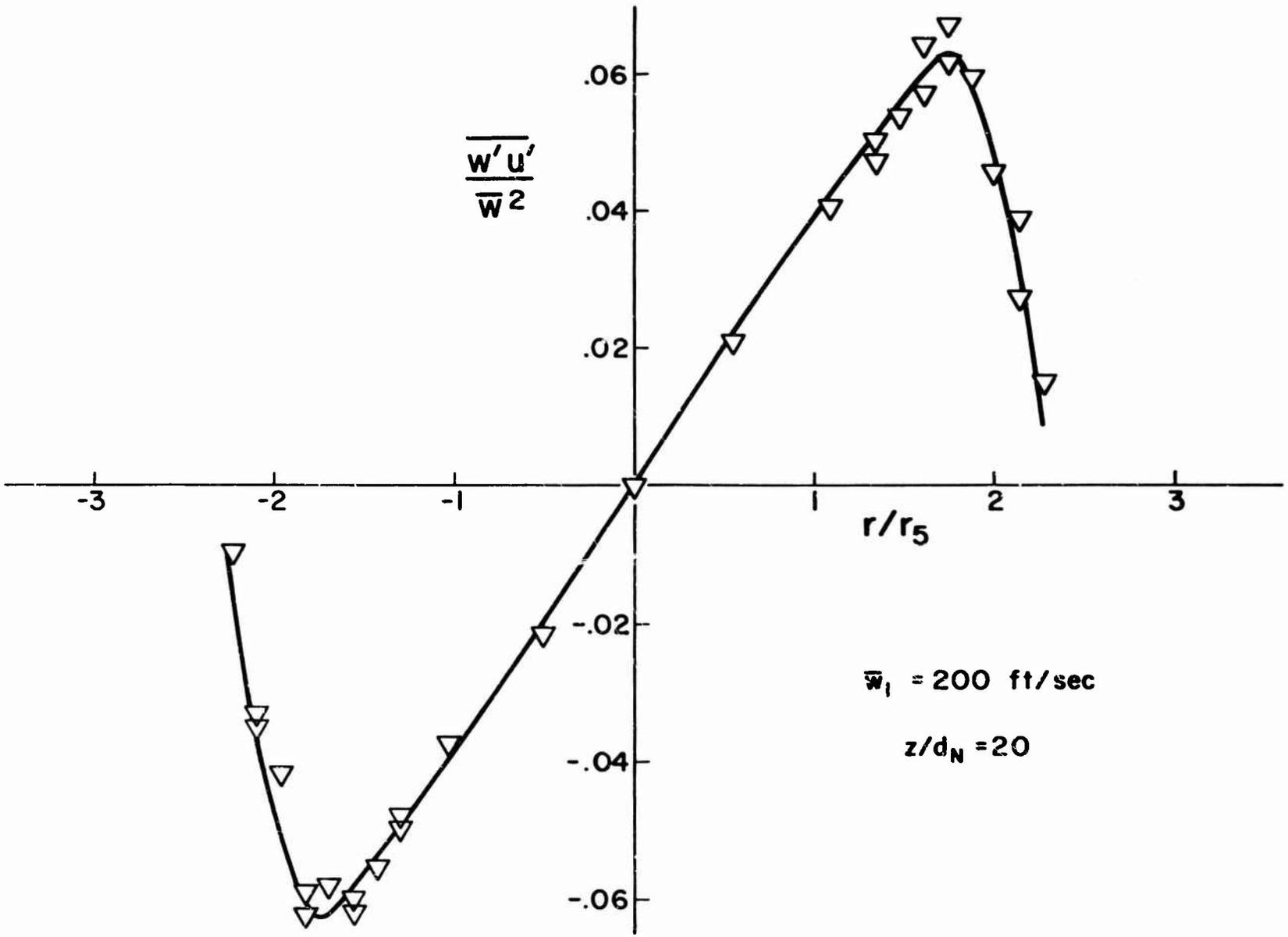

Figure 3.11. Radial distribution of turbulent shear correlation in the free jet.

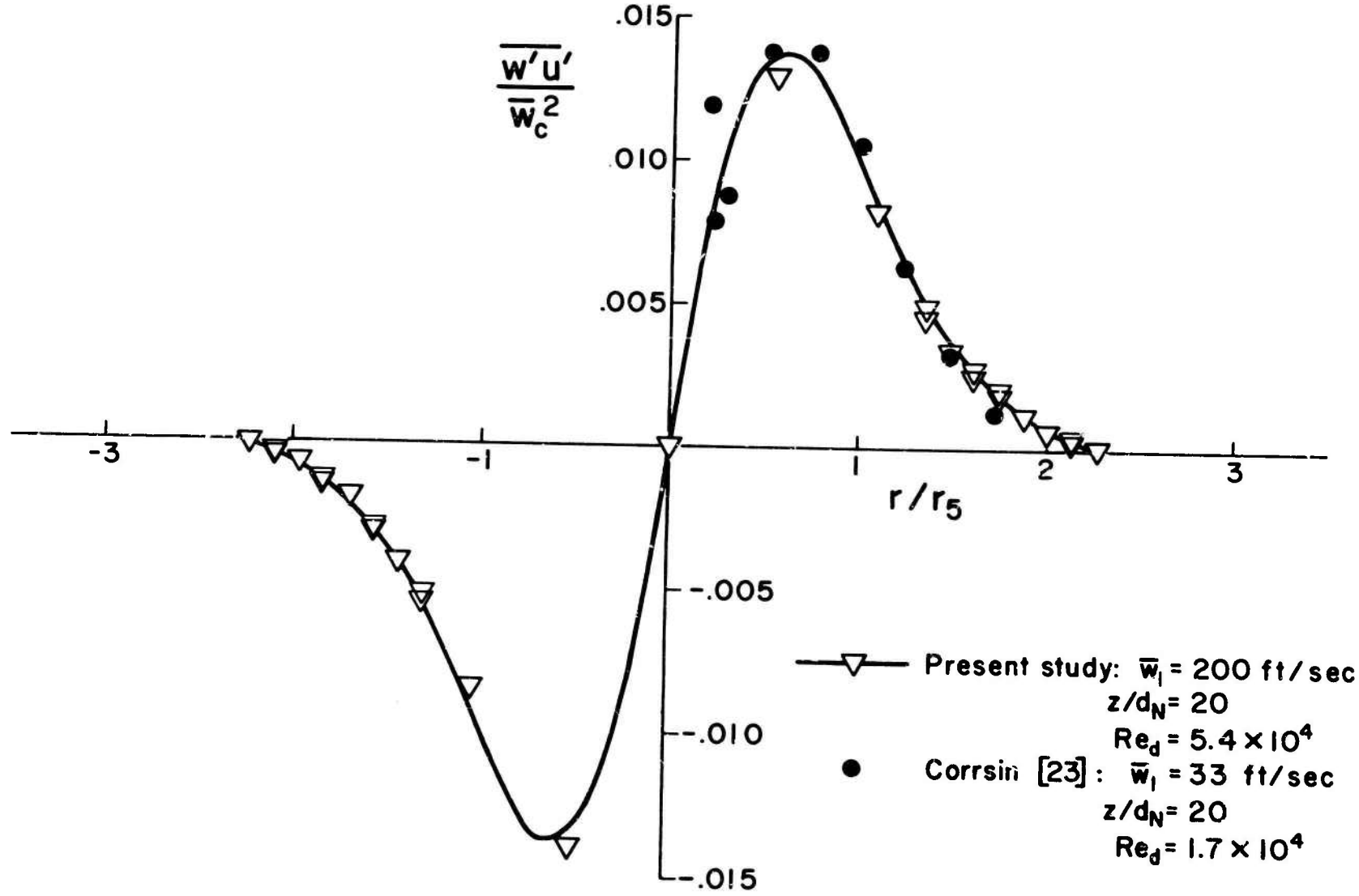

Figure 3.12. Radial distribution of turbulent shear correlation in the free jet.

At this point, it can be concluded on the basis of the measurements just presented, that the turbulent characteristics of the free jet used in this study agree well with turbulence measurements made in other free jets. In view of its well-behaved microstructure, it would appear that the heat transfer measurements that will be reported later should be typical of those that will be found in free jets whose Reynolds numbers are high enough for fully developed turbulent jets to be established.

Impinging Jet Measurements.

Before the present series of tests were run, it was anticipated that the interaction between the free jet and the surface upon which it impinged might be such as to cause the jet to flap significantly. If this occurred, not only would the turbulence level in the jet be grossly changed but the heat transfer and pressure distributions on the plate could no longer be properly related to the characteristics of the free jet in the plane of impingement. In order to check on the possibility of such flapping interactions, detailed measurements of the mean and fluctuating components of velocity just upstream of the impingement plate on the centerline of the jet were made for z/d_N = 10, 20, 30, 40, and 50. All surveys were made for a nozzle velocity of 200 ft/sec. These results are given in Figs. 3.13 through 3.17. The data are plotted both as a function of z/d_N and as a function of the distance upstream of the plate z' made nondimensional with the local free jet half-radius. It may be seen from an inspection of Figs. 3.13 through 3.17 that at all locations of the impingement plate in the jet the mean and turbulent velocities away from the plate approached the values measured in the free jet closely enough so as to indicate that no serious jet flapping existed. Near the core (z/d_N = 10) the upstream influence of the plate extends some two jet half-breadths which at this location is roughly two nozzle diameters. In the developed jet, the upstream influence becomes fixed at approximately 1.6 jet half-breadths.

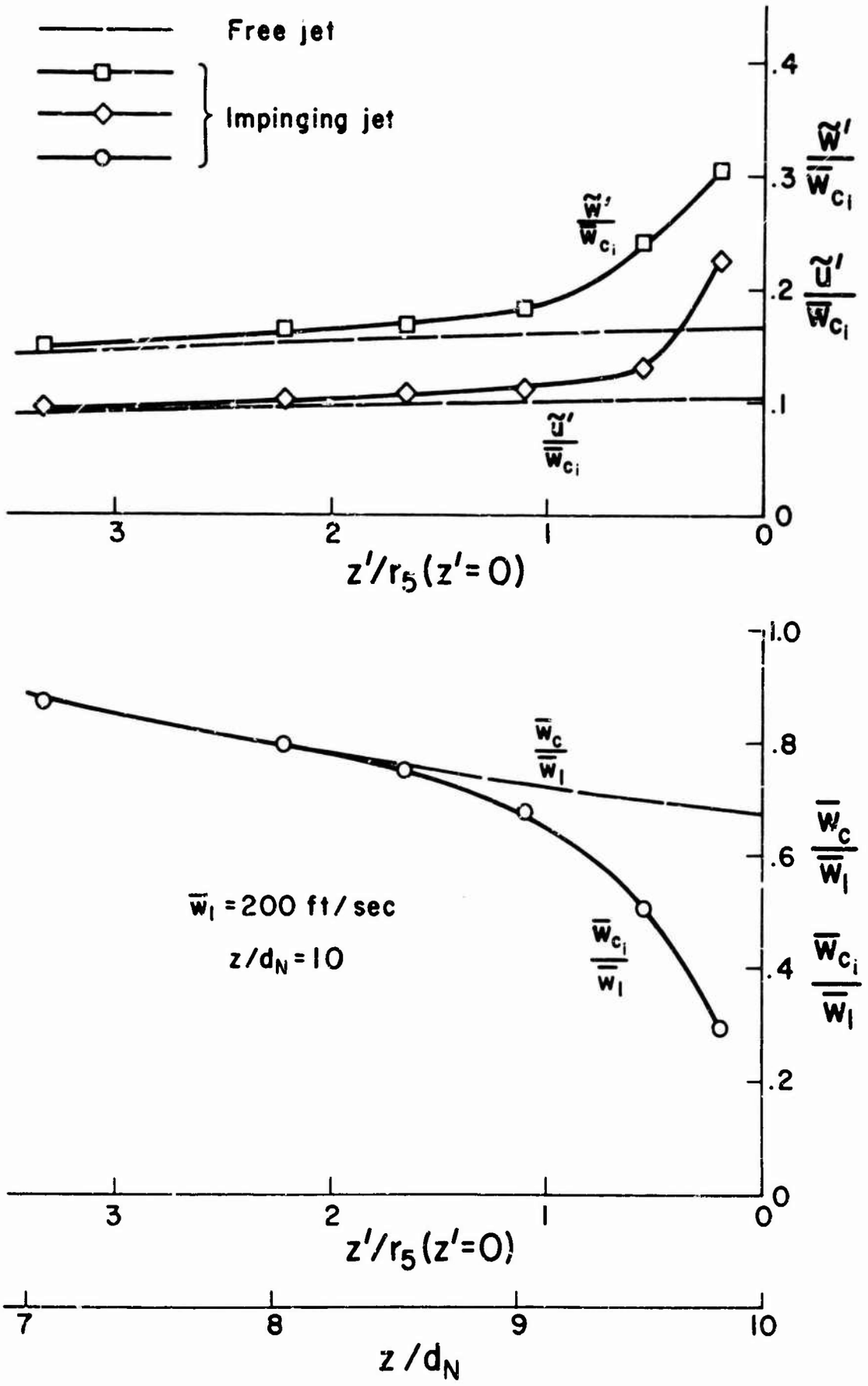

Figure 3.13. Mean and turbulent velocities measured on the centerline upstream of the impingement plate. $z/d_N = 10$

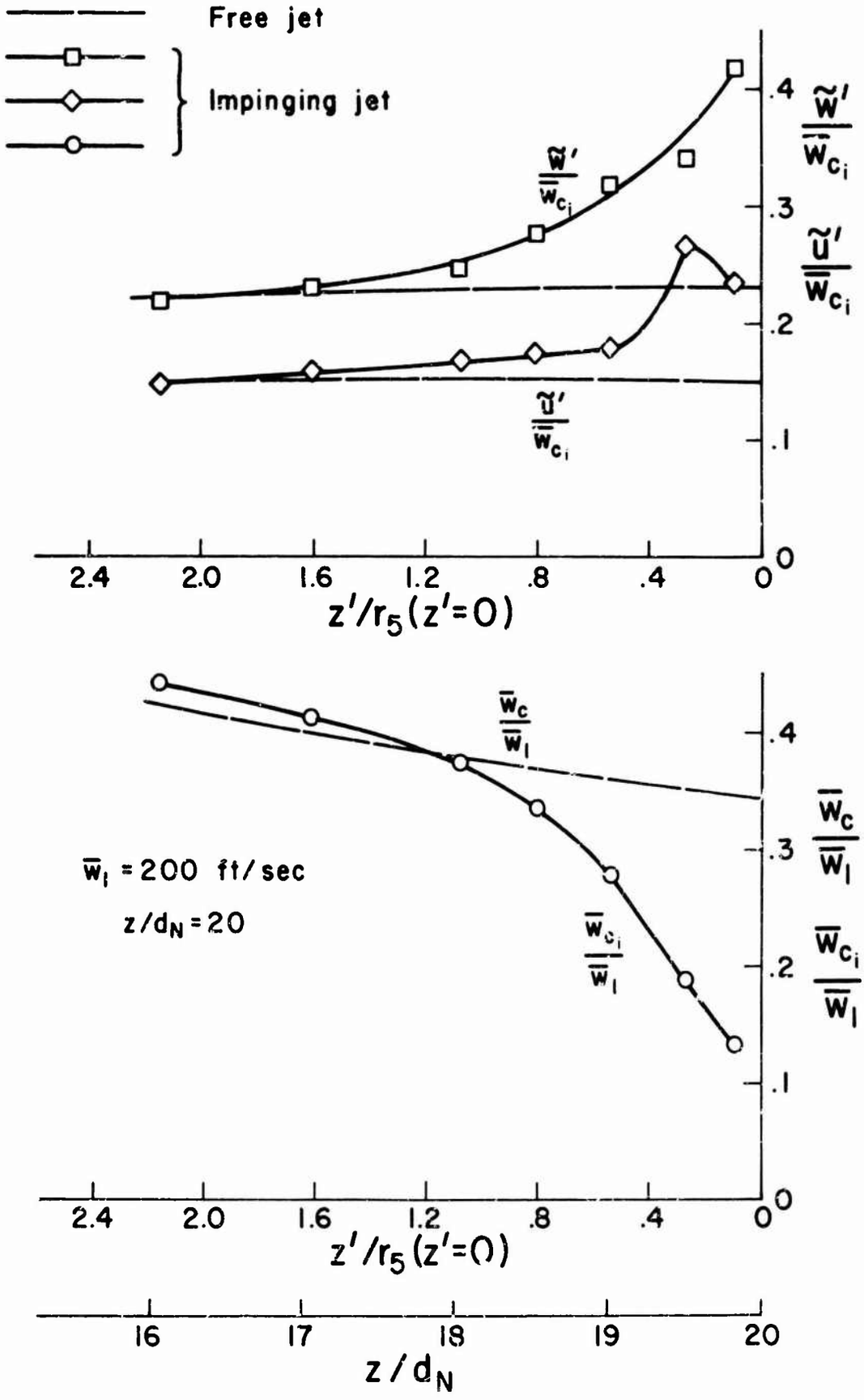

Figure 3.14. Mean and turbulent velocities measured on the centerline upstream of the impingement plate. z/d_N = 20

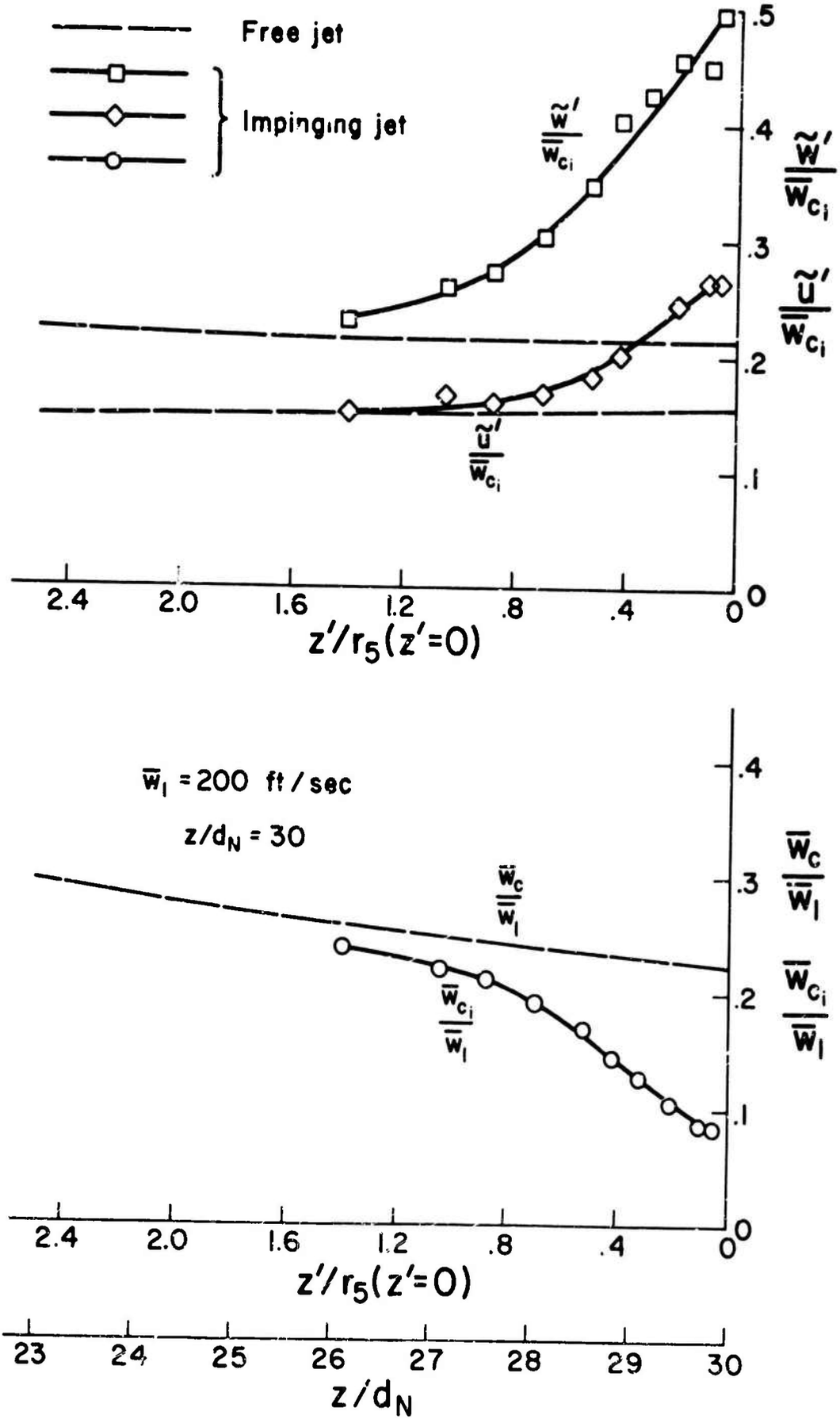

Figure 3.15. Mean and turbulent velocities measured on the centerline upstream of the impingement plate. $z/d_N = 30$

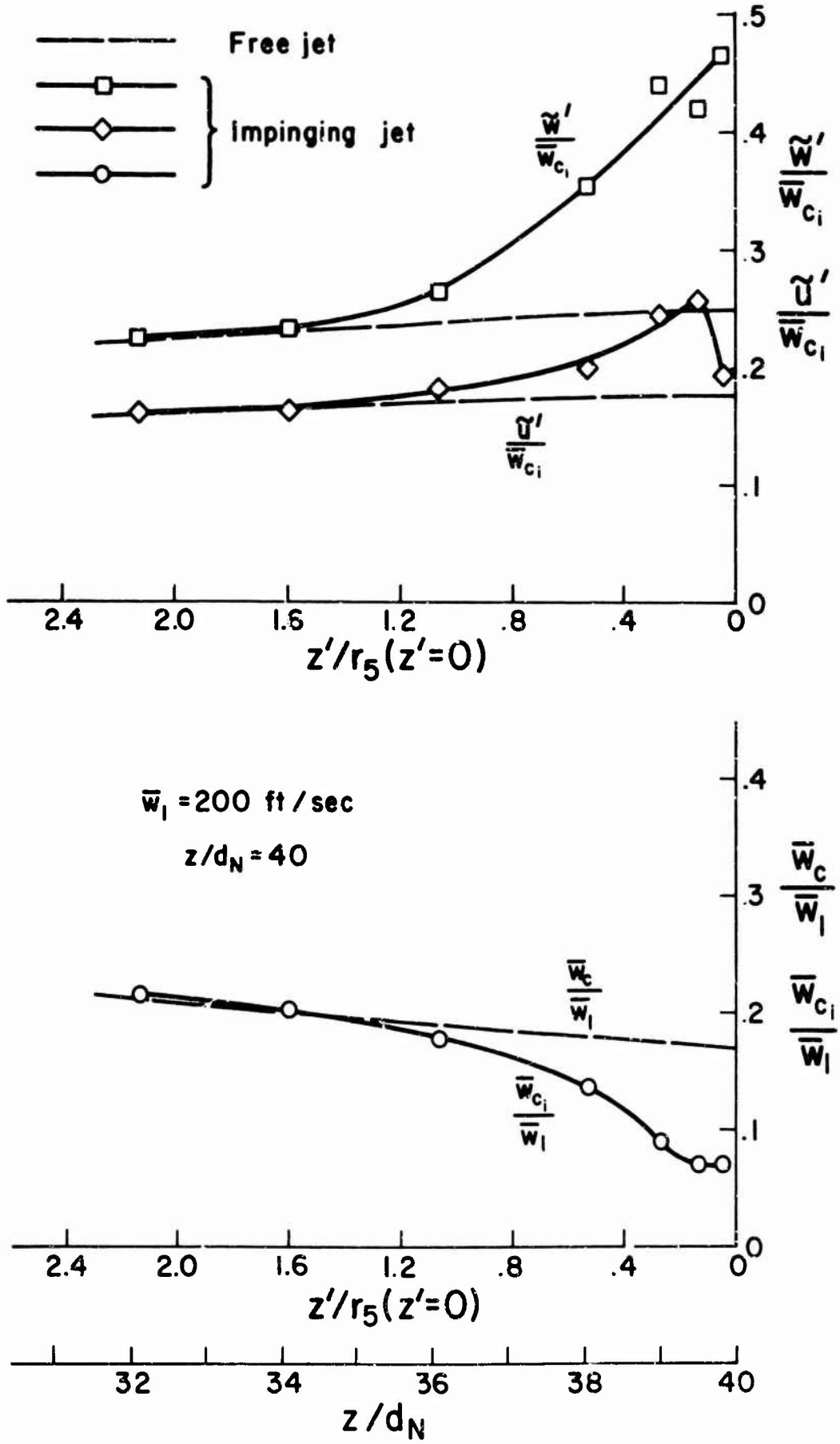

Figure 3.16. Mean and turbulent velocities measured on the centerline upstream of the impingement plate. $z/d_N = 40$.

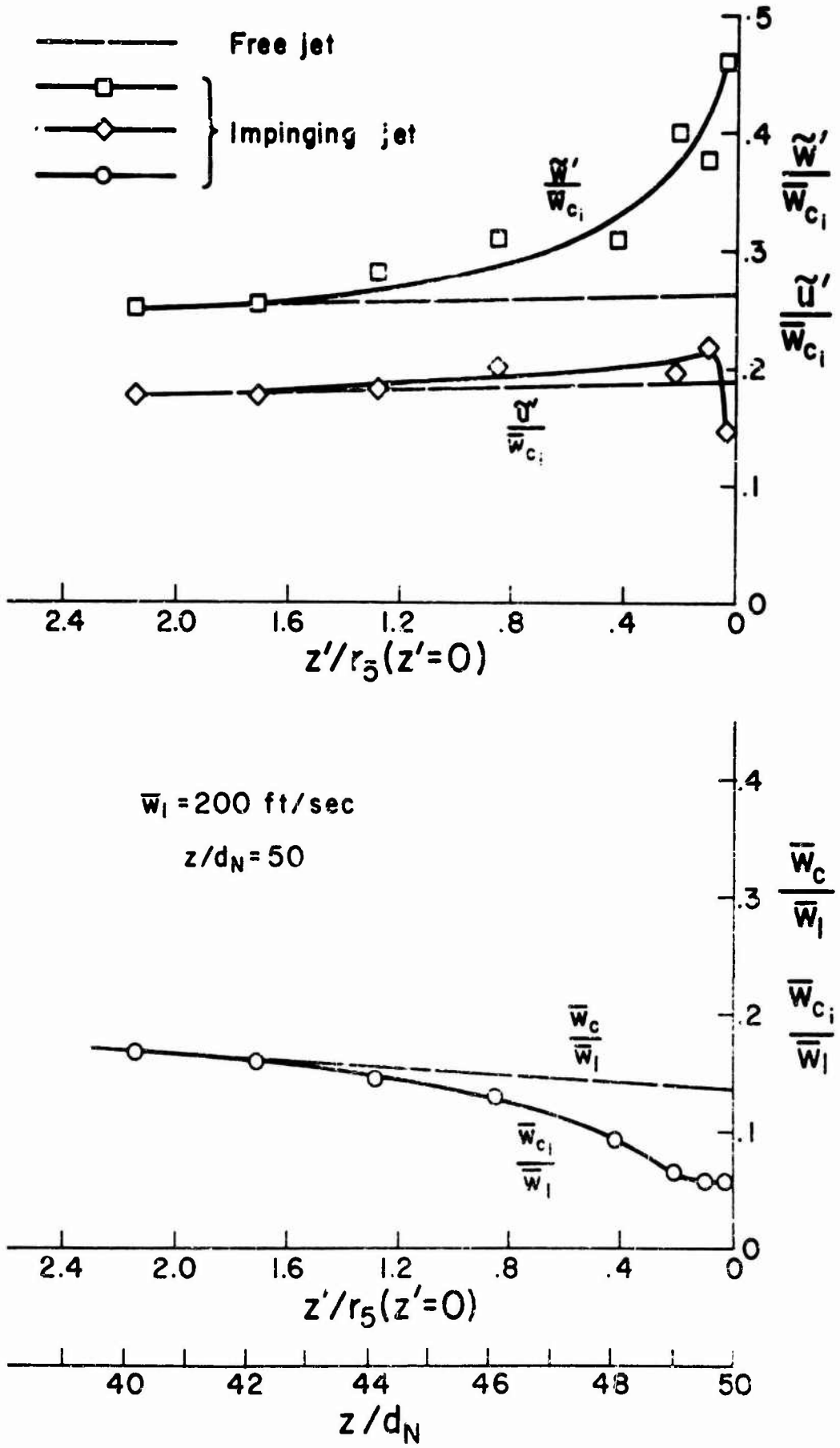

Figure 3.17. Mean and turbulent velocities measured on the centerline upstream of the impingement plate. $z/d_N = 50$.

4. EXPERIMENTAL RESULTS - PRESSURE MEASUREMENTS

Before going on to discuss the heat transfer measurements that were made, one more set of measurements which were designed to complete the specifications of the free jet being employed should be presented. Measurements were made of the fluctuations in total pressure on the centerline of the free jet and at the stagnation point of the impingement plate. These measurements were made at 200 ft/sec for axial positions z/d_N = 10, 20, and 30. The nondimensional spectra of these total pressure fluctuations in the free jet are shown in Fig. 4.1. As in the case of the other turbulent spectra which have been reported, it would appear that total pressure fluctuations also become of similar form for $z/d_N > 20$.* The spectra of $\overline{p'^2}$ at the stagnation point of the impingement plate are shown in Fig. 4.2. Here again the spectra appear similar for $z/d_N \geq 20$ except for what is felt to be an experimental difficulty at the higher frequencies. It is of some interest to compare these data with the measurements obtained by Strong, Siddon, and Chu [27] for a jet of nozzle Reynolds number $Re_d = 2.8 \times 10^5$ and at $z/d_N = 7$. While one would not expect these spectra to agree exactly, the general forms of the spectra are similar.

The spectra just presented can be integrated to obtain $\overline{p'^2}/q_c^2$. These nondimensional total pressure fluctuations are plotted in Fig. 4.3 as a function of z/d_N. It is easily seen from these results that the root-mean-square pressure fluctuation at the stagnation point of the impingement plate is roughly 70 percent of the rms total pressure fluctuation in the free jet at an equivalent z/d_N. One may also note the good agreement between the present measurements and those of Strong, et al.

---

* The lack of similarity of these spectra at the higher wave numbers, although this has not yet been traced down, is thought to be due to difficulties in obtaining a proper transfer function for the pressure transducer at the higher frequencies.

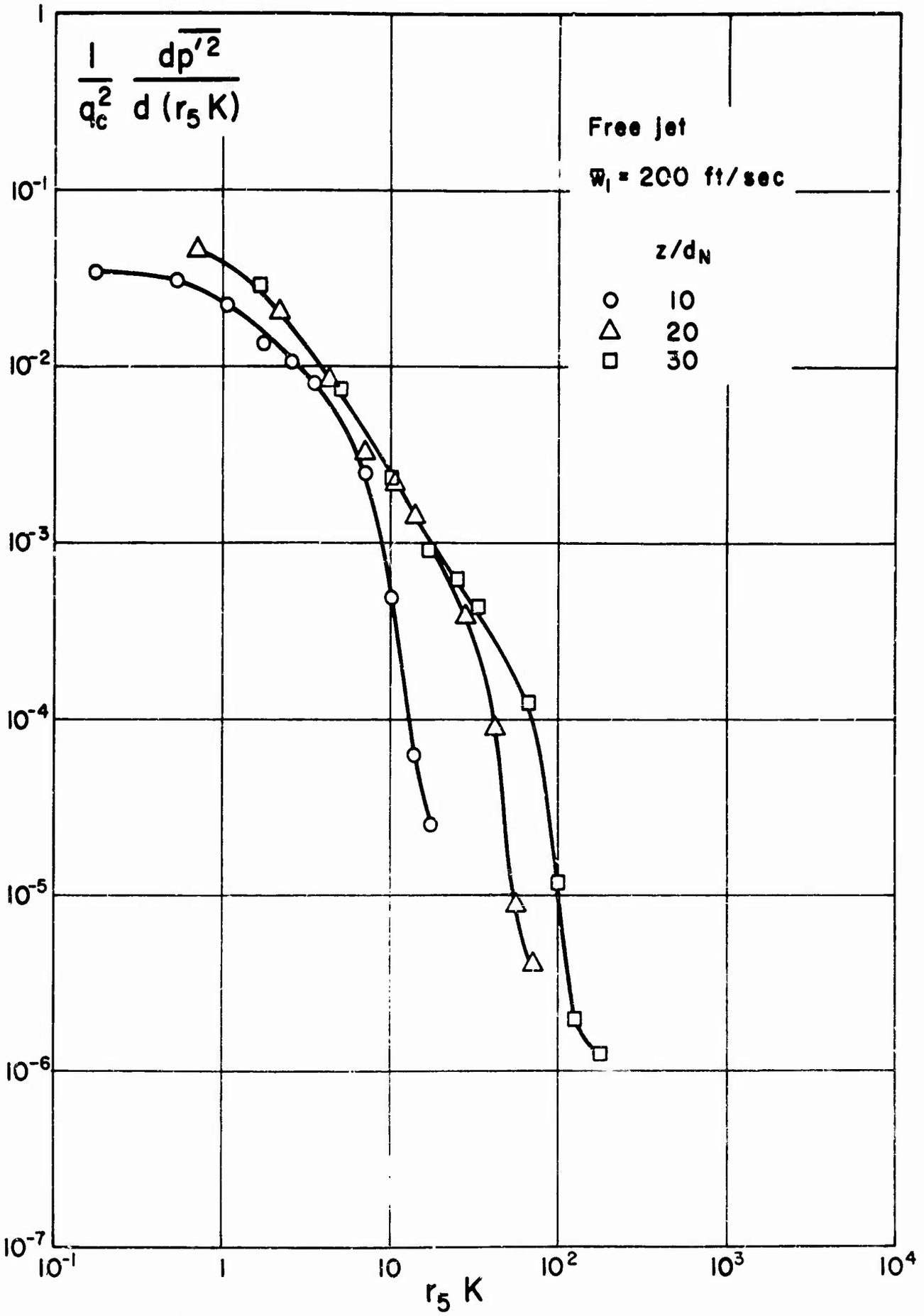

Figure 4.1. Spectra of the fluctuating total pressure on the centerline of the free jet.

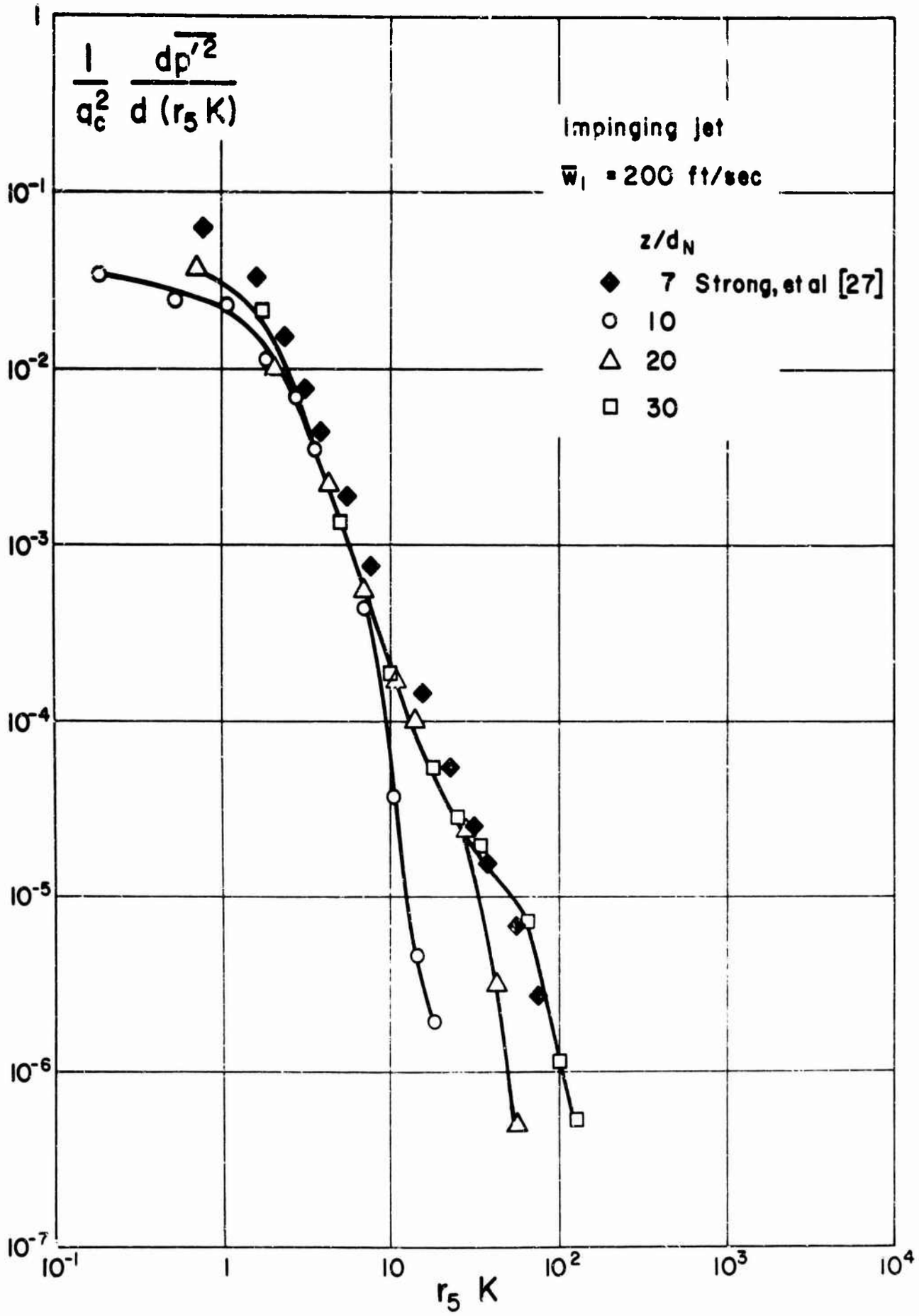

Figure 4.2. Spectra of the fluctuating total pressure at the stagnation point of the impinging jet.

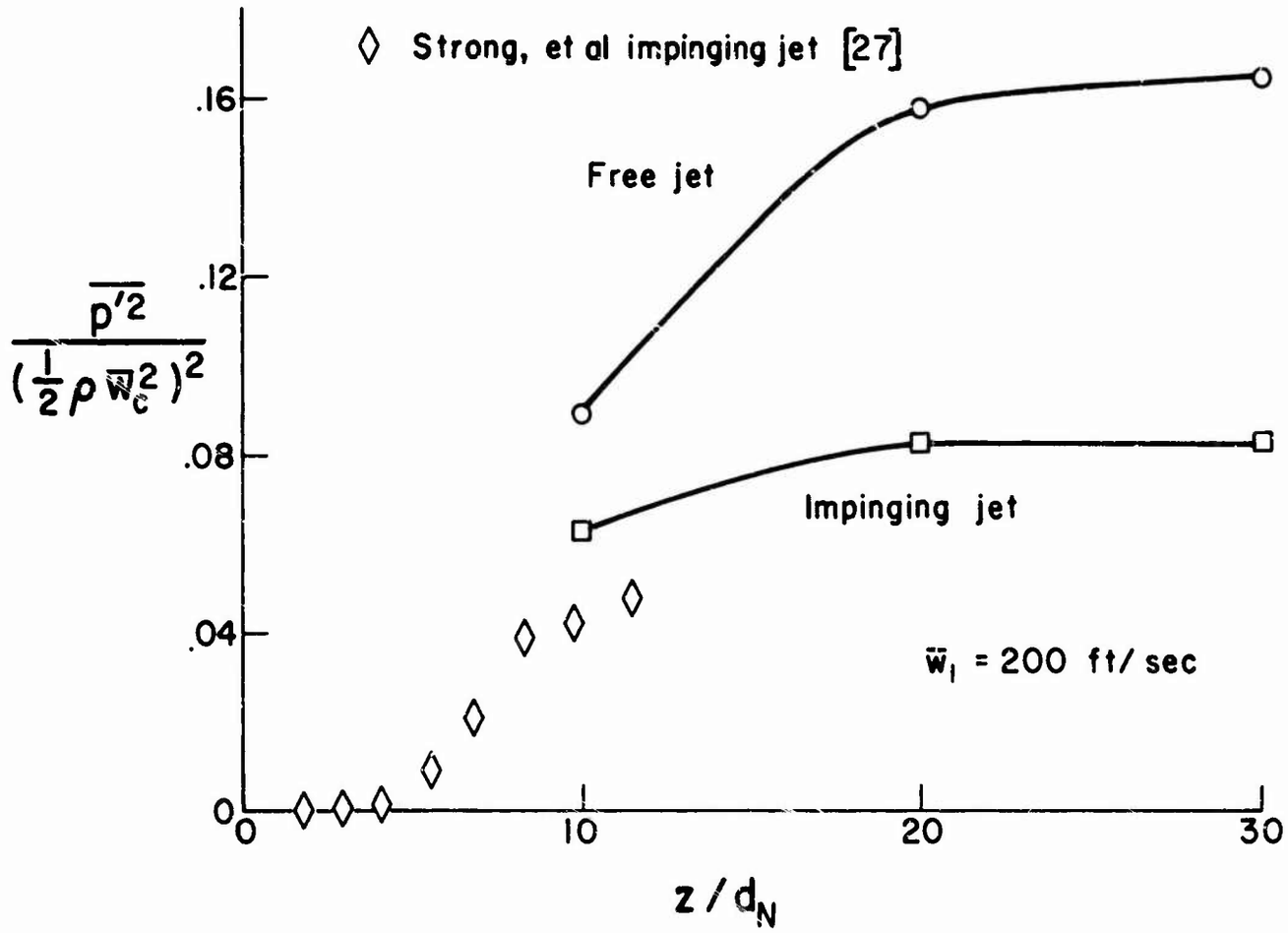

Figure 4.3. Nondimensional total pressure fluctuations on the centerline of the free and impinging jets.

5. EXPERIMENTAL RESULTS - HEAT TRANSFER

Having presented a fairly detailed description of the free jet in which this study of impingement heating was carried out, we now proceed to a discussion of the actual heat transfer measurements. Table 5.1 indicates the heat transfer distribution tests which were made. Listed in the table are the nozzle velocities and z/d_N for which measurements were made together with the pertinent values of local centerline velocity, jet half-breadth, and local Reynolds number. Note the approximate constancy of Re_5 with z/d_N for a fixed nozzle velocity. This constancy is expected in the developed region of the free jet.

Figures 5.1 and 5.2 are typical plots of heat transfer distributions on the impingement plate. These particular distributions of film coefficient $h = \dot{q}/\Delta T$ versus r have been selected as they were taken at the lowest and highest Reynolds numbers at which tests were made. It will be noted that the general character of these curves follows the behavior discussed in the introduction of this report; that is, the stagnation point heating is relatively high compared to the wall heating at low Reynolds number and this ratio becomes smaller as the Reynolds number is increased. Some liberty has been taken in fairing the curves in Figs. 5.1 and 5.2 as a result of knowledge of the behavior of the various individual heat gages gained during the performance of many tests. In general, it was found that the heat transfer near the stagnation point behaved in a manner similar to that of a laminar boundary layer on a surface having the same pressure distribution. The heat transfer rates were, however, a factor of 1.5 to 2 times larger than the calculated laminar values. Away from the stagnation point on the plate, it was found that the heat transfer behaved in a manner similar to a normal turbulent boundary layer which developed in an external flow having a free stream velocity equal to the local maximum velocity in the wall jet. A more precise statement of this behavior is given in [28] which reports a theoretical study done in conjunction with the present experimental study.

Table 5.1

$\frac{z}{d_N}$		$\bar{w}_1$, ft/sec			
		200	300	500	700
7	$\bar{w}_c$ =	177 ft/sec			
	r_5 =	.345 in.			
	Re_5 =	3.12×10^4			
10	$\bar{w}_c$ =	134	224	401	
	r_5 =	.450	.398	.386	
	Re_5 =	3.08×10^4	4.55×10^4	7.89×10^4	
15	$\bar{w}_c$ =	90	149	257	
	r_5 =	.670	.583	.572	
	Re_5 =	3.16×10^4	4.44×10^4	7.51×10^4	
20	$\bar{w}_c$ =	69	109	190	
	r_5 =	.931	.838	.790	
	Re_5 =	3.28×10^4	4.67×10^4	7.67×10^4	
30	$\bar{w}_c$ =	45	70	120	168
	r_5 =	1.43	1.39	1.33	1.30
	Re_5 =	3.28×10^4	4.97×10^4	8.15×10^4	1.12×10^5

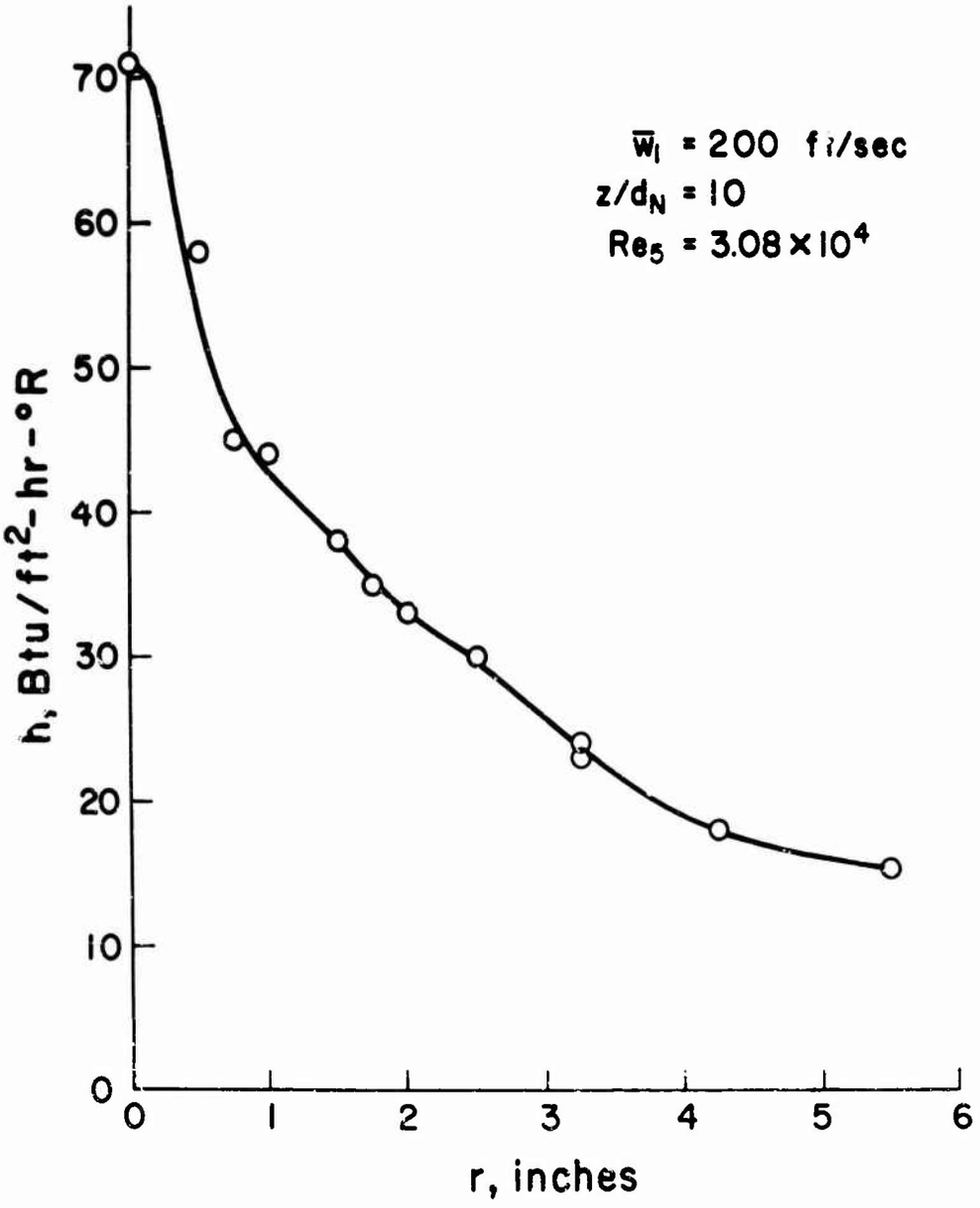

Figure 5.1. Radial distribution of measured film coefficient h for jet impingement on a flat plate.

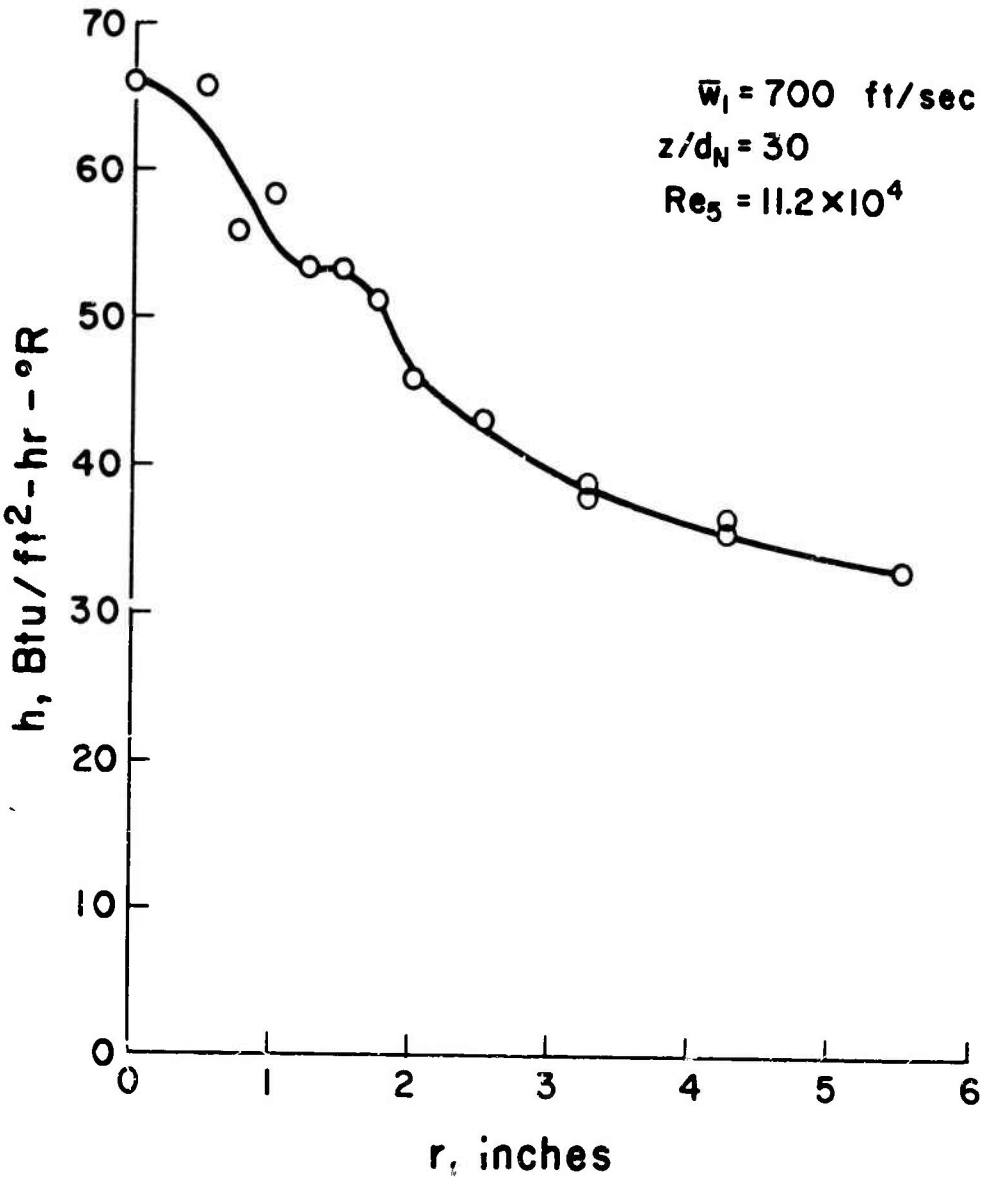

Figure 5.2. Radial distribution of measured film coefficient h for jet impingement on a flat plate.

Because of the great difference between the behavior of the heat transfer at and near the stagnation point and in the developed wall jet, it is convenient to discuss the measurements in these regions separately.

Stagnation Point Heat Transfer.

In Fig. 5.3 the measured stagnation point heat rates made dimensionless by means of the expected laminar heat transfer rates are plotted as functions of z/d_N. The laminar heat transfer rates were obtained from the relation [29]

$$\dot{q}_{lam} = \frac{c_p}{\sqrt{2Pr}} \sqrt{\rho\mu\left(\frac{du_e}{dr}\right)_{r=0}} (T_c^0 - T_w) \qquad (5.1)$$

For the particular conditions at which these tests were run, this relation reduces to

$$\frac{\dot{q}}{\Delta T} = 6.95 \times 10^{-1} \sqrt{\left(\frac{du_e}{dr}\right)_{r=0}} \qquad (5.2)$$

For each of the test conditions, the stagnation point velocity gradient $(du_e/dr)_{r=0}$ was evaluated from the data given in [1], and these are the exact values of $\dot{q}_{lam}$ used in Fig. 5.3. Before going on to discuss Fig. 5.3, it will be useful to note that if the stagnation point velocity gradient is written

$$\left(\frac{du_e}{dr}\right)_{r=0} = \alpha \frac{\bar{w}_c}{r_5} \qquad (5.3)$$

then Eq. (5.1) can be written in the form of a Nusselt number and a Reynolds number based on the local free jet half-breadth as

$$Nu_5 = \sqrt{\frac{\alpha Pr}{2}} \sqrt{Re_5} \qquad (5.4)$$

where Pr is the Prandtl number.

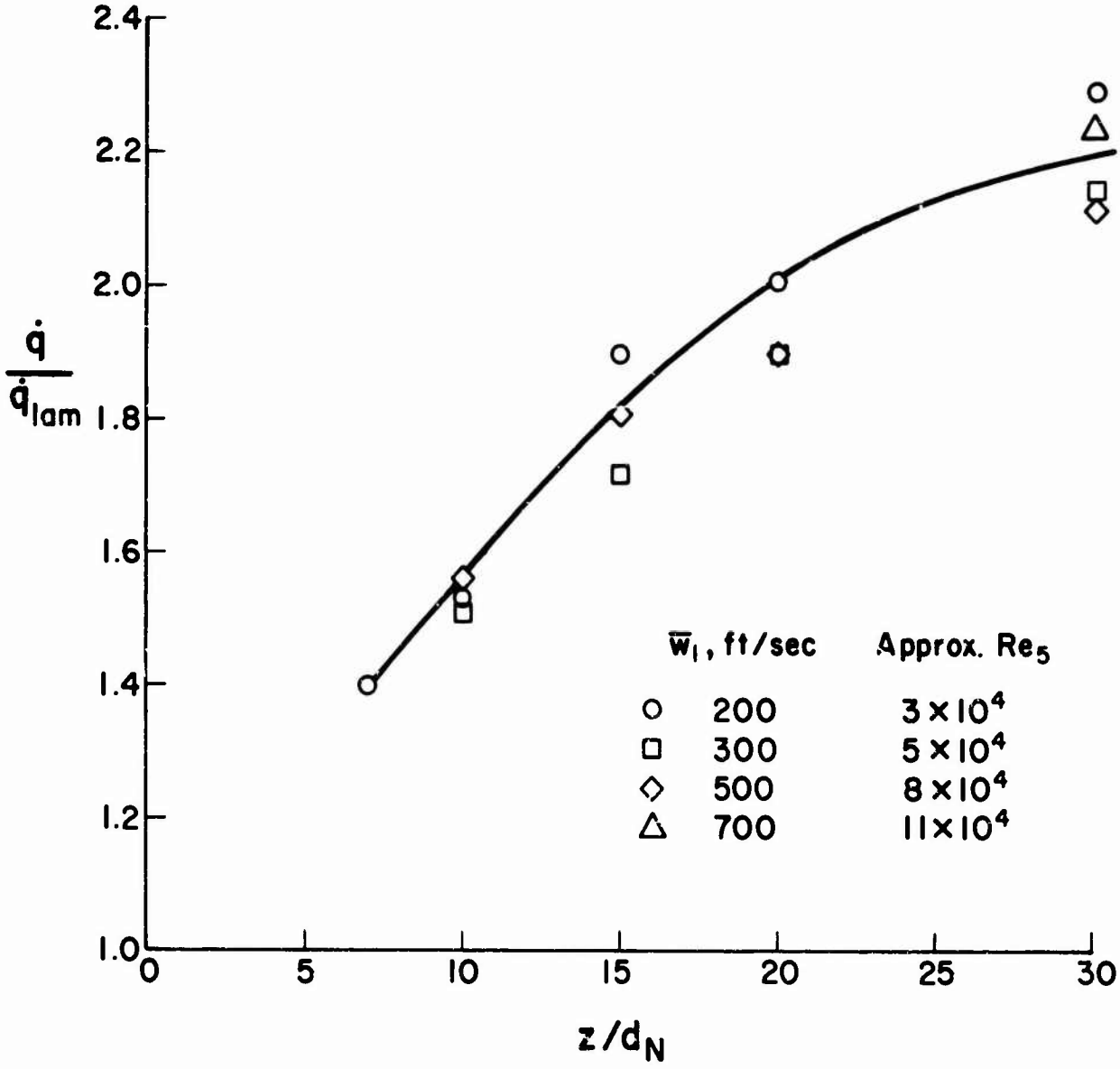

Figure 5.3. Ratio of measured heat transfer to that predicted by laminar theory at the stagnation point of the impinging jet.

If α is taken to be the value found for fully developed free jets, namely, $\alpha = 1.13$ [1] , then for the conditions of these tests

$$\frac{Nu_5}{\sqrt{Re_5}} = 0.635 \tag{5.5}$$

Returning to Fig. 5.3, it may be seen that the stagnation point heat transfer is larger than that predicted for a true laminar flow by a factor that is a function of z/d_N . There does not seem to be any consistent effect of Reynolds number that can be discerned from the data. Comparing Fig. 5.3 with Fig. 3.5 and noting the somewhat similar behavior of the two curves might lead one to suspect that it was the turbulence level in the jet prior to stagnation that was causing the increased laminar heat transfer rates. As mentioned in the introduction, similar increases in stagnation point heat transfer have been measured on spheres and cylinders in flows having approximately homogeneous turbulence produced by grids. In these experiments it has been pointed out that there are two primary parameters that affect the results; the relative turbulent intensity and the ratio of the integral scale of the turbulence to the scale of the body in question. In a free jet one of these parameters is suppressed, since, as has been shown earlier, the ratio of integral scale to the local scale length is a constant.* In view of this, there is shown in Fig. 5.4 a plot of $\dot{q}/\dot{q}_{lam}$ versus the average relative turbulent intensity in the free jet $\tilde{k}'/\bar{w}_c$, where

$$\tilde{k}' = \frac{1}{3}\sqrt{2\overline{u'^2} + \overline{w'^2}} \tag{5.6}$$

There is seen to be a general increase in $\dot{q}/\dot{q}_{lam}$ with turbulent intensity, but the scatter of the data at the higher intensities

*In a fully developed free jet, the only local scale length is, of course, the half-breadth of the jet.

is somewhat large. This scatter is somewhat larger than can be attributed to any one step in arriving at data plotted in Fig. 5.4, but perhaps an accumulation of differences can account for the scatter when one considers the problem of going from conditions defined in a free jet to conditions in a given jet impingement. In spite of the scatter evident in Fig. 5.4, it is clear that there does not seem to be any strong effect of Reynolds number.

It is of interest to compare the results just presented with the results of recent investigators for the effect of turbulence on heat transfer to cylinders in a uniform turbulent stream. It must be realized that this is not exactly a legitimate comparison since it compares results from two-dimensional flow with those of axisymmetric flow, and results from homogeneous turbulence with results from nonhomogeneous turbulence. In addition, in one circumstance, the velocity gradient at the stagnation point is caused by body curvature while in the other the same gradient is caused by the rotational velocity profile of the impinging jet. Nevertheless, on Fig. 5.5, which is a repetition of the data given in Fig. 12 of [12], we have plotted the results of our measurements. In order to have rough equivalence, the Reynolds number based on diameter, used by Smith and Kuethe, has been replaced by the Reynolds number based on twice the half-breadth in plotting the free jet data. It can be seen that the order of magnitude of the effect of turbulence is about the same as has been found by other investigators. In detail, however, the results are quite different. Close examination of the data shows that the effect of Reynolds number is not nearly as pronounced in our axisymmetric free jet results as has been found to be the case for cylinders in uniform turbulent flow.

Before going on to discuss the heat transfer away from the stagnation point, it may be useful to present, in Fig. 5.6, a plot of $Nu_5/\sqrt{Re_5}$ versus Reynolds number, together with the expected accuracy of determining $Nu_5/\sqrt{Re_5}$ that results from the measurement of $\dot{q}$ and the evaluation of $\dot{q}_{lam}$ from measured

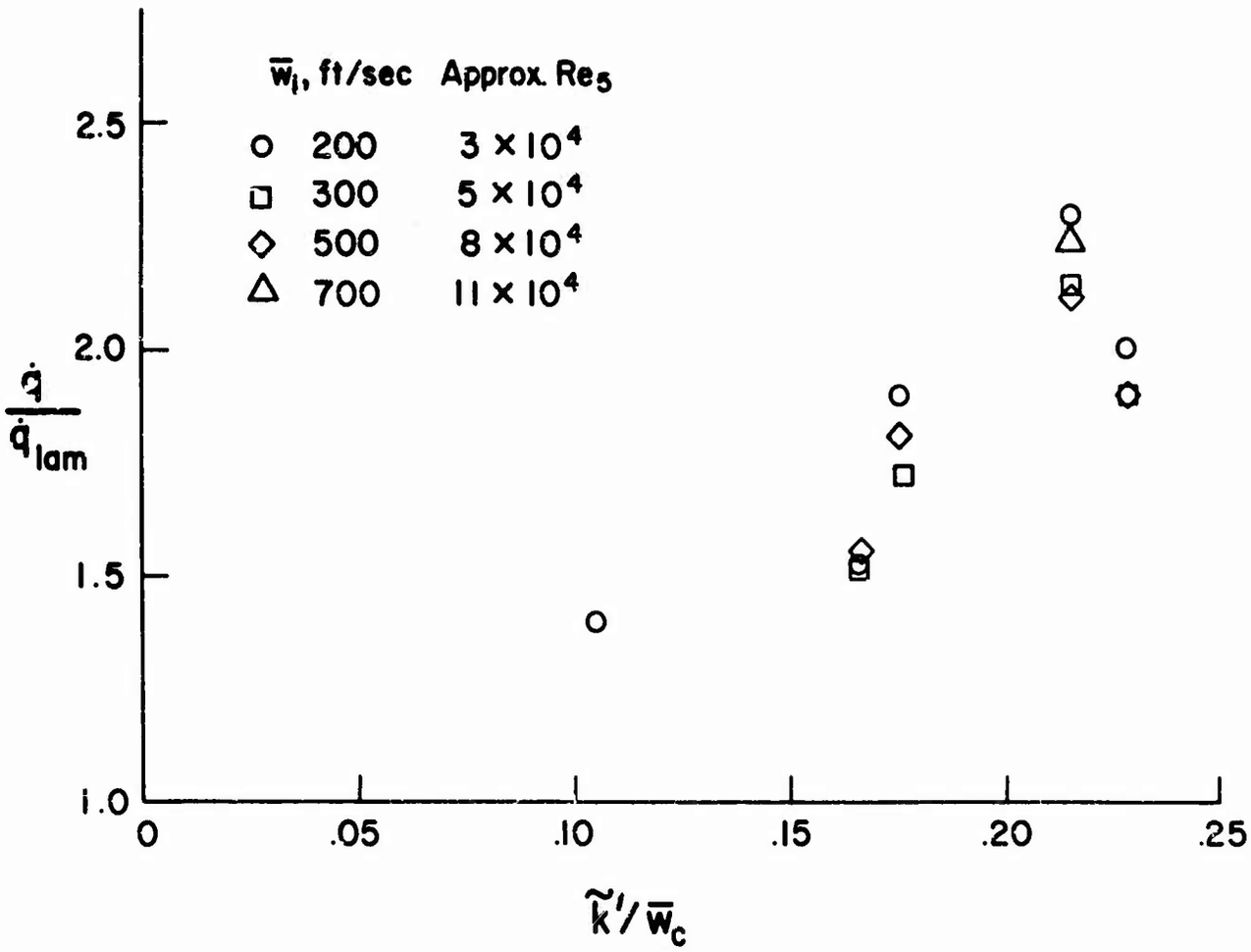

Figure 5.4. Ratio of measured-to-theoretical laminar heat transfer as a function of relative jet turbulent intensity.

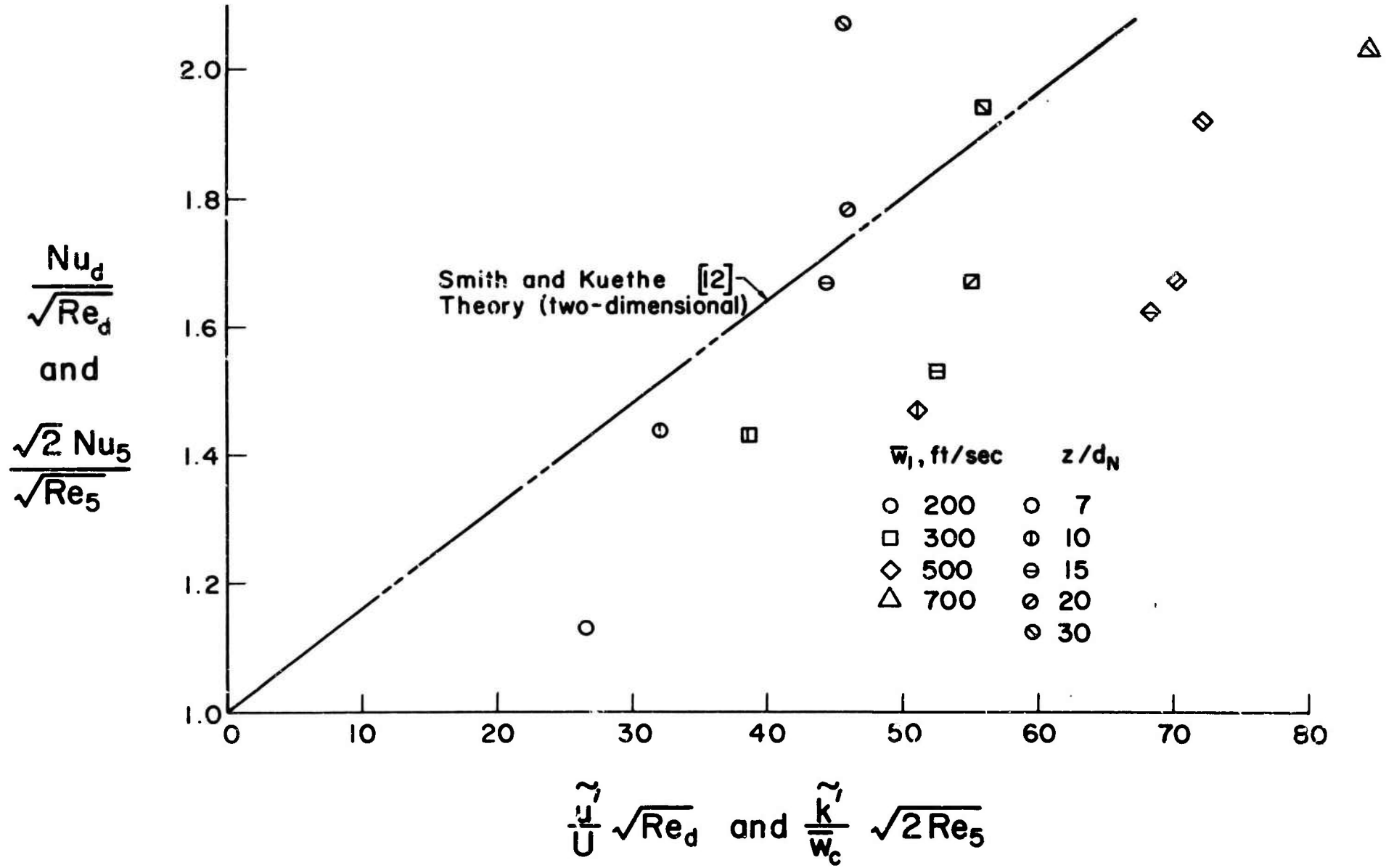

Figure 5.5. Comparison of measured heat transfer for the axisymmetric impinging jet with that predicted by the two-dimensional theory of [12].

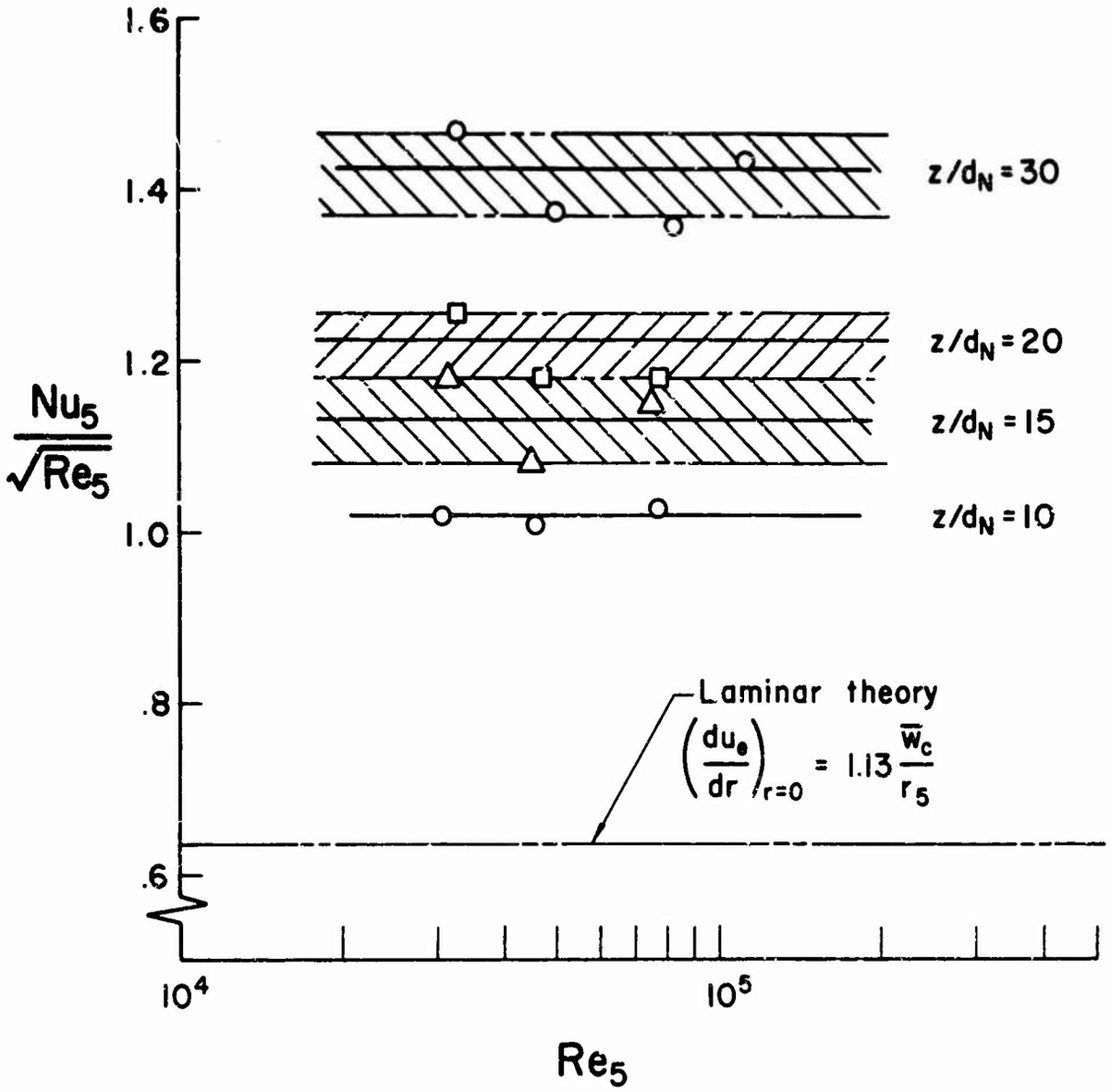

Figure 5.6. Measured heat transfer as a function of local Reynolds number.

values of $(du_e/dr)_{r=0}$. It would appear, as has been stated earlier, that there is no discernible effect of Reynolds number that can be gleaned from these data.

Heat Transfer Close to the Stagnation Point.

Close to the stagnation point, the boundary layer behaves as a laminar layer disturbed by having embedded in it the turbulence carried in from the free jet. In the experiments reported here, this region is not well instrumented. The number of heat transfer gages in this region near the stagnation point was not large and these gages proved, unfortunately, to be some of those which had large variations from the mean in their behavior. As a result of these variations, it is difficult to make detailed comments concerning the measured distributions of heat transfer near the stagnation point. It does appear, however, that the actual heat transfers fall off with r/r_5 at a rate slightly greater than that predicted by correcting the normal distribution of laminar heat transfer by a turbulence factor equal to that measured at the stagnation point. This may be seen from an inspection of Fig. 5.7 where the measured heat transfers near the stagnation point are compared for the case of $z/d_N = 30$. Although a great deal more work is needed before the exact nature of this near-stagnation point heat transfer fall-off is understood, it is suggested that, for most engineering computations at large Reynolds numbers, sufficient accuracy will be achieved by applying the stagnation point turbulence correction factor to the normal laminar heat transfer rates in order to estimate local heating near the stagnation point of impinging flows. If such a procedure is followed, it will be found that the heat transfer in the region near the stagnation point will be proportional to the square root of Re_5 and will be a decreasing function of r/r_5 similar to the distributions shown in Fig. 1.3.

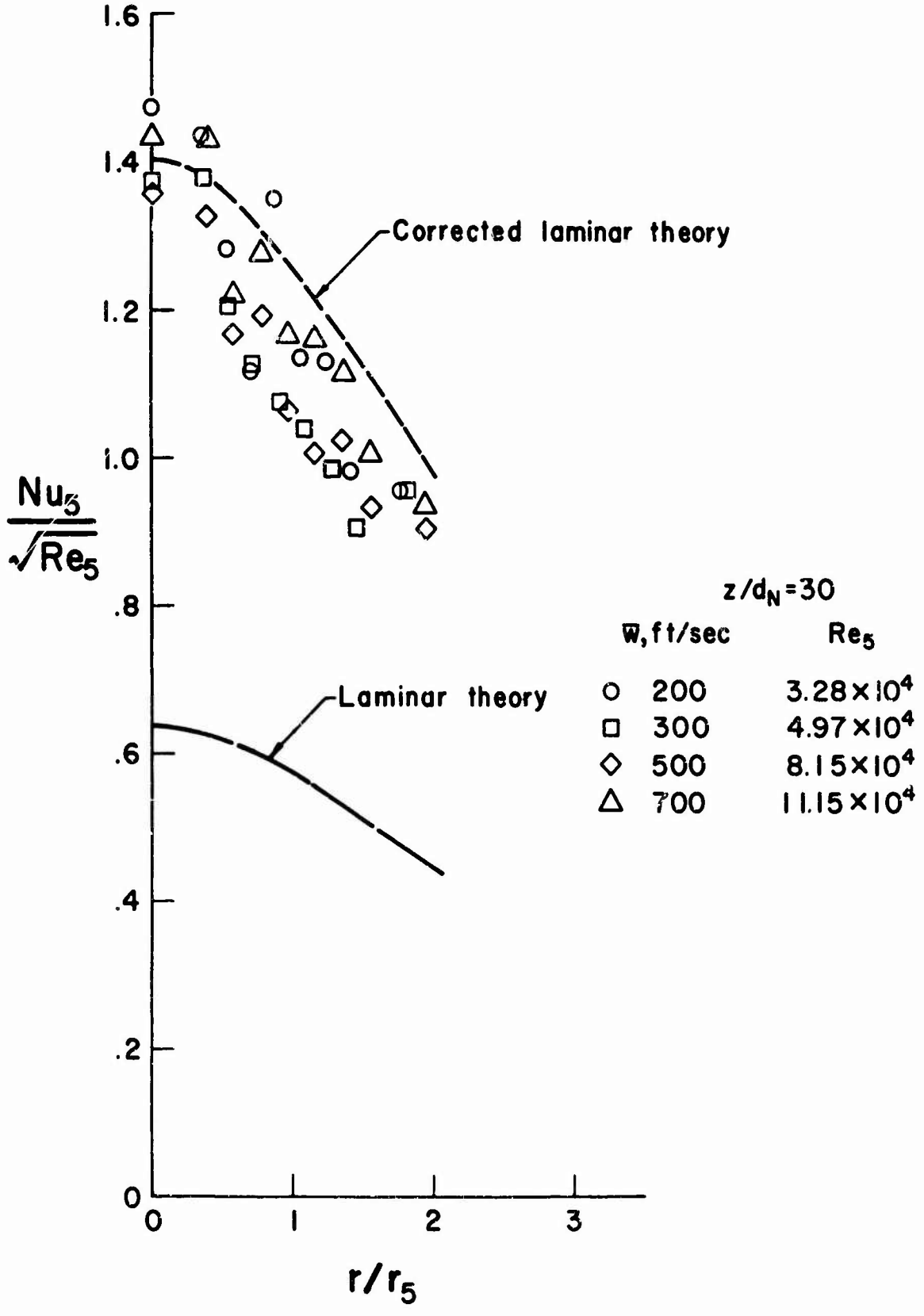

Figure 5.7. Heat transfer close to the stagnation point.

Heat Transfer Far from the Stagnation Point.

Once transition has occurred in the developing axially symmetric wall jet at a point away from the stagnation point, the behavior of the heat transfer is quite different from that in the vicinity of $r = 0$. Indeed, based on a simplified analysis of the development of a turbulent boundary layer in a flow whose external velocity falls off as does the maximum velocity in the wall jet, one would expect, at large distances from the stagnation point, i.e., $r/r_5 \gg 1$, that the Nusselt number based on the length r would be proportional to the eight-tenths power of the Reynolds number based on r_5, namely,

$$Nu = \frac{\dot{q}r}{k\Delta T} = \text{const } (Re_5)^{.8} \tag{5.7}$$

or, if $Nu_5 = qr_5/k\Delta T$,

$$\frac{Nu_5}{(Re_5)^{.8}} = \text{const } \frac{r_5}{r} \tag{5.8}$$

In view of this relation for $r/r_5 \gg 1$, we might expect a generalization of Eq. (5.8) for smaller r/r_5 to be of the form

$$\frac{Nu_5}{(Re_5)^{.8}} = f\left(\frac{r}{r_5}\right) \tag{5.9}$$

In Figs. 5.8 through 5.11 the measured heat transfer distributions have been plotted in the form indicated by Eq. (5.9), namely, as Nu_5 as a function of r/r_5. It should be noted that the scatter of the data is largest in Fig. 5.8 and in particular for the cases of z/d_N of 20 and 30. These conditions represented the lowest heat transfer rates measured and are those for which the experimental errors are largest. As the Reynolds number was

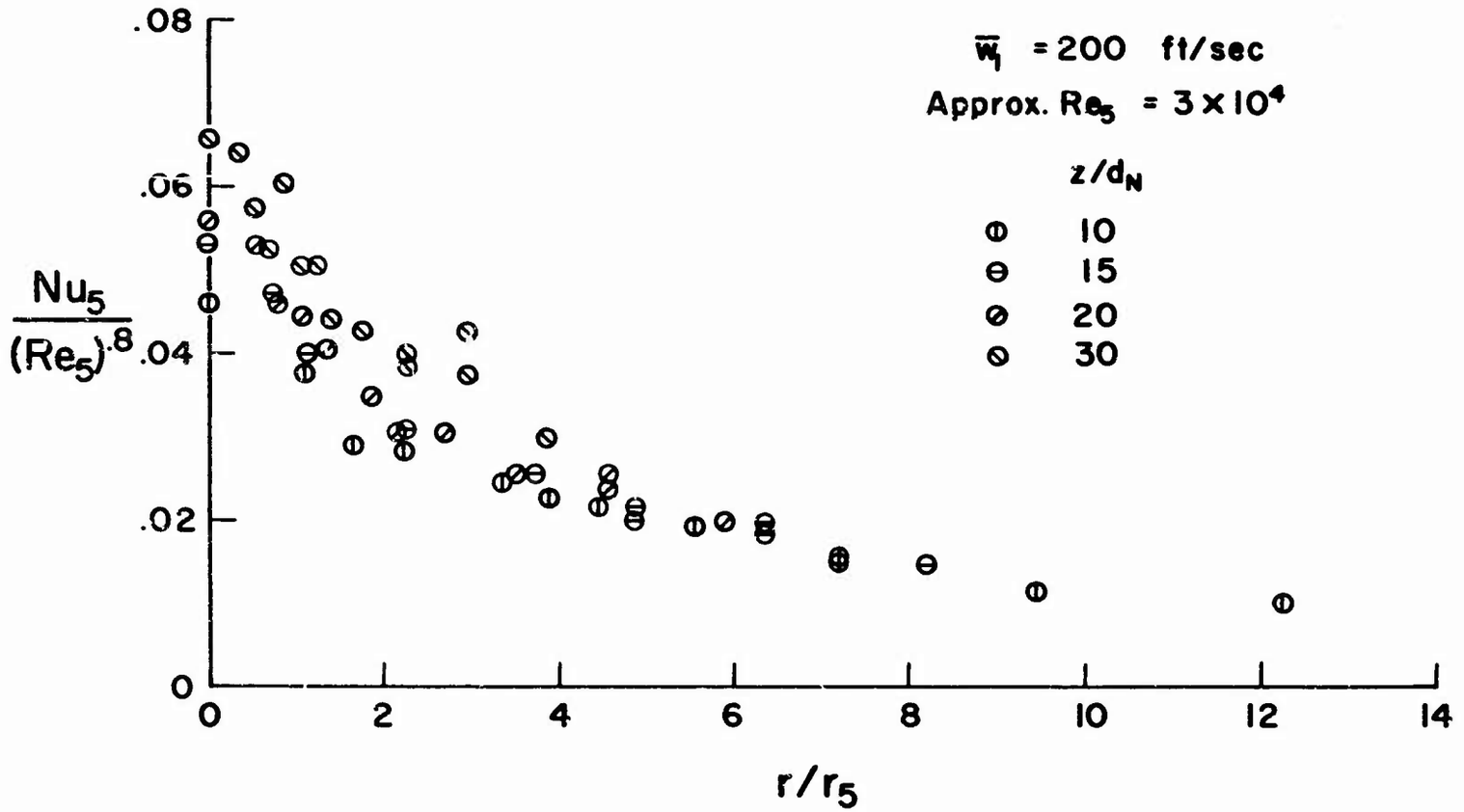

Figure 5.8. Measured heat transfer distribution with $Nu_5 = hr_5/k$.
$Re_5 \approx 3 \times 10^4$

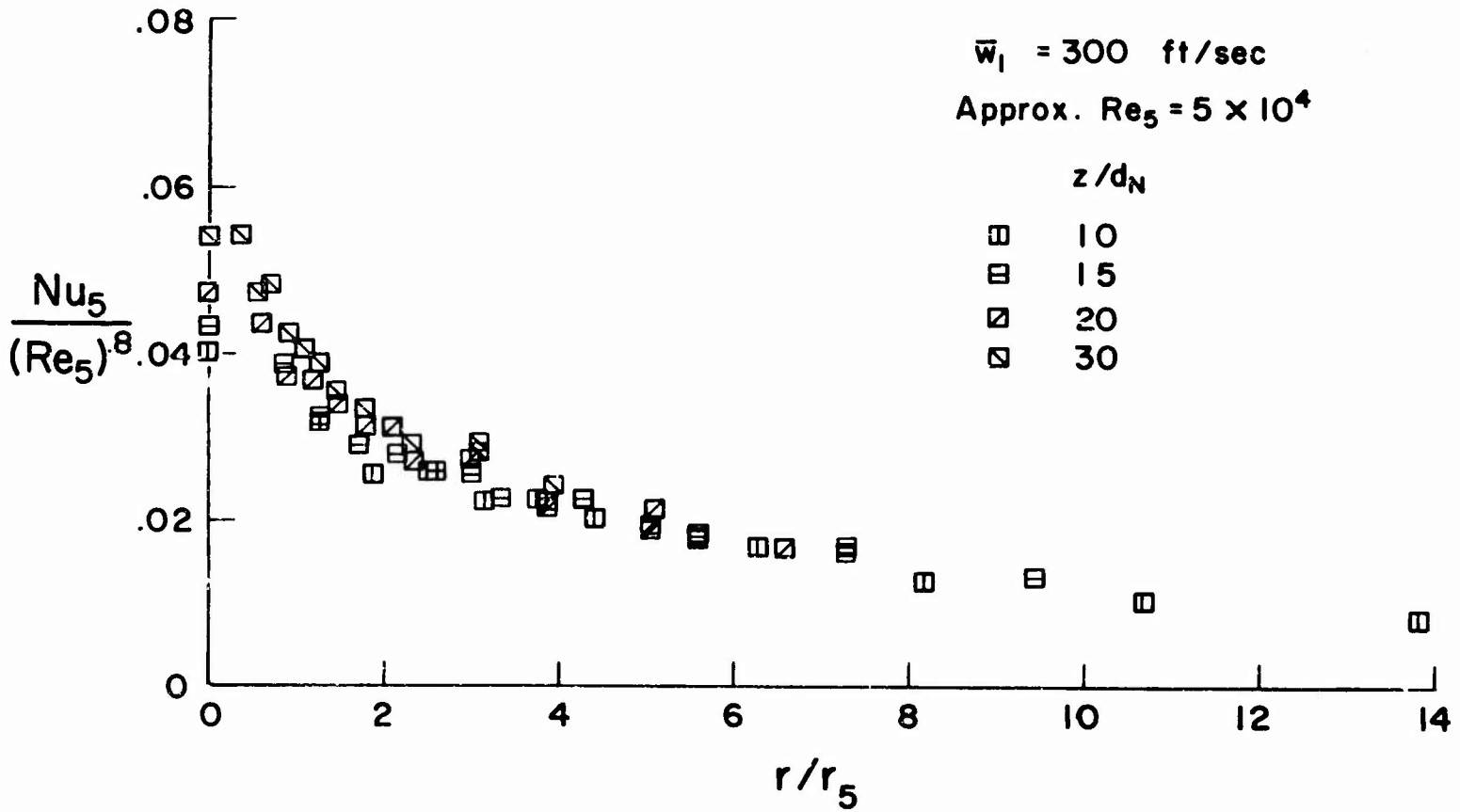

Figure 5.9. Measured heat transfer distribution with $Nu_5 = hr_5/k$.
$Re_5 \approx 5 \times 10^4$

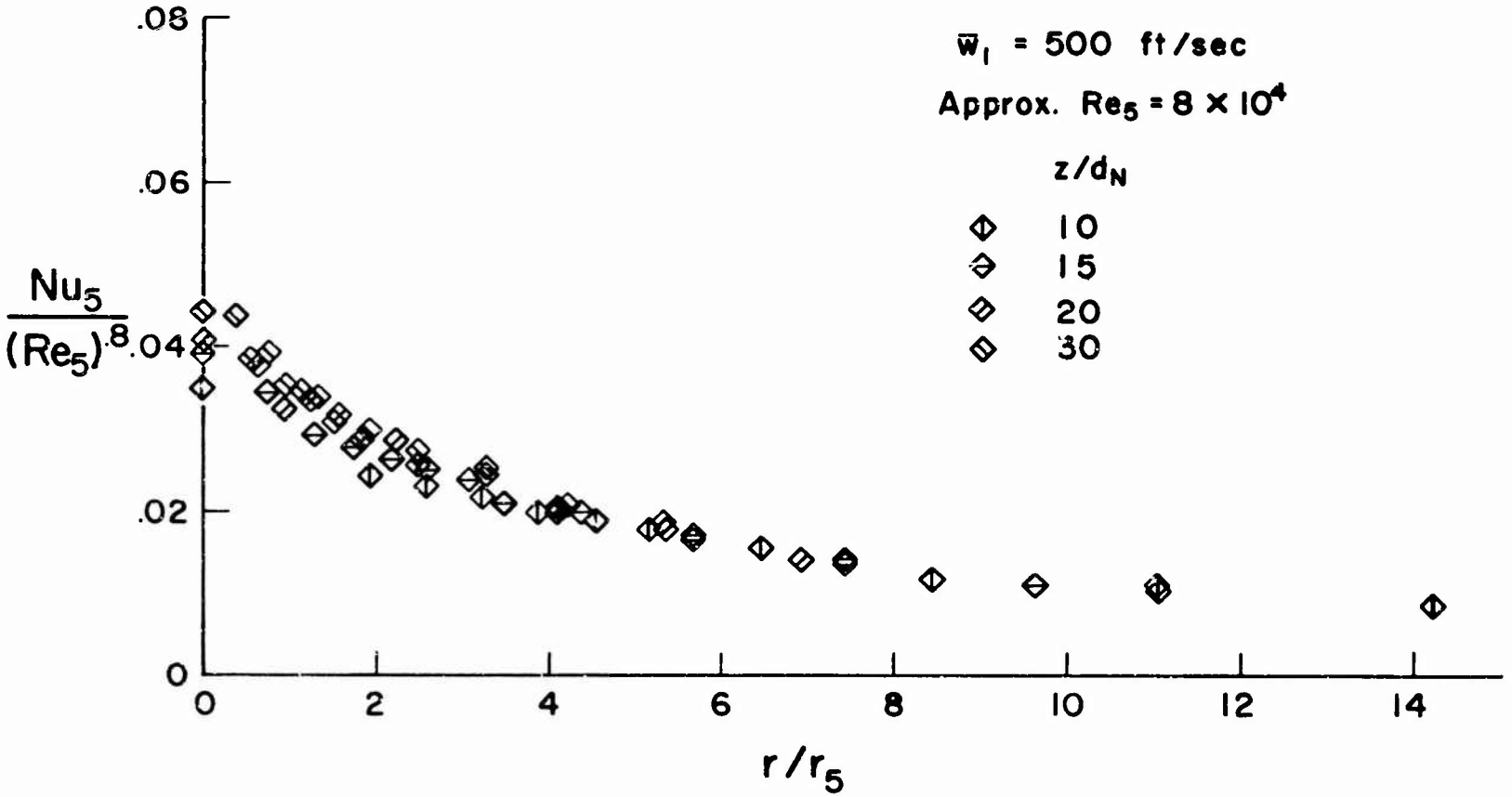

Figure 5.10. Measured heat transfer distribution with $Nu_5 = hr_5/k$.
$Re_5 \approx 8 \times 10^4$

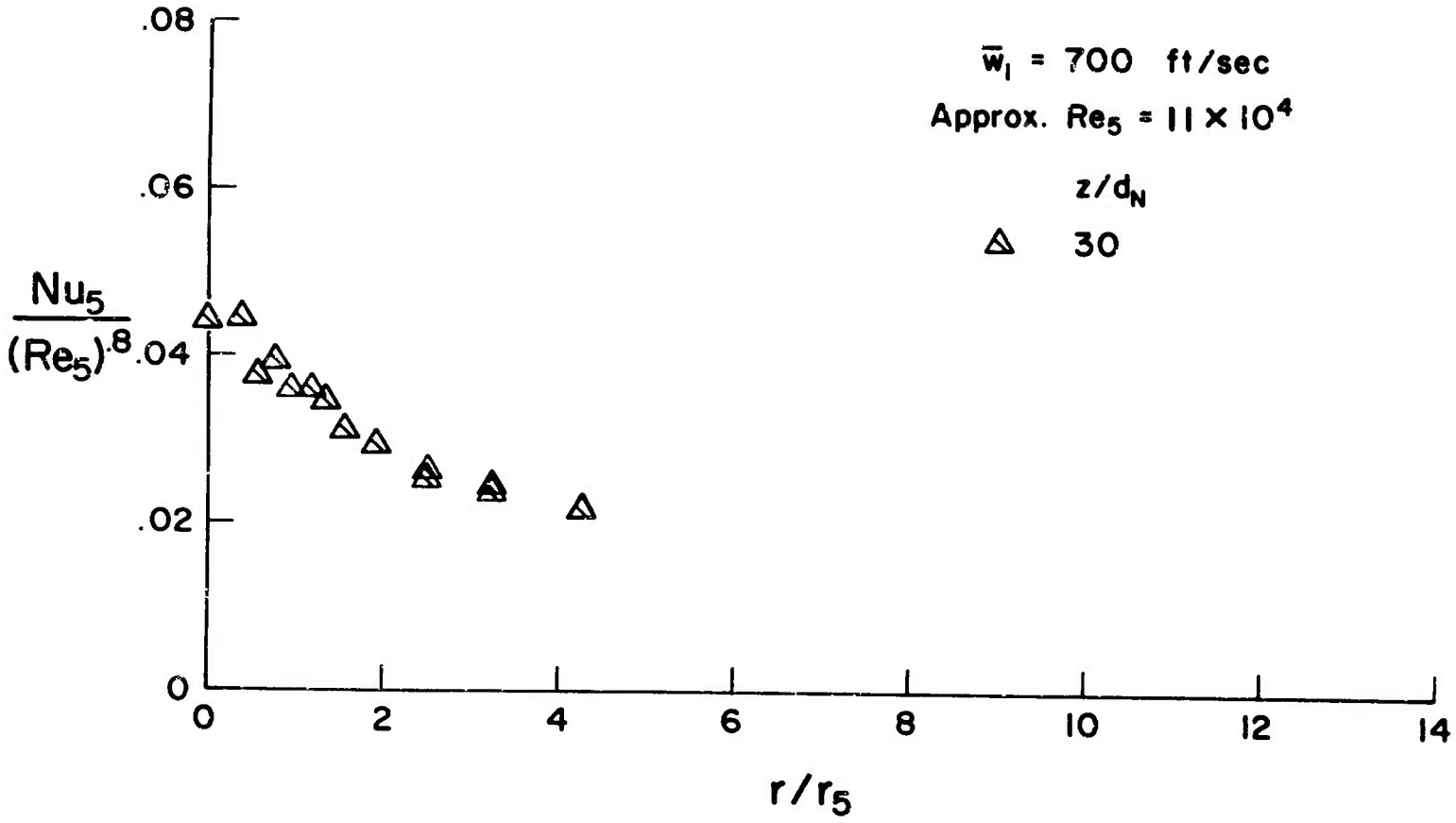

Figure 5.11. Measured heat transfer distribution with $Nu_5 = hr_5/k$. $Re_5 \approx 11 \times 10^4$

increased and the general level of heat transfer increased, the scatter in the data decreases (see Figs. 5.9 through 5.11).

When the data are plotted as in Figs. 5.8 through 5.11 for a fixed Reynolds number, only one curve of Nu_5 versus r/r_5 should result at $r/r_5 \gg 1$. Thus the data scatter at large r/r_5 in these figures is truly a measure of experimental accuracy which for low velocity and large z/d_N was poor. On the other hand, when all the data shown in Figs. 5.8 through 5.11 and obtained at different Reynolds numbers are plotted on the same graph as is done in Fig. 5.12, the fact that for r/r_5 equal to approximately 2 or greater all the data fall on one curve within the expected experimental accuracy indicates that a relationship such as that given in Eq. (5.9) is valid.

Rosenbaum and Donaldson, in a theoretical study done in conjunction with the present work [28], have derived a theoretical expression for the turbulent heat transfer below an impinging jet. Their result for the case when Reynolds analogy is assumed to hold is plotted in Fig. 5.12 for reference.

The success of the simple correlation suggested by Eq. (5.9) encourages one to attempt a correlation of the form given in Eq. (5.7) in order to obtain a description of the behavior of jet impingement heat transfer at large r/r_5. Figures 5.13 through 5.16 are the result of plotting our measurements in this form. As before, one sees a more pronounced scatter in the data at low speeds and large z/d_N. In addition, the only data which yield information concerning the large r/r_5 behavior of the parameter $Nu_5/(Re_5)^{.8}$ are those taken at $z/d_N = 10$ and 15. Inspection of the data does indicate, however, that an asymptote may be approached at large r/r_5. Further investigation is needed, but on the basis of present data, it would appear that heat transfers at large r/r_5 might be computed on the basis of the following formula

$$Nu = \frac{\dot{q}r}{k\Delta T} = 0.12(Re_5)^{.8} \qquad (5.10)$$

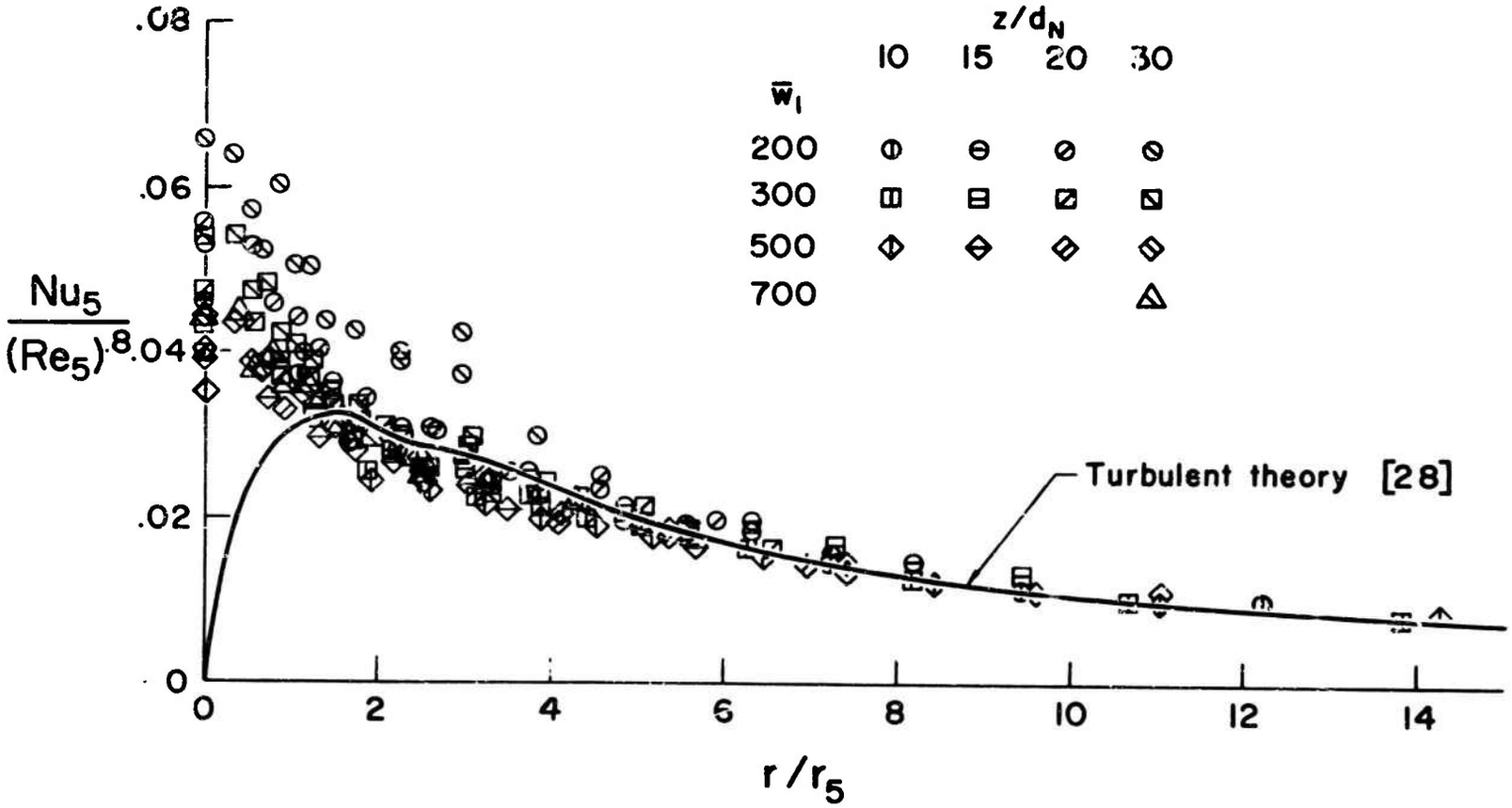

Figure 5.12. Comparison of measured heat transfer data for all Reynolds numbers.

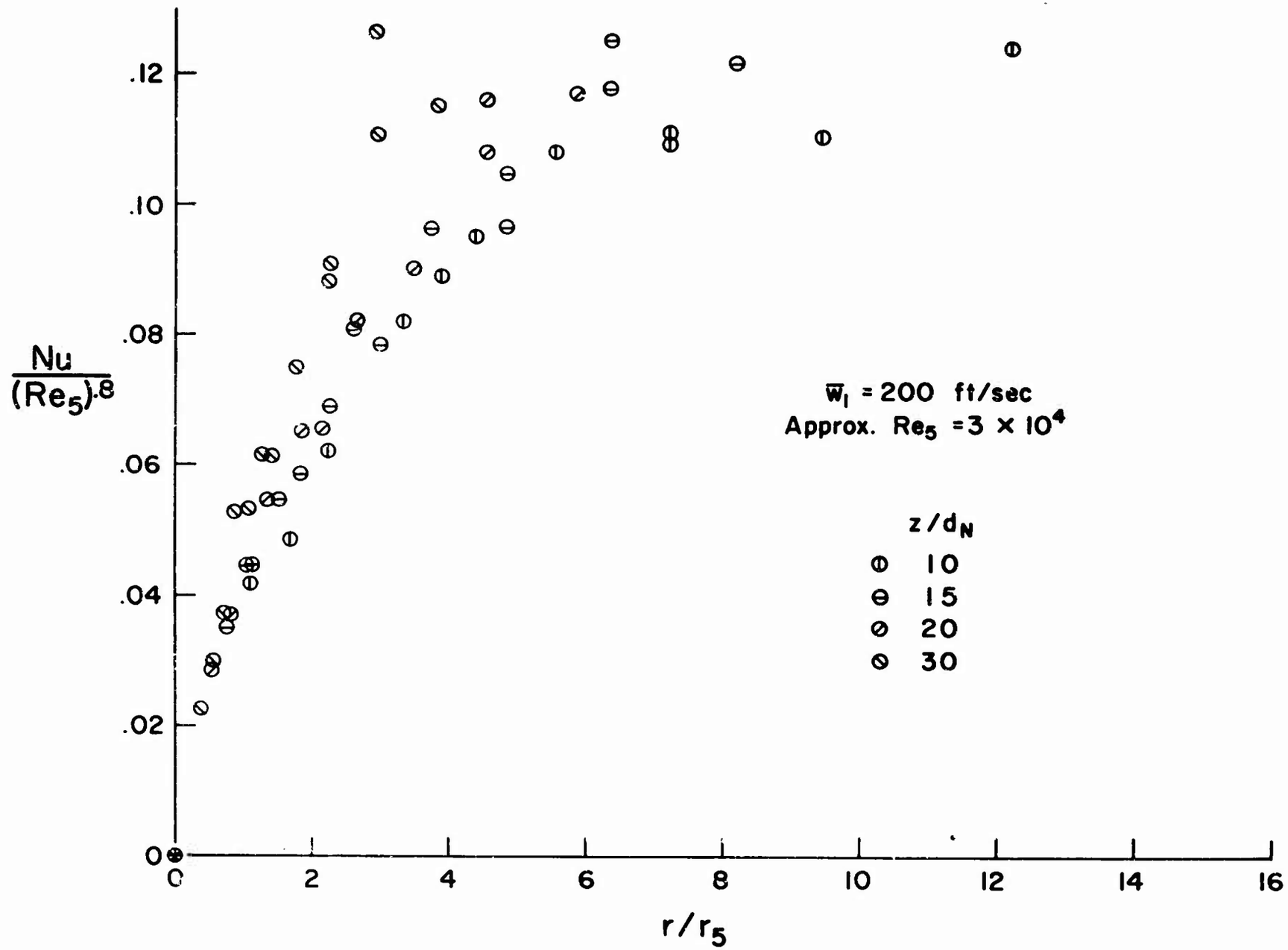

Figure 5.13. Measured heat transfer distribution with $Nu = hr/k$. $Re_5 \approx 3 \times 10^4$.

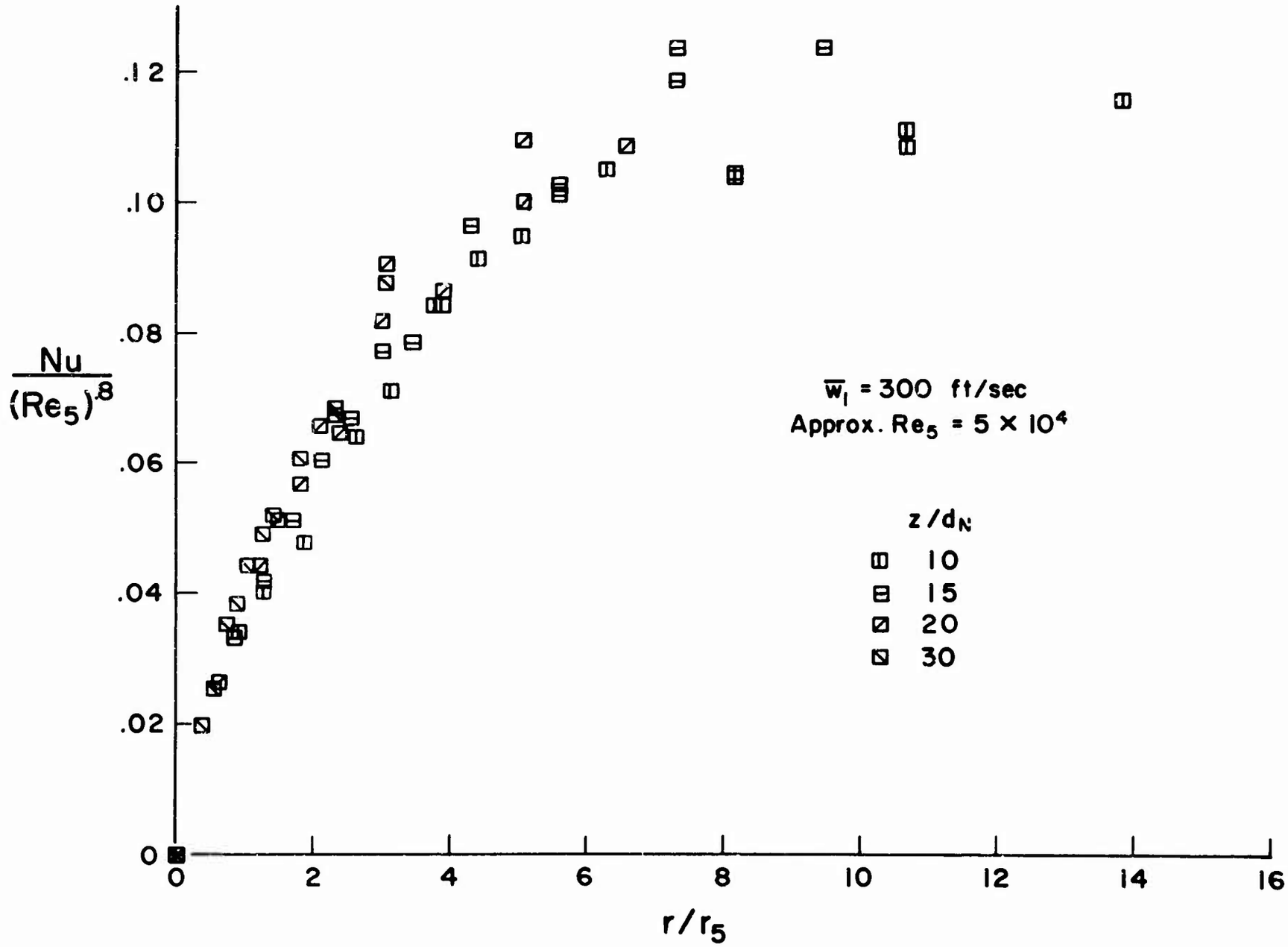

Figure 5.14. Measured heat transfer distribution with $Nu = hr/k$. $Re_5 \approx 5 \times 10^4$.

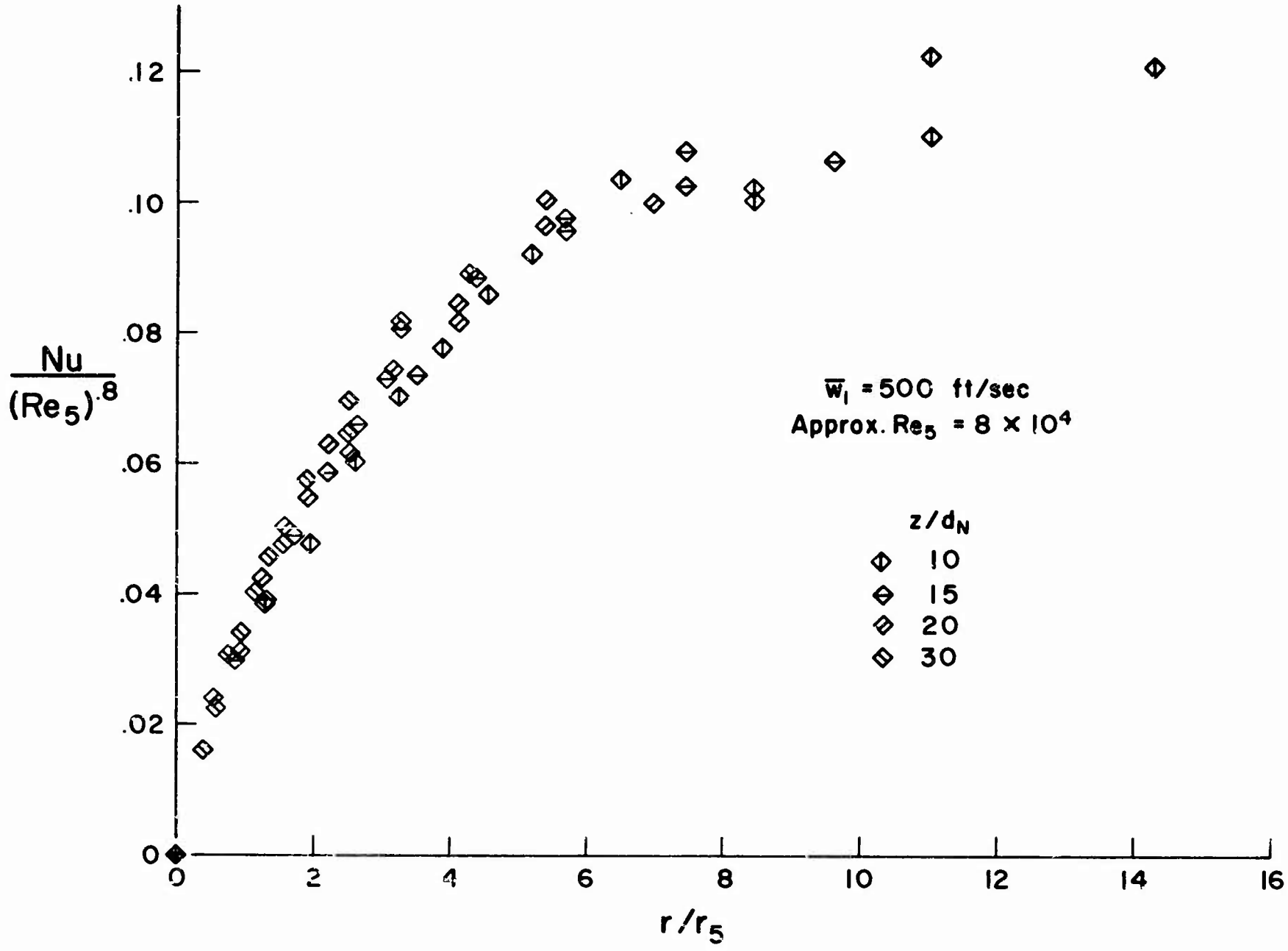

Figure 5.15. Measured heat transfer distribution with $Nu = hr/k$. $Re_5 \approx 8 \times 10^4$.

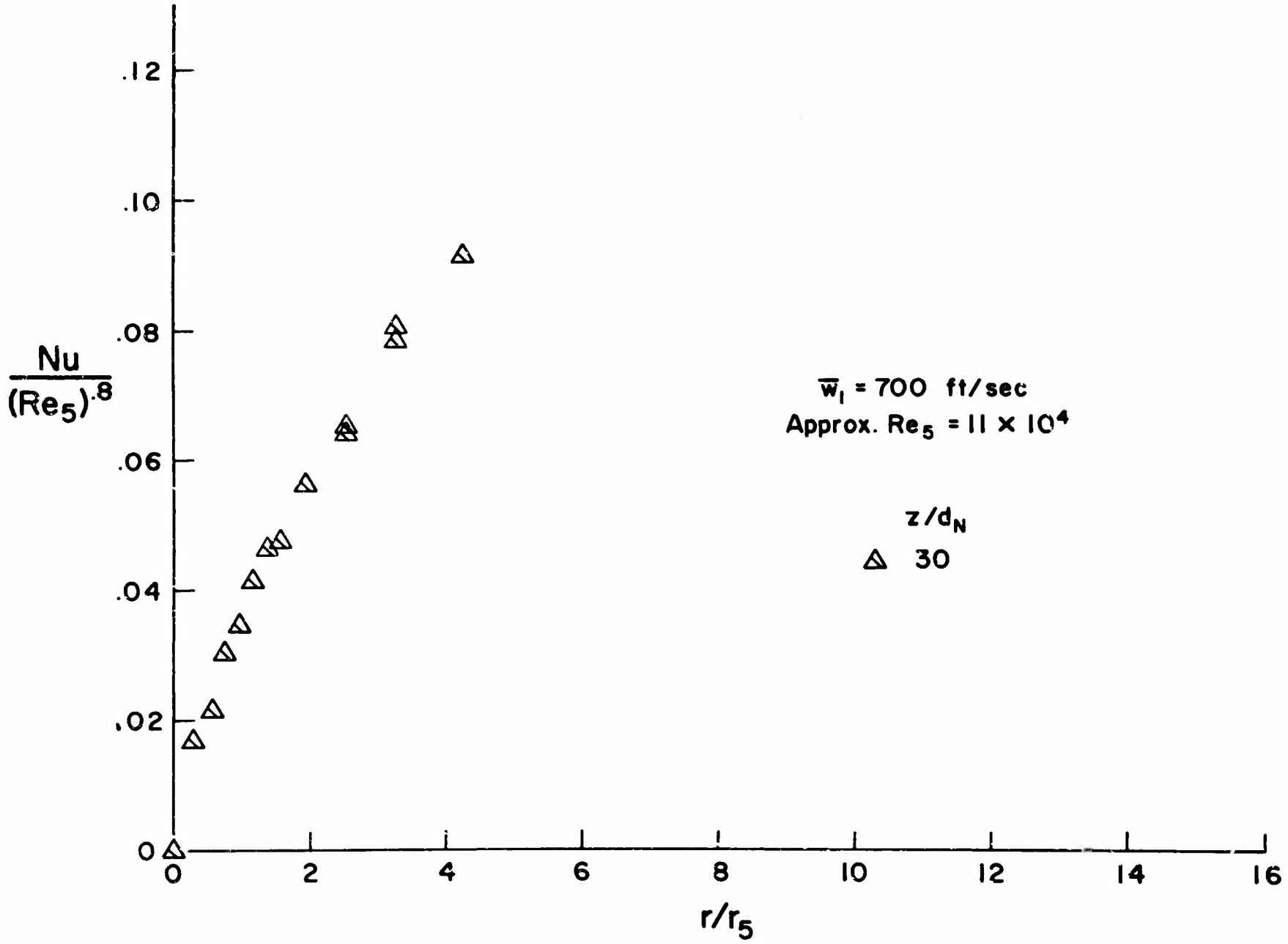

Figure 5.16. Measured heat transfer distribution with $Nu = hr/k$. $Re_5 \approx 11 \times 10^4$.

Comparison with Other Results.

In general, the heat transfer results obtained in this study agree well with the results of other investigators. It will, perhaps, suffice to compare our results with those of Gardon and Cobonpue [14]. In the upper part of Fig. 5.17, a comparison is made of radial heat transfer distributions for the most nearly equivalent conditions. It is seen that the agreement is excellent. The lower portion of Fig. 5.17 shows the axial variation of $\dot{q}/\dot{q}_{lam}$. In this case the agreement at the two downstream stations is not good, with the values of $\dot{q}/\dot{q}_{lam}$ measured by Gardon and Cobonpue falling some 27 percent below those of the present study. At present, the reason for this disagrement is not understood.

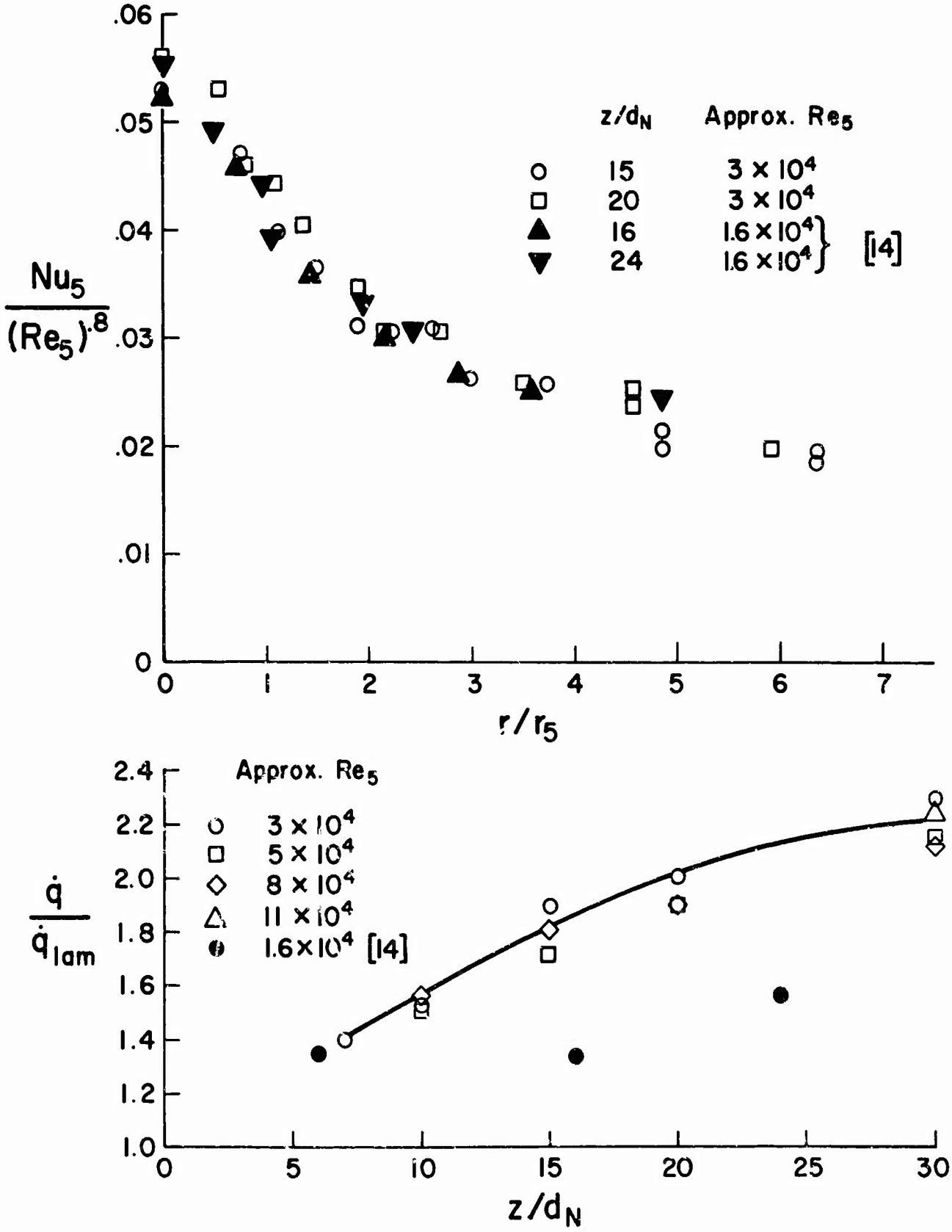

Figure 5.17. Comparison of heat transfer data with that of Gardon and Cobonpue [14].

6. DISCUSSION

It was the purpose of the present investigation to develop a rationale for computing the heat transfer that results when a jet impinges on a surface. It appears from the results just presented that the following procedure should yield results that will suffice for most engineering purposes.

In the region near the stagnation point, the heat transfer should be computed by first computing the laminar heat transfer that would take place on a surface having the same pressure distribution as that on the impingement plate. A constant correction factor is then to be applied to these results to account for the structure of the turbulent jet. The appropriate correction factor, which is a function of z/d_N and not of Reynolds number, is to be obtained from the results given in Fig. 5.3.

Farther away from the stagnation point, the heat transfer should be computed on the basis of the technique given by Rosenbaum and Donaldson [28] and plotted in Fig. 5.12. At most Reynolds numbers of interest, adequate results will be obtained by assuming the larger of these two results to be the proper local heat transfer rate.

Very far from the stagnation point, it appears that the heat transfer film coefficient falls off as $1/r$, and for large r/r_5 the heat transfer may be estimated from the approximate formula

$$Nu = \frac{\dot{q}r}{k\Delta T} = 0.12 \frac{r_5}{r}$$

7. SUMMARY

The results of an experimental study of the heat transfer below normally impinging jets have been presented. These results have been correlated on the basis of the local mean flow and turbulent characteristics of the free jet that would exist in the plane of impingement were the plane to be removed. In order to make these local correlations possible, a rather extensive survey of the free jet used in the experiments was made that could be used in connection with previous studies of the local mean character of the jet. On the basis of the method of local correlation which is developed, a rationale for computing heat transfer distributions below impinging jets is suggested.

8. CITED REFERENCES

1. Snedeker, R.S. and Donaldson, C.duP. Experiments on free and impinging underexpanded jets from a convergent nozzle. ARAP Report No. 63, September 1964.

2. Snedeker, R.S. and Donaldson, C.duP. Experiments on the oblique impingement of underexpanded jets on a flat plate. ARAP Report No. 64, April 1965.

3. Reiber, H. Mitt. Forschungsarbeiten 269, 1 (1925).

4. Comings, E.W., Clapp, J.T., and Taylor, J.F. Air turbulence and transfer processes: flow normal to cylinders. Ind. and Eng. Chem. 40, 6, 1076 (1948).

5. Maisel, D.S. and Sherwood, T.K. Evaporation of Liquids into Turbulent Gas Streams. Chem. Eng. Prog. 46, 3, 131 (1950).

6. Giedt, W.H. Trans. ASME 71, 375 (1949).

7. Zapp, G.M. MSE Thesis. Oregon State University, 1950.

8. Van Der Hegge Zijnen, B.G. Heat transfer from horizontal cylinders to a turbulent air flow. Appl. Sci. Res. A7, 205 (1957).

9. Schnautz, J.H. Ph.D. Thesis. Oregon State University, 1958.

10. Seban, R.H. J. Heat Trans. 82, 101 (1960).

11. Kestin, J., Maeder, P.F., and Sogin, H.H. Z. Angew. Math. Phys. 12, 115 (1961).

12. Smith, M.C. and Kuethe, A.M. Effects of turbulence on laminar skin friction and heat transfer. Phys. Fluids 9, 12, 2337 (1966).

13. Vickers, J.M.F. Heat transfer coefficients between fluid jets and normal surfaces. Ind. and Eng. Chem. 51, 8, 967 (1959).

14. Gardon, R. and Cobonpue, J. Heat transfer between a flat plate and jets of air impinging on it. Proc. 1961 Intern'l Heat Transfer Conf., 454. Univ. of Colorado, August 1961.

15. Huang, G.C. Investigations of heat-transfer coefficients for air flow through round jets impinging normal to a heat-transfer surface. J. Heat Transfer 85, 237 (1963).

16. Gardon, R. and Akfirat, J.C. Heat transfer characteristics of impinging two-dimensional air jets. ASME Paper No. 65-HT-20, August 1965.

17. Gardon, R. and Akfirat, J.C. The role of turbulence in determining the heat transfer characteristics of impinging jets. Intern'l J. Heat and Mass Transfer 8, 9, 1261-1272 (1965).

18. O'Connor, T.J., Comfort, E.H., and Cass, L.A. Turbulent mixing of axisymmetric jets of partially dissociated nitrogen with ambient air. AVCO Corp. Tech. Rept. RAD-TR-65-18, July 1965.

19. Rose, W.G. Some corrections to the linearized response of a constant-temperature hot-wire anemometer operated in a low speed flow. J. Appl. Mech. 29, 554 (1962).

20. Westkaemper, J.C. An analysis of slug-type calorimeters for measuring heat transfer from exhaust gases. AEDC Tech. Note 60-202, November 1960.

21. Westkaemper, J.C. On the error in slug-type calorimaters caused by surface-temperature mismatch. J. Aerospace Sci. 28, 11, 907 (1961).

22. Wehofer, S. Rocket heat transfer measuring devices and techniques. AEDC Tech. Doc. Rept. 63-93, July 1963.

23. Corrsin, S. Investigation of flow in an axially symmetrical heated jet of air. NACA ACR 3L23, December 1943.

24. Corrsin, S. and Uberoi, M.S. Further experiments on the flow and heat transfer in a heated turbulent air jet. NACA Rept. 998, 1950.

25. Laurence, J.C. Intensity, scale, and spectra of turbulence in the mixing region of a free subsonic jet. NACA Rept. 1292, 1956.

26. Gibson, M.M. Spectra of turbulence in a round jet. J. Fluid Mech. 15, 161 (1963).

27. Strong, D.R., Siddon, T.E. and Chu, W.T. Pressure fluctuations on a flat plate with oblique jet impingement. UTIA Tech. Note 107, February 1967.

28. Rosenbaum, H. and Donaldson, C.duP. An analysis of jet impingement heat transfer. ARAP Report No. 101, March 1967.

29. Lees, L. Laminar heat transfer over blunt nosed bodies at hypersonic flight speeds. Jet Propulsion 26, 4 (1956).

APPENDIX

Notation system used for flow variables.

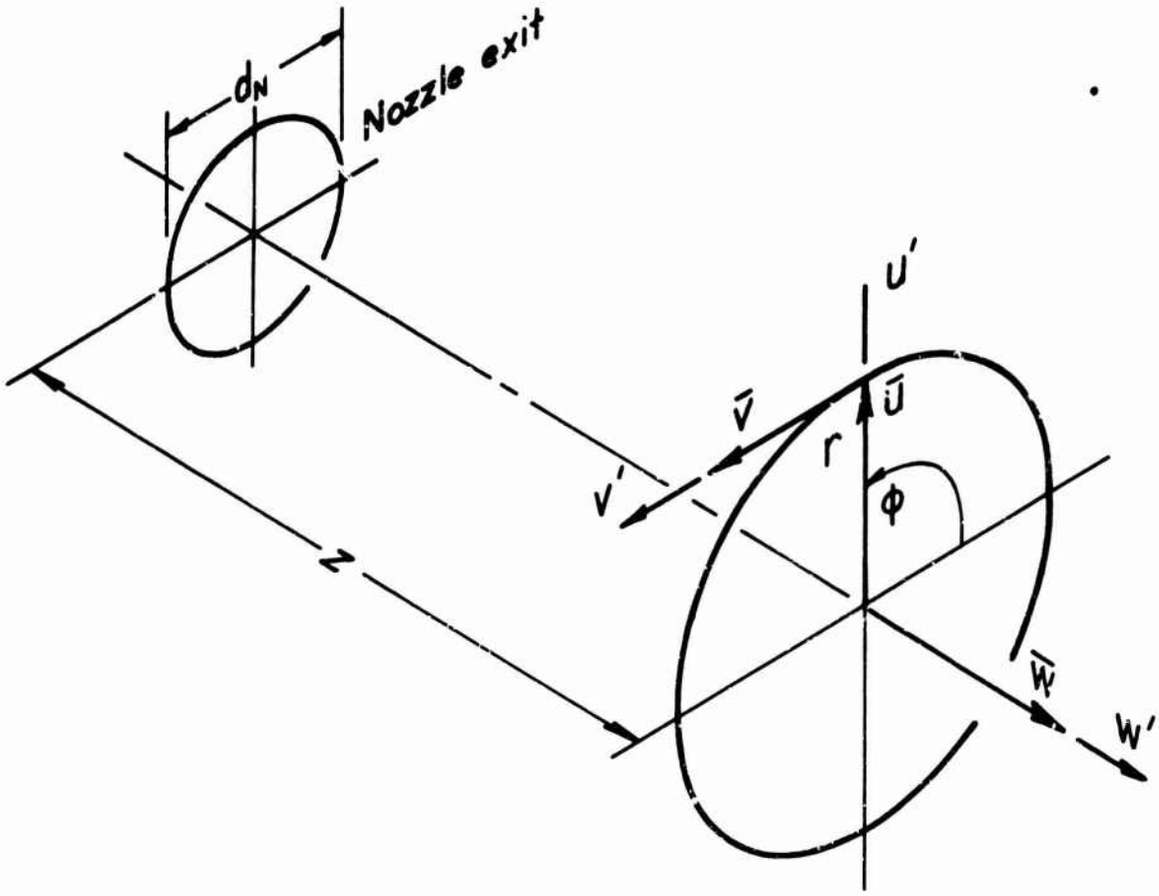

$u = \bar{u} + u'$ = total instantaneous radial velocity

$v = \bar{v} + v'$ = total instantaneous tangential velocity

$w = \bar{w} + w'$ = total instantaneous axial velocity

$\tilde{u}' = \sqrt{\overline{u'^2}}$

$\tilde{v}' = \sqrt{\overline{v'^2}}$ root-mean-square turbulent components

$\tilde{w}' = \sqrt{\overline{w'^2}}$

$p = \bar{p} + p'$ = instantaneous total pressure

$\tilde{p}' = \sqrt{\overline{p'^2}}$ = root-mean-square total pressure fluctuation

z = axial coordinate

ϕ = tangential coordinate

r = radial coordinate

APPENDIX (continued)

Schematic of axisymmetric, subsonic turbulent jet flow

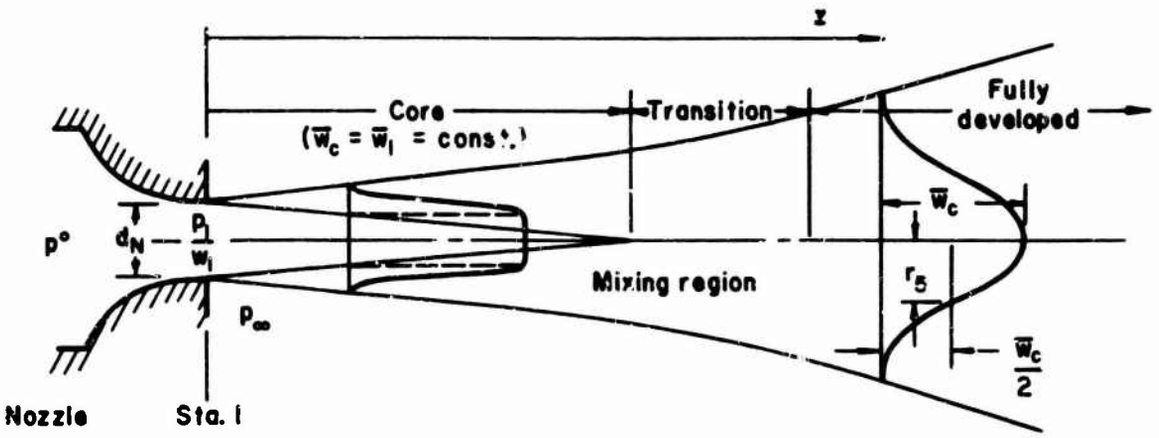

$\bar{w}_1$ = mean velocity at nozzle exit plane

$\bar{w}_c$ = mean velocity on the jet centerline

r_5 = jet half-breadth; radius at which $\bar{w} = \bar{w}_c$?

d_N = diameter of nozzle exit

Unclassified

Security Classification

DOCUMENT CONTROL DATA - R & D

(Security classification of title, body of abstract and indexing annotation must be entered when the overall report is classified)

1. ORIGINATING ACTIVITY (Corporate author) Aeronautical Research Associates of Princeton, Inc. 50 Washington Road, Princeton, New Jersey	2a. SECURITY CLASSIFICATION Unclassified 2b. GROUP

3. REPORT TITLE

A Study of the Mean and Turbulent Structure of a Free Jet and Jet Impingement Heat Transfer

4. DESCRIPTIVE NOTES (Type of report and inclusive dates)

Technical Report

5. AUTHOR(S) (First name, middle initial, last name)

Colemen duP. Donaldson
Richard S. Snedeker
David P. Margolis

6. REPORT DATE	7a. TOTAL NO. OF PAGES	7b. NO. OF REFS
December 1966	84	29

8a. CONTRACT OR GRANT NO	9a. ORIGINATOR'S REPORT NUMBER(S)
b. ~~xxxxxxxx~~ Nonr-3903(00)(x) ARPA Order No. 149-60 c. d.	ARAP Report No. 96 9b. OTHER REPORT NO(S) (Any other numbers that may be assigned this report)

10. DISTRIBUTION STATEMENT

Distribution of this document is unlimited.

11. SUPPLEMENTARY NOTES	12. SPONSORING MILITARY ACTIVITY

13. ABSTRACT

The results of an experimental study of the heat transfer below normally impinging jets are presented. These results are correlated on the basis of the local mean flow and turbulent characteristics of the free jet that would exist in the plane of impingement were this plane to be removed. In order to make these local correlations possible, a rather extensive survey of the turbulent characteristics of the free jet used in the experiments is made that can be used in connection with previous studies of the local mean character of the jet. On the basis of the method of local correlations which is developed, a rationale for computing heat transfer distributions below impinging jets is suggested.

DD FORM 1473

Unclassified

Security Classification

Impinging jet heat transfer
Turbulence in free and impinging jets
Impinging jets
Heat transfer
Effect of turbulence on heat transfer